

**Design, Synthesis, and Characterization of Nucleoside Based Probes to Evaluate the Role of Human Histidine Triad Nucleotide Binding Protein 1 in Mu Opioid Receptor and N-Methyl-D-Aspartate Receptor Cross Regulation**

A DISSERTATION  
SUBMITTED TO THE FACULTY OF  
THE UNIVERSITY OF MINNESOTA  
BY

**Maxwell Dalton Dillenburg**

IN PARTIAL FULFILLMENT OF THE REQUIREMENTS  
FOR THE DEGREE OF  
DOCTOR OF PHILOSOPHY

**Advisor: Dr. Carston R. Wagner**

June 2023

## **Acknowledgements**

I would like to sincerely thank my advisor, Dr. Rick Wagner, for his mentorship during my graduate career. Dr. Wagner's scientific curiosity and creativity are always inspiring and have contributed greatly to my professional development. Beyond Dr. Wagner's great scientific leadership, I thank him for his personal support and patience during my many years in lab. I am grateful to have been able to spend time in Dr. Wagner's lab, where he has developed a multidisciplinary space providing an excellent opportunity for student collaboration. I have had the opportunity to work with both fantastic students in our lab and many great scientists around the world. I would like to thank the many graduate students with whom I have shared the lab, both your professional support and friendship were instrumental for my success. I want to specifically thank Alex Strom and Trent West for all the mentorship they provided. Thank you to my committee members Dr. Carrie Haskell-Luevano, Dr. Will Pomerantz and Dr. Carolyn Fairbanks for taking the time to serve on my committee.

I want to give a special thank you to all my collaborators: Dr. Carolyn Fairbanks, Dr. Cristina Peterson, Kelley Kitto, Dr. Rafal Dolot, Dr. Luciana Jesus da Costa, and Dr. Romario Mattos. I appreciate all your hard work in these projects, and I am grateful to have had the opportunity to collaborate with all of you. I want to specifically thank Dr. Cristina Peterson for the many years of collaboration.

I would like to express my deepest appreciation to my friends and family for their support during this journey. The positivity you all provide to my life has been vital to helping me overcome some of the more difficult times. This dissertation is dedicated to my wife, Bailey; I could not have done this without you.

## Abstract

The histidine triad nucleotide binding protein 1 (HINT1) has widespread expression across tissues and is involved in several biological processes including CNS function, tumor suppression, and mast cell activation. HINT1 participates in these processes through protein-protein interactions with G protein-coupled receptors, transcription factors, and other proteins. Recently, it has been discovered that HINT1 is critical to the cross-regulatory interactions of the mu opioid receptor (MOR) and N-methyl-D-aspartate receptor (NMDAR) via mediation of a series of protein assemblies. Interestingly, though HINT1 is largely known for the involvement of its phosphoramidase activity in the metabolism of clinically approved antiviral ProTides, the contribution of this enzymatic activity to these interactions is unknown. To probe the role of HINT1, and specifically the HINT1 active site, in MOR-NMDAR cross talk, we have developed two series of HINT1 active-site inhibitors and evaluated their activity using *in vivo* models of these interactions. Specifically, we examined the effect of spinal administration of HINT1 inhibitors on the blockade of morphine's inhibition of NMDA evoked behaviors and the inhibition of endomorphin-2 tolerance. These findings are supported by *in vitro* characterization of HINT1 binding using X-ray crystallography, isothermal titration calorimetry, and a continuous fluorescence assay to evaluate inhibition of HINT1 catalysis. Together, these studies detail the SAR of HINT1 inhibitors on MOR-NMDAR crosstalk and demonstrate the utility of these inhibitors as probes to evaluate the intriguing role of HINT1 *in vivo*.

## **Table of Contents**

Acknowledgements	i
Abstract	ii
Table of Contents	iii
List of Tables	vi
List of Figures	viii
Disclosure of Publications	ix

## **Chapter I: The Many Faces of Histidine Triad Nucleotide Binding Protein 1 (HINT1)**

i. Abstract	2
ii. Introduction	4
iii. HINT1 Structure	5
iv. HINT1 Catalytic Functions	8
a. Substrate Specificity	8
b. Kinetic Mechanism	14
c. Potential Biological Functions of HINT1 Catalysis	18
d. Prodrug Activation	19
v. HINT1 in Biological Pathways	24
a. Central Nervous System	24
b. Tumor Suppression and Tumorigenesis	29
c. Mast Cell Activation	31
vi. Summary and Future Directions	32



vii.	References	34
viii.	Supplemental Information	50

## **Chapter II: Inhibition of HINT1 Modulates Spinal Nociception and NMDA Evoked Behavior in**

### **Mice**

i.	Abstract	54
ii.	Introduction	55
iii.	Results	57
iv.	Conclusions	70
v.	Materials and Methods	75
vi.	References	87
vii.	Supplemental Information	92

## **Chapter III: Development of HINT1 Inhibitors to Selectively Modulate MOR-NMDAR Cross**

### **Regulation**

i.	Abstract	95
ii.	Introduction	96
iii.	Results	100
iv.	Conclusions	117
v.	Materials and Methods	121
vi.	References	129
vii.	Supplemental Information	134

## Appendix

### i. NMR Spectra

159

## List of Tables

### Chapter II

1. HINT1 Carbamate Inhibitor Dissociation Constants and Yields	59
2. HINT1 Sulfamate Inhibitor Dissociation Constants	61
3. HINT1 Inhibitor NMDA Evoked Behavior ED <sub>50</sub> Values	68
4. X-Ray Crystallography Statistics	92

### Chapter III

1. HINT1 Carbamate Inhibitor Inhibition Constants	107
2. HINT1 Acyl-Sulfamate Inhibitor Inhibition Constants	108
3. Crystallographic parameters and data collection statistics (S1)	156
4. Refinement Statistics	158

## List of Figures

### Chapter I

TOC Figure	3
Figure 1: HINT1 Crystal Structure	6
Figure 2: HINT1 Interacting Molecules	9
Figure 3: HINT1 Substrate Kinetics	11
Figure 4: HINT1 Kinetic Mechanism	15
Figure 5: Structures of Isolated Transition States of HINT1 Catalysis	17
Figure 6: Clinically Approved ProTides	20
Figure 7: ProTide Activation Mechanism	22
Figure 8: Role of HINT1 in Downregulation of MOR signaling via NMDAR	27
Figure S1: Sequence Alignment of Human HINT Isoforms	51
Figure S2: Sequence Alignment of HINT1 homologs	52

### Chapter II

Figure 1: HINT1-Inhibitor Co-Crystal Structures	63
Figure 2: Carbamate vs Acyl-Sulfamate Inhibitor Bound HINT1 Structures	65
Figure 3: NMDA Evoked Behavior Assay Results	67
Figure 4: Endomorphin-2 Tolerance Assay Results	69
Figure 5: Carbamate vs Acyl-Sulfamate Inhibitor Electron Density	73

### Chapter III

Figure 1: HINT1 Substrates and Previously Developed HINT1 Inhibitors	99
Scheme 1: Synthetic Strategy for Preparation of Nucleoside Precursors 6a and 6b	102
Scheme 2: Synthetic Scheme for the Preparation of Target Compounds 8-10	103
Scheme 3: Synthetic Scheme for the Preparation of Target Compounds 13 and 14	104
Figure 2: Co-crystal structures of Compounds 8-10, 13, 14 bound to HINT1	109
Figure 3: Comparison of Nucleoside Positioning for HINT1 Inhibitors	110
Figure 4: Comparison of Acyl-Sulfamate Side Chains for Compounds 13 and 14 Bound to HINT1	111
Figure 5: NMDA Evoked Behavior and Thermal Hyperalgesia Results	114
Figure 6: HINT1 Inhibitor Analgesia Results	115
Figure 7: HINT1 Inhibitor Endomorphin-2 Tolerance Results	116
Figure 8: HINT1 Inhibitor Molecular Surfaces	120
Figure S1: Compound 8 Inhibition Kinetics	150
Figure S2: Compound 9 Inhibition Kinetics	151
Figure S3: Compound 10 Inhibition Kinetics	152
Figure S4: Compound 14 Inhibition Kinetics	153
Figure S5: Compound 15 Inhibition Kinetics	154

## Disclosure of Publications

This work has utilized portions of manuscripts that have been previously published, previously submitted, or will be submitted for publication. The manuscripts that have been adapted for this work are listed below. These works have been repurposed with the expressed written permission of the copyright holder and/or authors.

**Dillenburg M**, Smith JA, Wagner CR. The Many Faces of Histidine Triad Nucleotide Binding Protein 1. [*Under review*]

Shah RM, Peterson C, Strom A, **Dillenburg M**, Finzel B, Kitto KF, Fairbanks C, Wilcox G, Wagner CR. Inhibition of HINT1 Modulates Spinal Nociception and NMDA Evoked Behavior in Mice. ACS Chemical Neuroscience 2019 10 (10), 4385-4393

**Dillenburg M**, Peterson C, Kitto KF, Dolot R, Fairbanks C, Wagner CR. Development of HINT1 Inhibitors to Selectively Modulate MOR-NMDAR Cross Regulation. [*In preparation*].

## Chapter I

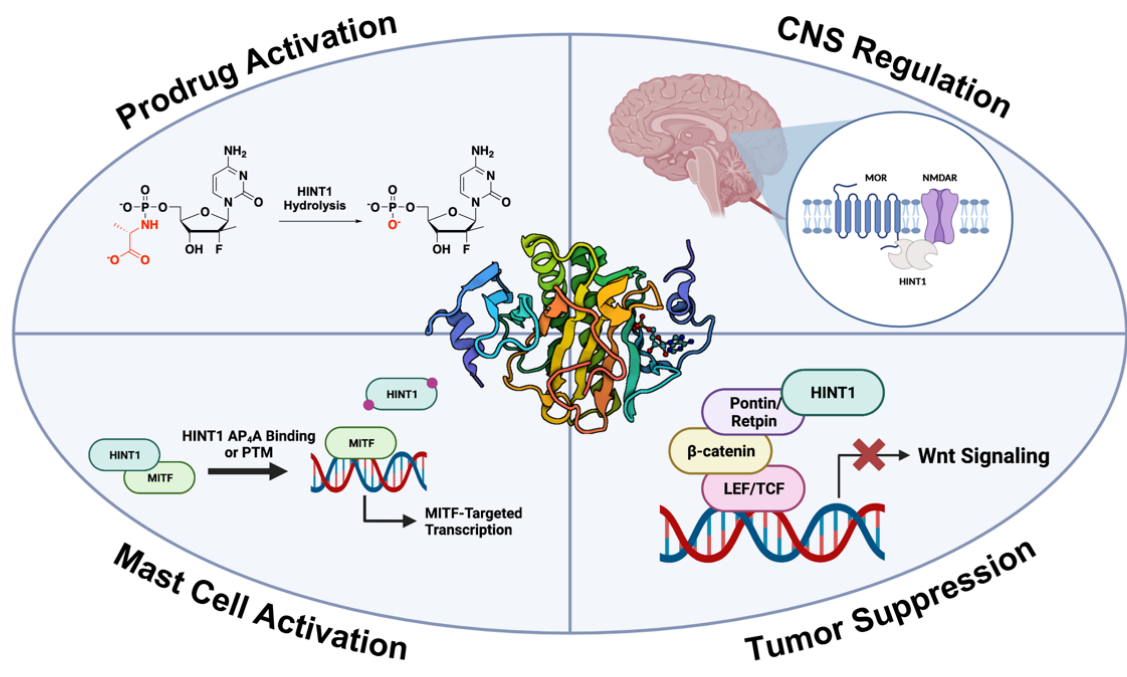
### The Many Faces of Histidine Triad Nucleotide Binding Protein 1 (HINT1)

## **Abstract**

The histidine triad nucleotide binding protein 1 (HINT1) is a nucleoside phosphoramidase that has garnered interest due to its widespread expression and participation in a broad range of biological processes. Herein, we discuss the role of HINT1 as a regulator of several CNS functions, tumor suppressor, and mast cell activator via its interactions with multiple G-protein coupled receptors and transcription factors. Importantly, altered HINT1 expression and mutation is connected to the progression of multiple disease states, including several neuropsychiatric disorders, peripheral neuropathy, and tumorigenesis. Additionally, due to its involvement in the activation of several clinically used phosphoramidate prodrugs, tremendous efforts have been made to better understand the interactions behind nucleoside binding and phosphoramidate hydrolysis by HINT1. We detail the substrate specificity and catalytic mechanism of HINT1 hydrolysis while highlighting the structural biology behind these efforts. The aim of this review is to summarize the multitude of biological and pharmacological functions in which HINT1 participates, while addressing the areas of need for future research.

Keywords: Histidine Triad Nucleotide Binding Protein, ProTide, Pronucleotide, Inherited peripheral neuropathy, pain, opioid tolerance, amino acyl t-RNA synthetase





## Introduction

Histidine triad nucleotide binding proteins (HINTs) are members of the ubiquitous and ancient superfamily of histidine triad (HIT) enzymes. HIT proteins are linked by their ability to hydrolyze an array of functionalized nucleotide monophosphate molecules into their respective monophosphate products.<sup>1</sup> In the case of HINT proteins, they display phosphoramidase and acyl-adenylate hydrolase activity reliant on their catalytic triad of histidines. This catalytic triad of histidine residues, patterned His-X-His-X-His-X-X, where X is a hydrophobic residue, are conserved across HINT proteins.<sup>2,3</sup> There are three human HINT isoforms, hHINT1, hHINT2, and hHINT3 located in the cytosol, mitochondria, and nucleus respectively, each having a wide array of binding partners while maintaining the crucial catalytic triad of histidine residues (**Figure S1**).<sup>4</sup>

<sup>5</sup> This review will focus on the most well studied HINT protein, HINT1. HINT1 is known to be involved in numerous protein-protein interactions, contributing to biochemical processes ranging from nociception to mast cell activation.<sup>6, 7</sup> However, the mechanism behind HINT1's involvement in these processes is not well understood. Crucially, it is not known whether the catalytic activity of HINT1 is vital to these processes or if the protein is behaving as a multifaceted scaffold. Though the cellular role of this catalytic activity is unclear, the mechanism and substrate specificity of HINT1 catalysis has been an area of great interest due its involvement in the activation of nucleoside phosphoramidate prodrugs, a crucial class of antiviral therapies.<sup>8</sup> The aim of this review is to summarize the efforts made into better understanding both the catalytic activity and protein-protein interactions of HINT1 across several biological pathways. Ultimately, these works have revealed the enigmatic nature of HINT1, a protein with a vital pharmacological role and seemingly puzzling combination of biological functions.

## HINT1 Structure

Currently, there are 59 published HINT1 crystal structures on the protein data base, with the earliest being published in 1997. Early structural work identified HINT1 as a 14 kDa protein that exists as a homodimer (**Figure 1A**).<sup>9</sup> Importantly, the first crystal structures identified the presence of the catalytic histidine triad in HINT1's active site, placing the protein in the HIT family. These catalytic histidines were identified to be His110, His112, and His114, which are located towards the protein's C-terminus (**Figure 1B**). Mutation of His112 to alanine or glycine was observed to prevent the formation of the adenylated HINT1 intermediate, indicating that His112 is the residue responsible for nucleophilic attack on the substrate phosphorous species.<sup>10</sup> In addition to the catalytic triad, a fourth histidine, His51, is located within the active site and contributes to the alignment of the histidine triad of HINT1 (**Figure 1B**). Analysis of bound HINT1 ligands reveals multiple key interactions required for binding of its nucleoside substrates. The carboxylic acid side of chain of Asp43 makes two tight hydrogen bonds with the 2'- and 3' hydroxyls of ribonucleosides, while a large hydrophobic pocket containing a series of conserved residues accommodates binding of the nucleobase (**Figure 1C**).<sup>11</sup> The active site contains the catalytic His112 that is responsible for the nucleophilic attack on the phosphorous of the nucleoside substrate. Co-crystal structures with bound non-hydrolysable HINT1 inhibitors uncovered more key interactions. It was demonstrated that Ser107 participates in a hydrogen bond with the acyl group of acyl-sulfamate inhibitors, which could indicate the importance of this residue for recognition of acyl-adenosine monophosphate (acyl-AMP) substrates.<sup>12</sup> Lastly, Trp123, located just outside the phosphoramidate binding pocket, is in position to interact with inhibitor or substrates via  $\pi$ - $\pi$  stacking or hydrophobic interactions.<sup>13</sup>

Figure 1

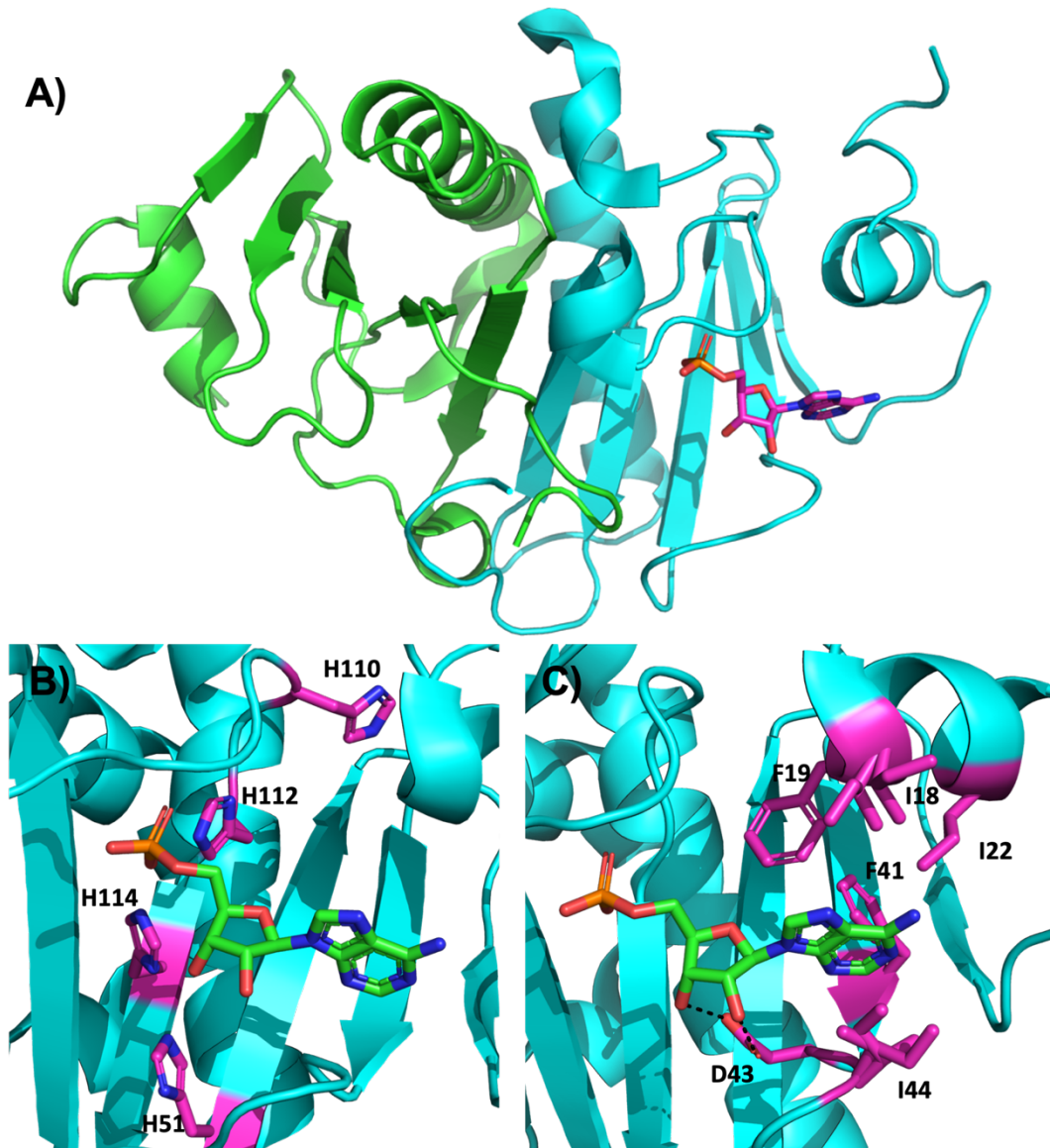


Figure 1. Crystal structures of AMP bound HINT1 Dimer (3TW2). (A) Overall cartoon structure of homodimeric human HINT1 bound to AMP, with each monomer depicted in a different color. (B) AMP in green bound to the HINT1 nucleoside binding site. The side chains of the histidine triad

(H110, H112, H114) and contributing His51 are labelled and highlighted in magenta. (C) AMP in green bound to the nucleobase binding pocket. The hydrophobic residues (I18, F19, I22, F41, and I44) forming the hydrophobic nucleobase binding pocket labelled in magenta. Key H-bonds from D43 to the 2'- and 3'-OH are measured and labelled in black, with the side chain of D43 highlighted in magenta.

## HINT1 Catalytic Functions

### Substrate Specificity

Early work by Brenner and co-workers evaluated the ability of various HINTs to hydrolyze a multitude of endogenous nucleotidylated substrates, including amino acids, sugars, and dinucleotides. Crucially, while, HINT homologs can differ in their termini, they maintain a similar active site structure, and each possesses the conserved catalytic triad of histidine residues (**Figure S2**). These studies demonstrated that the yeast homolog of human HINT1, known as Hnt1, could efficiently hydrolyze the phosphoramidate substrates AMP-NH<sub>2</sub>, AMP-N-alanine methyl ester, and AMP-N-ε-(N-α-acetyl lysine methyl ester), while dinucleotides, diphosphates, or adenylated sugars proved not to be substrates.<sup>14</sup> Subsequently, both *E.coli* homolog, hinT, and the Human ortholog, HINT1, were found to hydrolyze AMP-NH<sub>2</sub>, AMP-Morpholine, GMP-Morpholine, AMP-lysine and GMP-lysine.<sup>15</sup> Comparison of the specific activity of human HINT1 for AMP-NH<sub>2</sub> (**A1**), AMP-morpholine (**A2**), and AMP-lysine (**A3**) revealed HINT1 is able to accommodate a diverse set of leaving groups (**Figure 3A**). Similar to Hnt1, neither *E. coli* hinT or hHINT1 carried out significant hydrolysis of dinucleotides diphosphates.<sup>16</sup> Using a continuous fluorescence assay based on tryptamine or tryptophan containing nucleoside phosphoramidate monoester substrates, in which the indole moiety is quenched by the nucleoside base, Wagner and co-workers further evaluated HINT1 substrate specificity by examining a set of nucleoside phosphoramidate analogs with modifications to the nucleobase and ribose ring.<sup>17, 18</sup> Beginning with modifications to the nucleoside, the tryptamine functionalized adenosine and guanosine phosphoramidates, **B1** and **B2** respectively, displayed similar catalytic efficiencies ( $k_{cat}/K_m$ ) (**Figure 3B**). Replacement of the purine nucleobase with pyrimidine bases uracil (**3C**) and cytosine (**3D**) resulted in a decrease in

**Figure 2**

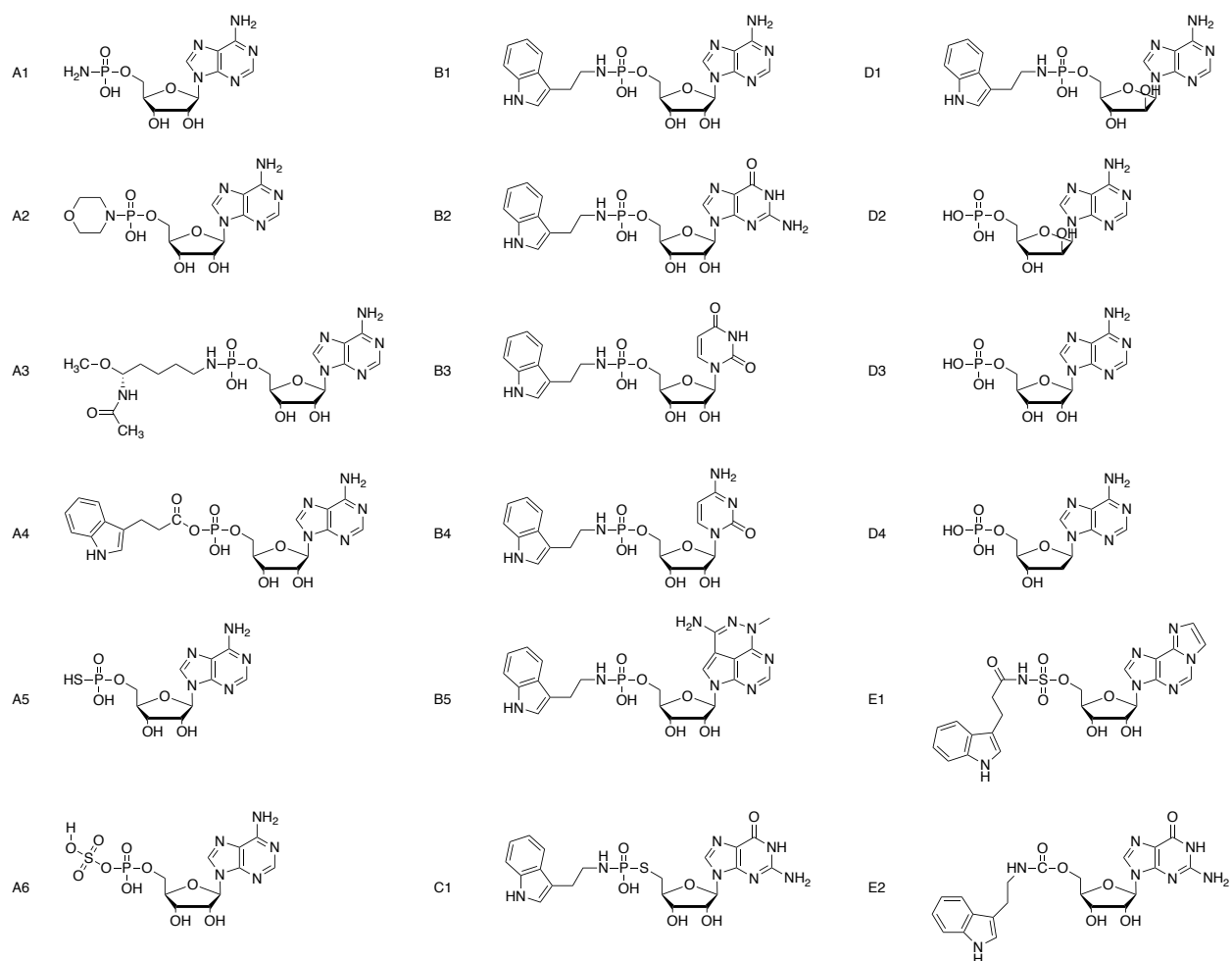


Figure 2. Structures of HINT1 interacting molecules. **Series (A)** Modifications to the leaving group for HINT1 substrates. **Series (B)** Modifications to the nucleobase with the corresponding tryptamine leaving group for HINT1 substrates. **Series (C)** HINT1 slow substrate used for isolating HINT1 catalytic intermediates. **Series (D)** Modifications to the ribose sugar for HINT1 substrates. **Series (E)** HINT1 inhibitors.

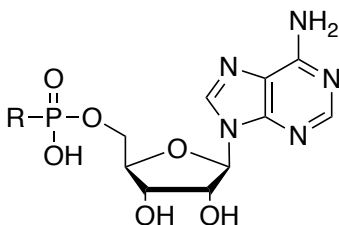
catalytic efficiency by roughly an order of magnitude, with the differences coming almost exclusively from changes to  $K_m$  (**Figure 3B**).<sup>17</sup> Co-crystal structures of bound purine and pyrimidine nucleoside ligands reveal that pyrimidines leave a portion of the hydrophobic nucleobase binding cleft unoccupied, while purines occupy much more of the space, giving an explanation to the purine preference.<sup>18</sup> Analysis of bound AMP and GMP to HINT1 revealed additional binding interactions making these favorable substrates. In the case of AMP, the exocyclic nitrogen forms a water mediated hydrogen bond with Pro28, while the exocyclic amine of GMP makes a direct hydrogen bond with the backbone carbonyl of His42. Additionally, substrates incorporating the non-natural nucleobase triciribine (**B5**) were hydrolyzed with a similar substrate specificity to that of the pyrimidine nucleobases.<sup>18</sup> Together, these data suggest that HINT1 displays a preference for purine over pyrimidine nucleobases, with the nucleobase binding cleft able to tolerate a range of larger nucleosides.

To examine the impact of changes to the ribose, particularly at the 2'- and 3'- hydroxyls, the Wagner group used a set of model substrates containing alterations to the ribose. Kinetic work comparing the adenosine phosphoramidate molecule (**B1**) and its arabinose analogue (**D1**) revealed a roughly 10-fold decrease in the catalytic efficiency due to the alteration of the stereochemistry at the 2'-carbon position (**Figure 3B**).<sup>17</sup> Comparison of the co-crystal structures of adenosine monophosphates (**D2**) and (**D3**) revealed that despite the stereochemical change at the 2'-carbon, they exhibit similar binding modes.<sup>18</sup> This was taken further with the complete removal of the 2'-hydroxyl using 2'-deoxy AMP (**D4**). Comparison of this crystal structure with AMP demonstrated again that the change at the 2'-carbon did not alter the binding mode.<sup>18</sup> This



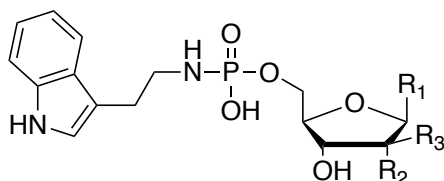
**Figure 3**

**A)**



	<b>R<sub>1</sub></b>	<b>hHINT1 Specific Activity (nmol nmol<sup>-1</sup> min<sup>-1</sup>)</b>
<b>A1</b>	NH <sub>2</sub>	196 ± 33
<b>A2</b>	Morpholine	45.0 ± 0.1
<b>A3</b>	Lysine	102 ± 19

**B)**



	<b>R<sub>1</sub></b>	<b>R<sub>2</sub></b>	<b>R<sub>3</sub></b>	<b>k<sub>cat</sub> (s<sup>-1</sup>)</b>	<b>K<sub>m</sub> (μM)</b>	<b>k<sub>cat</sub>/K<sub>m</sub> (x 10<sup>-7</sup> s<sup>-1</sup> M<sup>-1</sup>)</b>
<b>B1</b>	Adenine	OH	H	2.1 ± 0.1	0.13 ± 0.02	1.5 ± 0.3
<b>B2</b>	Guanine	OH	H	2.3 ± 0.7	0.21 ± 0.02	1.1 ± 0.1
<b>B3</b>	Uracil	OH	H	2.5 ± 0.3	2.2 ± 0.4	0.12 ± 0.05
<b>B4</b>	Cytosine	OH	H	1.2 ± 0.1	2.3 ± 0.4	0.06 ± 0.02
<b>B5</b>	Tricirbine	OH	H	0.77 ± 0.02	0.35 ± 0.02	0.22 ± 0.007
<b>D1</b>	Adenine	H	OH	1.1 ± 0.03	1.0 ± 0.06	0.11 ± 0.01

**Figure 3.** Kinetics data for two series of HINT1 substrates (Compound structures detailed in Fig.

2). (A) Specific activity of human HINT1 for a series of adenosine phosphoramidate substrates.

(B) Substrate specificity of human HINT1 following changes to the substrate nucleobase and ribose.

indicates that HINT1 can likely support an array of changes to the 2'-carbon position, as long as the five-membered ribose ring is maintained.

The importance of the phosphate group at the 5'-hydroxyl was also examined. The Wagner lab observed the phosphate group in two conformations, deemed a substrate and product conformation.<sup>18</sup> In most of the observed nucleoside monophosphate structures, each of the phosphate oxygens were positioned to interact with multiple hydrogen bond donors. Interestingly, the 5'-hydroxyl of the nucleoside was positioned to make two H-bonds in the product conformation, but only one in the substrate conformation, interacting with His112 only. The difference in this one H-bond may be responsible for the frequency of each of these conformers. Comparison of AMP with adenosine highlighted the importance of the phosphate moiety for HINT1 binding. Removal of the phosphate group of AMP resulted in an increase in the  $K_D$  by two-orders of magnitude, going from  $0.423 \pm 0.059 \mu\text{M}$  for AMP to  $55.9 \pm 9.9 \mu\text{M}$  for adenosine. Together, these studies have outlined a basic substrate model for HINT1 binding and catalysis.

In addition to its phosphoramidase and acyl-adenylate hydrolase activity, rabbit Hint was observed to desulfurize AMP $\alpha$ S (**A5**) and AMP $\text{SO}_4$  (**A6**) into nucleoside monophosphates *in vitro*, though they were 1- and 2- orders of magnitude, respectfully, less efficient substrates compared to AMPNH<sub>2</sub>.<sup>14</sup> This activity was further investigated by analyzing the hydrolysis of a series of nucleoside-5'-O-phosphorothioates (NMPS) by rabbit Hint. It was found that rabbit Hint was able to catalyze the hydrolysis of 5'-O-phosphothiorated ribonucleosides (A, G, C, and U) and

deoxynucleosides (dA, dG, dC, and dT) *in vitro*.<sup>19</sup> It is hypothesized that this catalytic activity could represent an important step in the metabolism of therapeutically relevant phosphorothioate oligonucleotides (PS-oligos). Metabolism of PS-oligos into the corresponding NMPS monomers has been well characterized.<sup>20</sup> HINT1 was proposed as potentially being responsible for conversion of these NMPS to the nucleoside monophosphate and H<sub>2</sub>S *in vivo*. This activity was confirmed in cellular lysates where NMPS was slowly hydrolyzed, resulting in the production H<sub>2</sub>S. Silencing of HINT1 by siRNA knockdown confirmed its participation in this conversion.<sup>21, 22</sup> Because endogenous H<sub>2</sub>S release has as a plethora of effects in cells, including neurotransmission, cell apoptosis, oxygen sensing, and many others, release of H<sub>2</sub>S due to HINT1 metabolism of NMPS could have a significant biological impact.<sup>23, 24</sup> Further studies *in vivo* are needed to examine the effects of this phenomenon.

Dimerization of HINT1 has been determined to play a crucial role in its substrate recognition. This was demonstrated via development of a monomeric HINT1 protein through mutation to Val97 at the dimerization interface.<sup>25</sup> Interestingly, circular dichroism of the monomeric HINT1 revealed similar stability to the wild-type HINT1. However, though the monomeric HINT1 had a similar  $k_{\text{cat}}$  for acyl-AMP hydrolysis (**A4**), its  $K_m$  was increased nearly 1000-fold compared to the wild-type dimeric hHINT1. Therefore, homodimerization likely does not contribute greatly to the stability of each HINT1 protomer, but the existence of the stable dimer is required for efficient catalysis. It is hypothesized that the tight dimerization interface allows for the contribution of one protomer C-terminus to influence the binding site of the other. The contribution of the C-terminal loop on substrate specificity was further investigated via comparison of HINT1 and echinT.

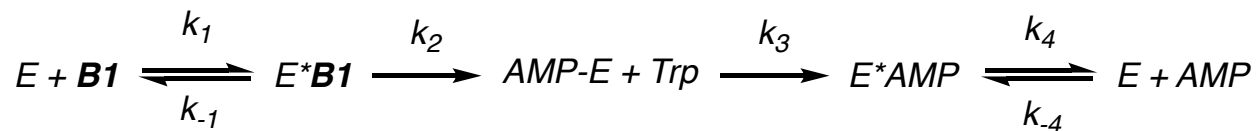
Though highly sequence similar, the two proteins have significant differences at the C-terminal loop, with *echinT* possessing a larger, more flexible loop.<sup>26</sup> Due to this flexibility, *echinT* can tolerate a wider array of phosphoramidate substrates compared to HINT1.<sup>17</sup> However, for non-sterically hindered compounds, HINT1 displays catalysis 3- to 32-fold more efficient than *echinT*. The impact of the C-terminal loops of HINT1 and *echinT* were examined directly by development of a pair of Hint chimeric proteins in which the C-terminus of one protein has been deleted and replaced by the C-terminus of the other. The HINT1 chimera containing the *echinT* C-terminus (Hs/*ec*) displayed nearly identical catalytic efficiencies compared to the wild-type *echinT*, while the *echinT* chimera containing the HINT1 C-terminus (*ec*/Hs) behaved similarly to the wild-type HINT1.<sup>26</sup> Further, *ec*/Hs chimera adopted the human enzyme preference for substrates containing L- tryptophan. Together, these studies highlight the importance of the C-terminus on HINT1 substrate recognition.

### **Kinetic Mechanism**

Investigations into the kinetic mechanism of HINT1 revealed that substrate hydrolysis likely occurs through a two-step double-displacement mechanism (**Figure 4**). This is analogous to another member of the HIT family, Fhit.<sup>27</sup> First, the substrate binds and undergoes rapid attack by the nucleophilic active site His112, releasing the alkyl-amine. Then, the intermediate HINT1-AMP is hydrolyzed followed by release of the AMP product. Stopped-flow fluorescence experiments demonstrated that catalysis occurs in two phases. First, an initial rapid burst phase comprised of substrate binding and nucleotidylation, followed by a linear phase consisting of partially rate limiting intermediate hydrolysis and product release.<sup>28</sup> Computational and catalytic

Figure 4)

A)



B)

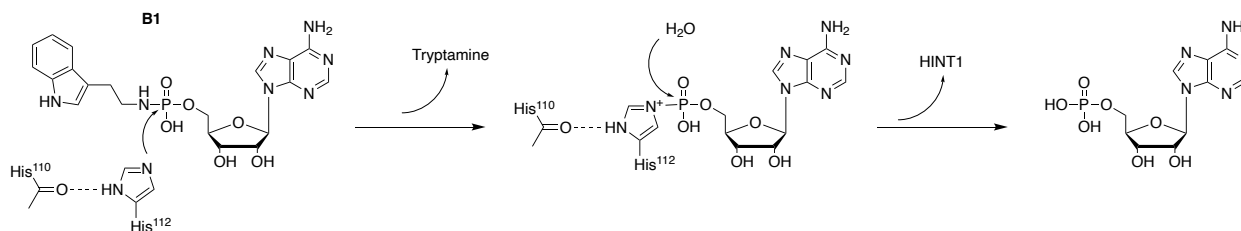
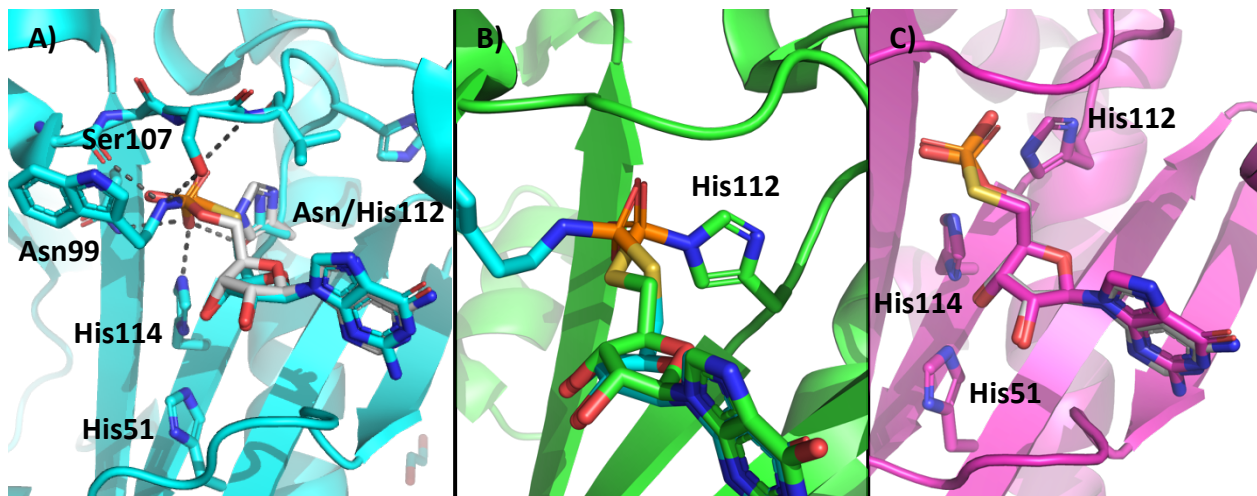


Figure 4. Kinetic mechanism of HINT1 acyl-AMP HINT1 hydrolysis. (A) Kinetic equation for hHINT1 hydrolysis of the tryptamine adenosine phosphoramidate **B1**. (B) Scheme for HINT1 hydrolysis of **B1**. His112 first attacks the substrate phosphorous, releasing tryptamine. Water then attacks the substrate/HINT1 complex, releasing HINT1 and the AMP product.

trapping experiments indicated that the partial rate limitation of product release is likely accompanied by a conformational change. This catalytic and kinetic mechanism was later supported through use of a slowly hydrolyzed thiophosphoramidate (**C1**), which in combination with HINT1 active site mutants allowed for capture of several intermediate structures using time dependent crystallography. Soaking of (**C1**) with the inactive HINT1 active site mutant H112N resulted in crystallographic capture of the enzyme\*substrate complex (**Figure 5A**). Next, (**C1**) was soaked with wild-type HINT1. The resulting crystal structure showed the presence of the guanylated intermediate with no electron density for the phosphoramidate leaving group (**Figure 5B**).<sup>29</sup> A longer soak of (**C1**) with wild-type HINT1 allowed for hydrolysis of the phosphorous-nitrogen bond, resulting in capture of the enzyme\*product complex (**Figure 5C**). Additionally, these structures identified a conserved water channel that may be involved in the proton transfers required for catalysis. Further studies determined that this water channel is gated by a pair of dynamic residues, Gln62 and Glu100, that form an ion-dipole pair 13 Å away from the active site.<sup>30</sup> Alterations to the pair of residues, particularly mutations to Gln62, resulted in significant changes to the steady-state  $k_{cat}$  and  $K_m$  during turnover of the fluorescent substrate TpAd (**B1**).<sup>30</sup> Disruption of the ion-dipole pair using the HINT1 variant Q62A resulted in a  $k_{cat}$  five-fold lower and a  $K_m$  10-fold lower than the wild-type variant for the HINT1 substrate (**B1**), resulting in a two-fold increase in the substrate specificity constant ( $k_{cat}/K_m$ ). Interestingly, this Q62A mutant also displayed a worse binding affinity for the HINT1 competitive inhibitor (**E1**). The connection of this long-range interaction to active site behavior could have an impact on the function of HINT1 in its numerous protein-protein interactions and warrants further investigation.

Figure 5



**Figure 5.** Isolated transition states of HINT1 hydrolysis of **C1**. **(A)** Overlay of the ES\* complex (teal, 5IPC) with a known AMP product complex (gray, 3TW2). H-bonds between **C1** and HINT1 are shown in black. Residues of interest are labelled in black. **(B)** Overlay of ES\* (teal, 5IPC) and the nucleotidylated HINT1 complex E\* (green, 5IPD). His112 is bound to the phosphorous center and the electron density for the tryptamine leaving group is no longer observed. **(C)** Overlay of the product of **C1** phosphoramidate hydrolysis (magenta, 5IPE) and AMP (gray, 3TW2).

## Potential Biological Functions of HINT1 Catalysis

Several studies have investigated potential biological roles for HINT1s enzymatic activity and its endogenous substrate. HINT1 has been found to interact with lysyl-tRNA synthetase (LysRS), which is known to generate LysRS-lysyl-AMP complexes. It has been hypothesized that these aminoacyl-adenylate complexes could be natural HINT1 substrates.<sup>10,31,32</sup> Indeed, radiolabeled HINT1-AMP complexes were observed following incubation of LysRS and HINT1 with [ $\alpha$ 32P]ATP. This evidence indicates that the product of the LysRS-ATP reaction is a substrate for HINT1. Furthermore, the formation of this species was dependent on the development of lysyl-AMP.<sup>10,25</sup> Examination of other amino acid-AMP substrates revealed that HINT1 has broad aa-AMP hydrolytic activity, with Trp123 playing a key role in substrate recognition.<sup>33</sup> This observed activity *in vitro*, combined with HINT1's known interactions with transcription factors MITF and USF2, implicates a potential role in transcription regulation, but further investigation of the cellular basis and context of the enzymatic activity is needed.<sup>34,35</sup> In addition to its active site-dependent catalytic activity, one recent study has claimed that HINT1 contains a second active site capable of zinc- and calmodulin-related sumoylase activity.<sup>36</sup> The authors hypothesize that this activity may contribute to the function of HINT1 in neuronal cells and disruption of this activity may be related to HINT1s involvement in certain neuropsychiatric disease states, but additional studies are needed, particularly given the significant distance found between the alleged active site residues.



## HINT1 Prodrug Activation

Though the endogenous substrate of HINT1 is currently unknown, its phosphoramidase activity is crucial to the metabolism of nucleotide phosphoramidate prodrugs. Nucleoside based drugs are important members of the antiviral and anticancer therapeutic armamentarium.<sup>37-39</sup> The activity of nucleoside analogs is typically dependent on their intracellular conversion to the corresponding 5'- mono-, di- and triphosphate. However, some nucleosides are poor substrates for the endogenous nucleoside kinases, especially those carrying out the first step, 5'-monophosphorylation.<sup>40-42</sup> In addition, cellular resistance to nucleoside base drugs can develop by down-regulation of the nucleoside kinase expression.<sup>41, 43</sup> While nucleoside 5'-monophosphates could in principle address the lack of kinase activity, they are not stable to plasma and are unable to cross the cell membrane.<sup>44</sup> Consequently, attempts have been made to by-pass the requirement for nucleoside kinase 5'-monophosphorylation by cloaking the phosphate in cell permeable and generally hydrophobic moieties.<sup>45, 46</sup> Although numerous pronucleotide strategies have been developed to accomplish this goal, the phosphoramidate based proTide approach has shown the most clinical success.<sup>47, 48</sup>

Aryloxy phosphoramidate triesters, commonly known as "ProTides", have had the greatest clinical impact of any nucleotide analogue phosphoramidate prodrug class, with three FDA-approved drugs (**Figure 6**). McGuigan and colleagues first reported aryloxy phosphoramidate prodrugs in 1992.<sup>49</sup> The story of ProTide development began with simple alkyloxy phosphoramidate derivatives of the HIV drug zidovudine, which were tested based on the hypothesis that the HIV protease could potentially hydrolyze the P-N bond of an amino acid

Figure 6

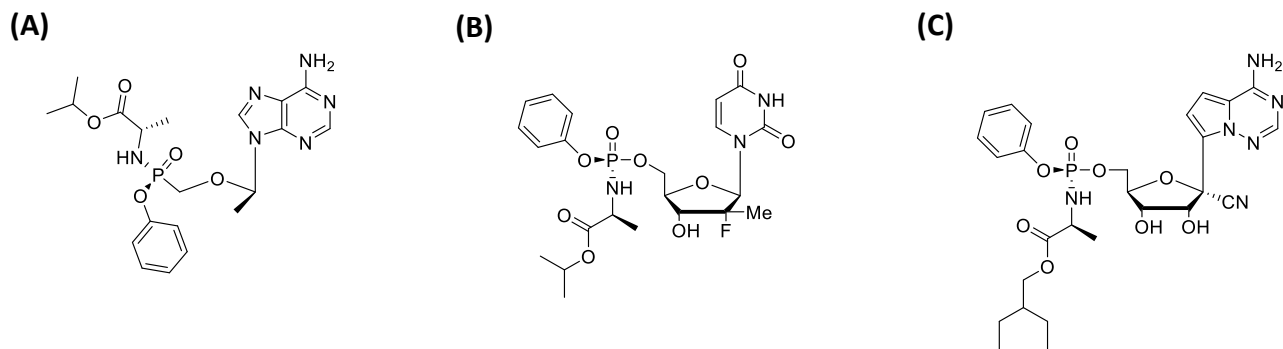
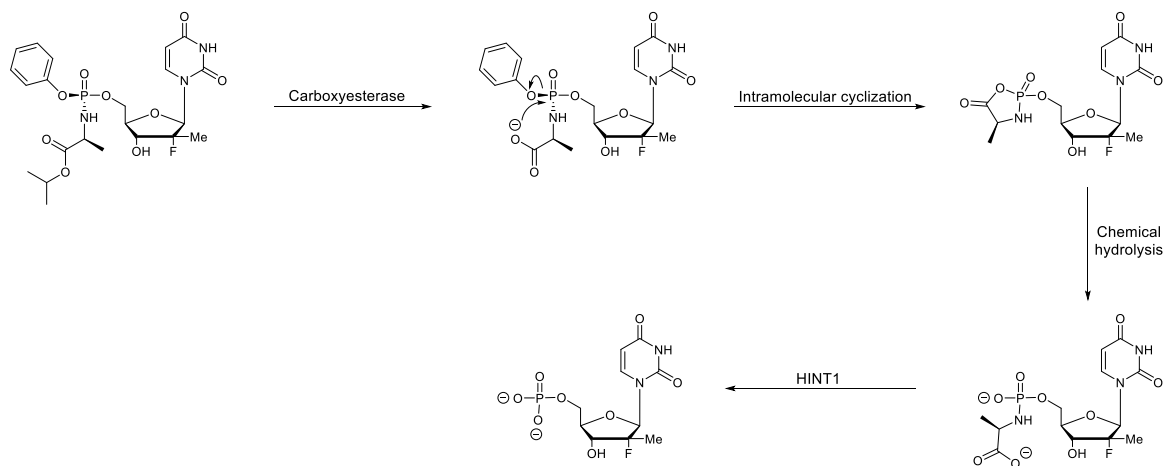


Figure 6. Clinically approved ProTides. (A) Tenofovir alafenamide (Vemlidy®) (B) Sofosbuvir (Sovaldi®) (C) Remdesivir (Veklury®).

linked to the phosphate group.<sup>50, 51</sup> The observation that zidovudine phosphoramidates had antiviral activity, while alkyloxy phosphotriesters did not, led to further exploration of the phosphoramidate masking group strategy. It was realized quickly thereafter that variation of the side chain of the amino acid impacted *in vitro* activity. Bulkier side chains, such as leucine and isoleucine diminished activity while alanine, glycine, and valine had similar activity.<sup>52</sup>

Subsequent investigations into carboxyester amino acid phosphoramidate monoesters helped elucidate the nucleotide phosphoramidase activity of HINT1 in the activation of nucleotide phosphoramidate prodrugs. Early on it was unclear whether a phosphoramidase was involved in activation to the monophosphate, or if the 5' O-P bond was first hydrolyzed by phosphorylases, and the resulting nucleoside re-phosphorylated by cellular kinases. Preliminary studies with thymidine kinase deficient permeabilized cells, as well as cell extracts, demonstrated the potential for enzymatic nucleoside phosphoramidate P-N hydrolysis by conversion of carboxymethyl ester amino acid phosphoramidate monoesters of fluorodeoxyuridine (FUdR) to the FUdR-monophosphate.<sup>38</sup> Subsequently, it was observed that treatment of CEM cells with a radiolabeled carboxymethyl ester amino acid phosphoramidate monoester of 3'-azido-3'-deoxythymidine (AZT) resulted in the production of AZT-monophosphate prior to the formation of AZT nucleoside.<sup>8</sup> In addition, when cells were treated with AZT carboxymethyl tryptophan phosphoramidate, the intracellular conversion of 3'-fluoro thymidine (FLT) carboxymethyl tryptophan phosphoramidate to FLT-monophosphate was found to be greatly reduced, consistent with P-N bond cleavage being carried out by an enzymatic mechanism.<sup>8</sup> Later, HPLC-MS based assays revealed that AZT monophosphate formed in CEM cells incubated with AZT carboxymethyl tryptophan phosphoramidate monoester, but not in cells incubated with AZT

**Figure 7**



**Figure 7.** ProTide activation mechanism. Steps of ProTide Activation: **(A)** Ester hydrolysis by carboxyesterase 1 or other carboxyesterase-type enzyme **(B)** Intramolecular cyclization via nucleophilic displacement of phenol by carboxylate **(C)** non-enzymatic chemical hydrolysis by water **(D)** phosphoramidate hydrolysis via HINT1 or another phosphoramidase-type enzyme.

alone, and that this could be blocked by pre-treating with carbamate analogues of AZT monophosphate.<sup>53</sup> Follow up experiments monitoring the decomposition of <sup>18</sup>O-labeled AZT phosphoramidate diesters demonstrated direct P-N bond cleavage in CEM cells and PBMCs.<sup>54</sup> Following reports that yeast and rabbit HINT1 were capable of hydrolyzing adenosine monophosphate phosphoramidates, a quantitative <sup>31</sup>P-based assay was developed to determine the total cell phosphoramidase activity in *E. coli*.<sup>14, 15</sup> Knocking out *E. coli* hinT completely blocked the conversion of adenosine 5'-monophosphoramidate to adenosine monophosphate indicating that *E. coli* hinT was responsible for all phosphoramidase activity in *E. coli*.<sup>15</sup> Wagner and colleagues sought to connect the phosphoramidase activity of human HINT1 to the previously reported phosphoramidase activity associated with nucleotide phosphoramidate prodrug activation in human cell lines. Consequently, a combination of T7 phage display, affinity chromatography, and a fluorogenic assay were employed to identify human HINT1 as the enzyme likely responsible for converting AZT tryptophan methyl ester phosphoramidate to AZT monophosphate.<sup>55</sup> Shortly thereafter, HINT1 would be identified as the phosphoramidase responsible for the final activation step of the phosphoramidate proTide, sofosbuvir.<sup>8, 56</sup> Treatment of cells in which HINT1 was knocked down by siRNA treatment with sofosbuvir resulted in reduced intracellular amounts of the corresponding nucleoside monophosphate.<sup>56</sup> Similarly for RDV, the formation of RDV-monophosphate from its parent phosphoramidate monoester was decreased by 50% in the presence of known HINT1 inhibitors indicating that HINT1 is a critical activator of RDV as well.<sup>57</sup>

ProTides are activated over three steps following cellular entry including two enzymatic activation steps (**Figure 7**). In the first step of ProTide activation, a carboxyesterase, usually

cathepsin A or carboxyesterase 1 (CES1), cleaves the ester group to reveal the carboxylic acid on the amino acid.<sup>56, 58</sup> Next, an intramolecular cyclization step displaces the aryloxy leaving group generating a cyclic acyl phosphoramidate intermediate that is subsequently hydrolyzed.<sup>59</sup> In the final step of ProTide activation, HINT1 hydrolyzes the P-N bond to give the nucleotide monophosphate which is then sequentially phosphorylated to give the active triphosphate species. It should be noted that amino acid phosphoramidate diesters are known to be capable of crossing the cellular membrane and being acted on by phosphoramidases directly. Derivatives of AZT, 5-fluorouracil deoxyribose (FUdR), and of guanosine-derived eIF4E inhibitors have demonstrated biological activity in vitro.<sup>38, 60, 61</sup>

## **HINT1 in Biological Pathways**

### **Central Nervous System**

HINT1 was first identified in neurons as a mu opioid receptor (MOR) interacting protein via a yeast two-hybrid study. Genetic knockout of HINT1 resulted in mice with an increased analgesic response and reduced tolerance towards opioids.<sup>62</sup> HINT1 was also shown to interact with the regulator of G-protein signaling RGSZ1 and RGSZ2 at its N-terminus. These interactions were shown to be crucial in regulating the MOR signaling pathway following opioid agonism.<sup>6,63</sup> The equilibrium of HINT1/RGSZ2 binding following MOR activation is believed to be crucial to recruiting PKC $\gamma$  to the MOR, where PKC $\gamma$  activation is vital to the downregulation of MOR signaling.<sup>64</sup> This early evidence led to the identification of HINT1 as a key regulator of the crosstalk

between the MOR and N-methyl-d-aspartate receptor (NMDAR).<sup>65</sup> Further investigation revealed that HINT1 interacts with PKC $\gamma$  in a redox-dependent manner to regulate the phosphorylation of MOR via crosstalk with NMDAR (**Figure 8**).<sup>64</sup> Garzon and co-workers have also demonstrated that HINT1 may play a similar role in mediating the activity of cannabinoid receptors as well as interact with transient receptor potential channels.<sup>66,67,68,69</sup>

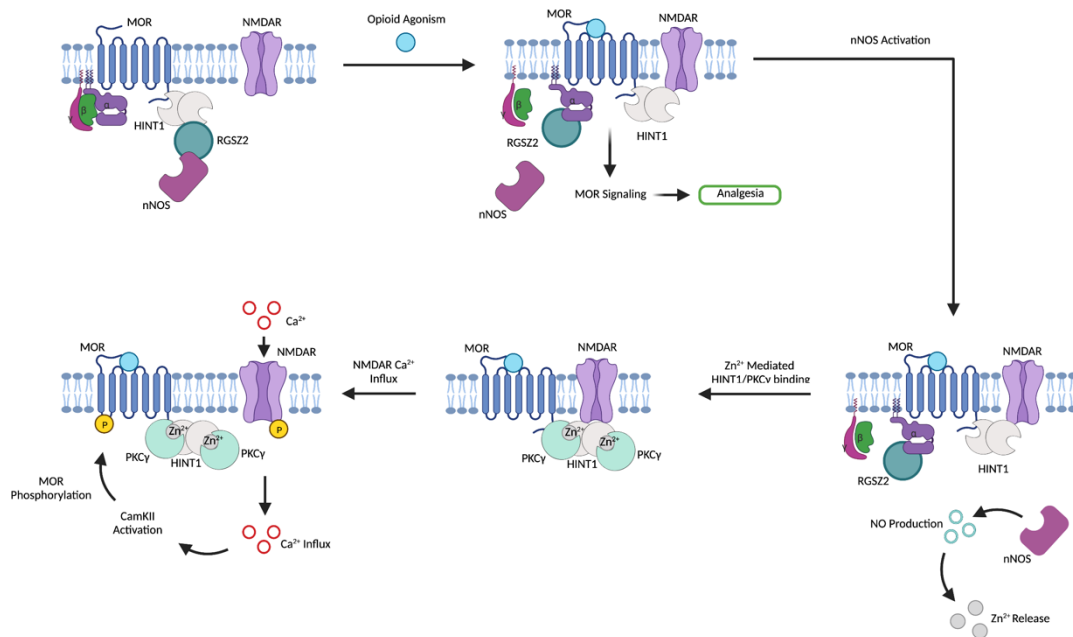
Analysis of HINT1 expression via immunostaining revealed that it has widespread expression in the mouse central nervous system, with relatively high levels in the olfactory system, cerebral cortex, and the hippocampus.<sup>70</sup> Later, researchers also observed enriched levels of HINT1 expression in the sciatic nerve, providing evidence for a potential role for HINT1 in the peripheral nervous system.<sup>71</sup> At the cellular level, HINT1 is primarily located in neurons and neuronal processes, with no immunoreactivity in astrocytes. In mice, HINT1 expression can be detected as early as 14 days following conception, indicating that HINT1 could play an important role in mouse brain development.<sup>70</sup> Genetic knockout of HINT1 resulted in increased anxiety and depression-related behaviors, identifying an important role for HINT1 in regulating the emotional behavior of mice.<sup>72,73</sup> However, there is evidence that this effect is age-dependent, as HINT1 deficiency in aged mice was tied to decreases in anxiety-like and depression-like behaviors.<sup>74</sup> In this study, Zhou and co-workers also identified age-dependent changes to HINT1 expression in the prefrontal cortex and hippocampus in mice, giving a potential mechanism behind these differences. Though how this change in expression contributes to these behaviors is not understood and requires further investigation.

Genetic mutations to HINT1 have been identified in connection to several neuropsychiatric disease states. Multiple single point mutations to HINT1 were potentially correlated with schizophrenia in a study conducted in Ireland.<sup>75</sup> Additionally, reduced expression of HINT1 was found in the dorsolateral prefrontal cortex and prefrontal cortex in patients with schizophrenia.<sup>76</sup> This connection is potentially due to the presence of HINT1 at the gene locus 5q31.2, which is highly associated with the disease.<sup>77</sup> HINT1<sup>-/-</sup> mice also displayed multiple schizophrenic-like phenotypes. Specifically, HINT1<sup>-/-</sup> mice displayed acute sensitivity in amphetamine-induced hyperlocomotor behavior assays compared to wild-type mice. This behavior is connected to dopaminergic signaling dysregulation which is often seen in schizophrenia.<sup>78</sup> Due to the high comorbidity of schizophrenia and nicotine dependence, the involvement of HINT1 was also investigated in this context.<sup>79</sup> Studies showed that several *HINT1* single nucleotide polymorphisms associated with schizophrenia also showed genetic association with nicotine dependence.<sup>80</sup> Further, it was observed that HINT1 expression was increased in mice following development of nicotine dependence.<sup>80</sup> Later studies found that HINT1<sup>-/-</sup> mice did not develop nicotine chronic place preference and had attenuated physical symptoms of nicotine withdrawal.<sup>81,82</sup> Interestingly, the effect of nicotine on HINT1<sup>-/-</sup> mice was found to be sex dependent, as nicotine did not alter anxiety-like behavior in female HINT1<sup>-/-</sup> mice.<sup>81</sup>

Significant evidence has gathered for the presence of HINT1 mutations in several forms of inherited peripheral neuropathies (IPNs). In these diseases, communication between the central nervous system and the body is disrupted, resulting in neurodegenerative and neuromuscular disorders. Nineteen variants of *HINT1* have been identified in patients with IPNs in North



**Figure 8**



**Proposed schematic pathway showing the role of HINT1 in downregulation of MOR signaling via NMDAR.** In the resting state, HINT1 is associated with the C-terminus of the MOR and the regulator of G-protein signaling, RGSZ2.<sup>6, 62</sup> Following activation of MOR by opioid therapy, G-protein signaling triggers activation of the nNOS pathway and subsequent generation of nitric oxide (NO) leading to the release of free zinc ions.<sup>64</sup> Additionally, RGSZ2 binds to the  $G\alpha$  subunit, freeing HINT1 to bind to C-terminus of the NR1 subunit of NMDAR. PKC $\gamma$  is then recruited to the cell membrane to bind HINT1 in a zinc dependent manner. RGSZ2 activation of PLC $\beta$  results in the release of DAG and subsequent activation of PKC $\gamma$ , which can then activate NMDAR via phosphorylation of the NR1 subunit.<sup>108</sup> The resulting calcium influx following NMDAR activation positively regulates the CaMKII signaling pathway, leading to phosphorylation of the mu opioid receptor and the development of opioid tolerance.

America, Europe, and Asia.<sup>83,84,85,86,87</sup> Focusing on a specific IPN, autosomal recessive axonal neuropathy with neuromyotonia (ARAN-NM), Zimòn and co-workers identified a series of *HINT1* mutations in patients using next-generation sequencing and subsequent cohort screening.<sup>71</sup> Eight *HINT1* mutations were identified, all of which contributed to mutations located near the dimer interface or the catalytic active site. Structural examination of six of these mutants was subsequently performed by Wagner *et al.*<sup>88</sup> Three of the mutations (R37P, G93D and W123\*) resulted in disruption of the dimer interface and significantly reduced catalytic activity. The H112N mutant is structurally similar to WT *HINT1* but is catalytically inactive due to the loss of the key catalytic His112. Two of the mutations (C84R and G89V), found on the *HINT1* surface, were similar in structure and activity to WT *HINT1*.<sup>88</sup> These mutations were found in a significantly higher percent of patients with NM, than without, establishing a connection between *HINT1* mutations resulting in monomeric *HINT1*, altered catalytic activity, or modifications of select surface residues and a specific phenotype of ARAN-NM. Interestingly, *HINT1* KO mice do not display a phenotype similar to that of IPNs, demonstrating that *HINT1* KO mice are not useful for replicating a peripheral neuropathy disease state.<sup>89</sup> Research identifying *HINT1* variants in patients with IPNs continues to be a growing field and is clinically necessary for distinguishing the many types of IPNs. However, more studies are needed to uncover the mechanism by which *HINT1* mutations shape the development of these diseases. In particular, the development of an animal model would be very useful. Studies determining whether mice incorporating the IPN mutations would reproduce the disease in mice should be carried out to assess this possibility.

Due to HINT1's observed involvement in multiple neurological processes, researchers have investigated its potential as a therapeutic target. The rational design of HINT1 inhibitors has taken advantage of the extensive analyses of HINT1 substrate specificity.<sup>90, 18</sup> Replacement of the phosphoramidate or acyl phosphate moieties of favored substrates with non-hydrolysable bioisosteres, such as carbamates and acyl-sulfamates (**E1** and **E2**), has resulted in low micromolar/high nanomolar competitive and non-competitive inhibitors.<sup>90,12,13</sup> Enzymatic inhibition of HINT1 using these inhibitors has been shown to decrease the development of acute morphine tolerance and enhanced opioid antinociception.<sup>91</sup> Interestingly, treatment of mice using the chronic constriction injury model with a HINT1 inhibitor decreased allodynia related to neuropathic pain following intracerebroventricular dosage.<sup>91</sup> Intrathecal administration of HINT1 inhibitors was also effective in reducing the development of acute endomorphin-2 tolerance and inhibited morphine's ability to block NMDA evoked behavior following NMDAR agonism in mice.<sup>13</sup> Taken together, the prevalence of HINT1 mutations in neuropsychiatric disorders and the efficacy of small molecule inhibition of HINT1 in mice demonstrates the need for further investigation into the role of HINT1 in these neurological processes and its potential as a therapeutic target.

### **Tumor Suppression and Tumorigenesis**

The first evidence of HINT1's role as a haploinsufficient tumor suppressor came from a genetic knockout of HINT1 in embryonic mouse cells. The researchers observed that deletion of the

*HINT1* gene resulted in an increased growth rate and spontaneous immortalization.<sup>92</sup> Additionally, treatment of *HINT1*<sup>-/-</sup> mice with the chemical carcinogen N-nitrosomethylbenzylamine resulted in increased gastric tumor development compared to their wild-type counterparts.<sup>92</sup> Further work established that the genetic knockout of *HINT1* enhances spontaneous mammary and ovarian tumor development and susceptibility to tumor growth following treatment with dimethylbenz(a)anthracene (DMBA).<sup>93</sup> Down-regulation of *HINT1* expression has been observed in hepatocellular carcinomas, human colon cancer cells, and human non-small lung cancer cell line, NCI-H522.<sup>94, 95,96</sup> Further, evaluation of commonly used immortalized cancer cell lines revealed relatively lower expression of *HINT1* in MCF7 and HeLA cells.<sup>97</sup>

*HINT1*'s role as a tumor suppressor is likely tied to its interactions with numerous transcription factors and apoptotic pathways. It was first uncovered that *HINT1* interacts with Pontin and Reptin, inhibiting  $\beta$ -catenin/T-cell factor-mediated transcription of Wnt genes, which are closely connected with carcinogenesis.<sup>98,99</sup> Transient transfection of *HINT1* in MCF-7 and SW480 cells resulted in increased apoptosis through upregulation of the pro-apoptotic p53 and Bax pathway and down-regulation of anti-apoptotic Bcl-2. Interestingly, cells expressing an enzymatically deficient mutant of *HINT1* (H112N) displayed similar pro-apoptotic behavior, indicating that the pro-apoptotic effect of *HINT1* transient expression is independent of its enzymatic activity.<sup>98</sup> This pro-apoptotic activity of *HINT1* was further observed in osteosarcoma cells.<sup>100</sup> Zhou and co-workers observed that *HINT1* is downregulated in osteosarcoma tissues. Transient expression of *HINT1* in osteosarcoma cells resulted in increased apoptosis via inhibition of FOXO1 expression,

which is known to regulate pro-apoptotic genes FasL and Bim.<sup>100</sup> Additionally, FOXO1 is known to interact with cyclinD1, which has a potential relationship with carcinogenesis due to its involvement in cell proliferation. These results are consistent with previous observations that HINT1 upregulation suppresses liver cell proliferation via inhibition of cyclinD1.<sup>101</sup> However, direct interaction of HINT1 and FOXO1 was not observed, suggesting further investigation is needed to delineate this mechanism.

### **Mast Cell Activation**

Mast cells play a crucial role in recognition of the pathogens and mediation of the immune response to parasites, as well as hypersensitivity reactions due to the release of histamine and other immune cell mediators.<sup>102</sup> Activation of mast cells is dependent on the microphthalmia-associated transcription factor (MITF), which regulates the expression of proteases, cytokine receptors, and cell adhesion molecules.<sup>103, 104, 105</sup> HINT1 was first identified to interact with MITF in a yeast two hybrid screening study, which demonstrated that binding of HINT1 to MITF downregulated the transcriptional activity of MITF by 94% *in vitro*, identifying a potential role for HINT1 in mast cell activation.<sup>35</sup> Vital to the interaction between HINT1 and MITF is the secondary messenger Ap<sub>4</sub>A.<sup>32</sup> There is evidence that upon activation of mast cells, LysRS produced Ap<sub>4</sub>A binds to HINT1, freeing MITF from this complex allowing for transcription of MITF related genes.<sup>106,32</sup> However, recent studies call into question the affinity of HINT1 to bind Ap<sub>4</sub>A *in vitro*.<sup>107</sup> The evidence as a whole suggests a role for HINT1 in the activation of mast cells, but the precise mechanism needs further evaluation.

## **Summary and Future Directions**

There is a growing interest in HINT1 due to its participation in a myriad of pharmacological and biological processes. Pharmacologically, HINT1's phosphoramidase activity is crucial for the metabolism of clinically used nucleoside phosphoramidase prodrugs. This phosphoramidase activity has been investigated thoroughly, resulting in a defined kinetic mechanism for HINT1 hydrolysis and establishment of the necessary structural parameters for HINT1 substrates. However, the connection between this enzymatic activity and HINT1's many biological roles remains to be established. The involvement of HINT1 in such a variety of processes, including the regulation of G-protein signaling in neurons, tumor suppression, and in mast cell activation make it an extremely interesting target for future investigations. Additionally, the association of HINT1 mutations or altered expression levels with the development of neuropsychiatric disease make it potentially therapeutically relevant. However, the exact mechanisms of HINT1's involvement in these processes are not completely understood. Further investigations into the specific mechanisms by which HINT1 contributes to these functions, particularly establishment of the role of its highly conserved enzymatic activity, will be crucial to defining the many cellular roles of HINT1.

## **Acknowledgements**

Financial support is gratefully acknowledged from NIAID (AI146049) and the University of Minnesota Foundation. Thank you to Jacob Smith for his contributions to the HINT1 Prodrug Activation section. TOC and Figure 9 created using BioRender.com.

## References

- (1) Krakowiak, A.; Fryc, I. [Histidine triad protein superfamily--biological function and enzymatic activity]. *Postepy Biochem* **2012**, *58* (3), 302-313.
- (2) Séraphin, B. The HIT protein family: a new family of proteins present in prokaryotes, yeast and mammals. *DNA Seq* **1992**, *3* (3), 177-179. DOI: 10.3109/10425179209034013.
- (3) Brenner, C. Hint, Fhit, and GalT: function, structure, evolution, and mechanism of three branches of the histidine triad superfamily of nucleotide hydrolases and transferases. *Biochemistry* **2002**, *41* (29), 9003-9014. DOI: 10.1021/bi025942q.
- (4) Rajasekaran, R.; Felser, A.; Nuoffer, J. M.; Dufour, J. F.; St-Pierre, M. V. The histidine triad nucleotide-binding protein 2 (HINT-2) positively regulates hepatocellular energy metabolism. *FASEB J* **2018**, *32* (9), 5143-5161. DOI: 10.1096/fj.201701429R.
- (5) Chou, T. F.; Cheng, J.; Tikh, I. B.; Wagner, C. R. Evidence that human histidine triad nucleotide binding protein 3 (Hint3) is a distinct branch of the histidine triad (HIT) superfamily. *J Mol Biol* **2007**, *373* (4), 978-989. DOI: 10.1016/j.jmb.2007.08.023.
- (6) Ajit, S. K.; Ramineni, S.; Edris, W.; Hunt, R. A.; Hum, W. T.; Hepler, J. R.; Young, K. H. RGSZ1 interacts with protein kinase C interacting protein PKCI-1 and modulates mu opioid receptor signaling. *Cell Signal* **2007**, *19* (4), 723-730. DOI: 10.1016/j.cellsig.2006.09.008.
- (7) Genovese, G.; Ghosh, P.; Li, H.; Rettino, A.; Sioletic, S.; Cittadini, A.; Sgambato, A. The tumor suppressor HINT1 regulates MITF and  $\beta$ -catenin transcriptional activity in melanoma cells. *Cell Cycle* **2012**, *11* (11), 2206-2215. DOI: 10.4161/cc.20765.



- (8) McIntee, E. J.; Rimmel, R. P.; Schinazi, R. F.; Abraham, T. W.; Wagner, C. R. Probing the mechanism of action and decomposition of amino acid phosphomonoester amidates of antiviral nucleoside prodrugs. *J Med Chem* **1997**, *40* (21), 3323-3331. DOI: 10.1021/jm960694f.
- (9) Brenner, C.; Garrison, P.; Gilmour, J.; Peisach, D.; Ringe, D.; Petsko, G. A.; Lowenstein, J. M. Crystal structures of HINT demonstrate that histidine triad proteins are GalT-related nucleotide-binding proteins. *Nat Struct Biol* **1997**, *4* (3), 231-238. DOI: 10.1038/nsb0397-231.
- (10) Chou, T. F.; Wagner, C. R. Lysyl-tRNA synthetase-generated lysyl-adenylate is a substrate for histidine triad nucleotide binding proteins. *J Biol Chem* **2007**, *282* (7), 4719-4727. DOI: 10.1074/jbc.M610530200.
- (11) Dolot, R.; Ozga, M.; Włodarczyk, A.; Krakowiak, A.; Nawrot, B. A new crystal form of human histidine triad nucleotide-binding protein 1 (hHINT1) in complex with adenosine 5'-monophosphate at 1.38 Å resolution. *Acta Crystallogr Sect F Struct Biol Cryst Commun* **2012**, *68* (Pt 8), 883-888. DOI: 10.1107/S1744309112029491.
- (12) Shah, R.; Strom, A.; Zhou, A.; Maize, K. M.; Finzel, B. C.; Wagner, C. R. Design, Synthesis, and Characterization of Sulfamide and Sulfamate Nucleotidomimetic Inhibitors of hHint1. *ACS Med Chem Lett* **2016**, *7* (8), 780-784. DOI: 10.1021/acsmchemlett.6b00169.
- (13) Shah, R. M.; Peterson, C.; Strom, A.; Dillenburg, M.; Finzel, B.; Kitto, K. F.; Fairbanks, C.; Wilcox, G.; Wagner, C. R. Inhibition of HINT1 Modulates Spinal Nociception and NMDA Evoked Behavior in Mice. *ACS Chem Neurosci* **2019**, *10* (10), 4385-4393. DOI: 10.1021/acchemneuro.9b00432.

- (14) Bieganowski, P.; Garrison, P. N.; Hodawadekar, S. C.; Faye, G.; Barnes, L. D.; Brenner, C. Adenosine monophosphoramidase activity of Hint and Hnt1 supports function of Kin28, Ccl1, and Tfb3. *J Biol Chem* **2002**, *277* (13), 10852-10860. DOI: 10.1074/jbc.M111480200.
- (15) Chou, T. F.; Bieganowski, P.; Shilinski, K.; Cheng, J.; Brenner, C.; Wagner, C. R. <sup>31</sup>P NMR and genetic analysis establish hintT as the only Escherichia coli purine nucleoside phosphoramidase and as essential for growth under high salt conditions. *J Biol Chem* **2005**, *280* (15), 15356-15361. DOI: 10.1074/jbc.M500434200.
- (16) Lima, C. D.; Klein, M. G.; Hendrickson, W. A. Structure-based analysis of catalysis and substrate definition in the HIT protein family. *Science* **1997**, *278* (5336), 286-290. DOI: 10.1126/science.278.5336.286.
- (17) Chou, T. F.; Baraniak, J.; Kaczmarek, R.; Zhou, X.; Cheng, J.; Ghosh, B.; Wagner, C. R. Phosphoramidate pronucleotides: a comparison of the phosphoramidase substrate specificity of human and Escherichia coli histidine triad nucleotide binding proteins. *Mol Pharm* **2007**, *4* (2), 208-217. DOI: 10.1021/mp060070y.
- (18) Maize, K. M.; Shah, R.; Strom, A.; Kumarapperuma, S.; Zhou, A.; Wagner, C. R.; Finzel, B. C. A Crystal Structure Based Guide to the Design of Human Histidine Triad Nucleotide Binding Protein 1 (hHint1) Activated ProTides. *Mol Pharm* **2017**, *14* (11), 3987-3997. DOI: 10.1021/acs.molpharmaceut.7b00664.
- (19) Ozga, M.; Dolot, R.; Janicka, M.; Kaczmarek, R.; Krakowiak, A. Histidine triad nucleotide-binding protein 1 (HINT-1) phosphoramidase transforms nucleoside 5'-O-phosphorothioates to nucleoside 5'-O-phosphates. *J Biol Chem* **2010**, *285* (52), 40809-40818. DOI: 10.1074/jbc.M110.162065.

- (20) Dias, N.; Stein, C. A. Antisense oligonucleotides: basic concepts and mechanisms. *Mol Cancer Ther* **2002**, *1* (5), 347-355.
- (21) Krakowiak, A.; Piotrkowska, D.; Kocoń-Rębowska, B.; Kaczmarek, R.; Maciaszek, A. The role of the Hint1 protein in the metabolism of phosphorothioate oligonucleotides drugs and prodrugs, and the release of H. *Biochem Pharmacol* **2019**, *163*, 250-259. DOI: 10.1016/j.bcp.2019.02.018.
- (22) Krakowiak, A.; Pawłowska, R.; Kocoń-Rębowska, B.; Dolot, R.; Stec, W. J. Interactions of cellular histidine triad nucleotide binding protein 1 with nucleosides 5'-O-monophosphorothioate and their derivatives - Implication for desulfuration process in the cell. *Biochim Biophys Acta* **2014**, *1840* (12), 3357-3366. DOI: 10.1016/j.bbagen.2014.08.016.
- (23) Łowicka, E.; Bełtowski, J. Hydrogen sulfide (H<sub>2</sub>S) - the third gas of interest for pharmacologists. *Pharmacol Rep* **2007**, *59* (1), 4-24.
- (24) Wang, R. Toxic gas, lifesaver. *Sci Am* **2010**, *302* (3), 66-71. DOI: 10.1038/scientificamerican0310-66.
- (25) Chou, T. F.; Tikh, I. B.; Horta, B. A.; Ghosh, B.; De Alencastro, R. B.; Wagner, C. R. Engineered monomeric human histidine triad nucleotide-binding protein 1 hydrolyzes fluorogenic acyl-adenylate and lysyl-tRNA synthetase-generated lysyl-adenylate. *J Biol Chem* **2007**, *282* (20), 15137-15147. DOI: 10.1074/jbc.M606972200.
- (26) Chou, T. F.; Sham, Y. Y.; Wagner, C. R. Impact of the C-terminal loop of histidine triad nucleotide binding protein1 (Hint1) on substrate specificity. *Biochemistry* **2007**, *46* (45), 13074-13079. DOI: 10.1021/bi701244h.

- (27) Huang, K.; Arabshahi, A.; Wei, Y.; Frey, P. A. The mechanism of action of the fragile histidine triad, Fhit: isolation of a covalent adenylyl enzyme and chemical rescue of H96G-Fhit. *Biochemistry* **2004**, *43* (23), 7637-7642. DOI: 10.1021/bi049762n.
- (28) Zhou, X.; Chou, T. F.; Aubol, B. E.; Park, C. J.; Wolfenden, R.; Adams, J.; Wagner, C. R. Kinetic mechanism of human histidine triad nucleotide binding protein 1. *Biochemistry* **2013**, *52* (20), 3588-3600. DOI: 10.1021/bi301616c.
- (29) Shah, R.; Maize, K. M.; Zhou, X.; Finzel, B. C.; Wagner, C. R. Caught before Released: Structural Mapping of the Reaction Trajectory for the Sofosbuvir Activating Enzyme, Human Histidine Triad Nucleotide Binding Protein 1 (hHint1). *Biochemistry* **2017**, *56* (28), 3559-3570. DOI: 10.1021/acs.biochem.7b00148.
- (30) Strom, A.; Shah, R.; Dolot, R.; Rogers, M. S.; Tong, C. L.; Wang, D.; Xia, Y.; Lipscomb, J. D.; Wagner, C. R. Dynamic Long-Range Interactions Influence Substrate Binding and Catalysis by Human Histidine Triad Nucleotide-Binding Proteins (HINTs), Key Regulators of Multiple Cellular Processes and Activators of Antiviral ProTides. *Biochemistry* **2022**, *61* (23), 2648-2661. DOI: 10.1021/acs.biochem.2c00506.
- (31) Lee, Y. N.; Razin, E. Nonconventional involvement of LysRS in the molecular mechanism of USF2 transcriptional activity in FcepsilonRI-activated mast cells. *Mol Cell Biol* **2005**, *25* (20), 8904-8912. DOI: 10.1128/MCB.25.20.8904-8912.2005.
- (32) Lee, Y. N.; Nechushtan, H.; Figov, N.; Razin, E. The function of lysyl-tRNA synthetase and Ap4A as signaling regulators of MITF activity in FcepsilonRI-activated mast cells. *Immunity* **2004**, *20* (2), 145-151. DOI: 10.1016/s1074-7613(04)00020-2.

- (33) Wang, J.; Fang, P.; Schimmel, P.; Guo, M. Side chain independent recognition of aminoacyl adenylates by the Hint1 transcription suppressor. *J Phys Chem B* **2012**, *116* (23), 6798-6805. DOI: 10.1021/jp212457w.
- (34) Wang, L.; Li, H.; Zhang, Y.; Santella, R. M.; Weinstein, I. B. HINT1 inhibits beta-catenin/TCF4, USF2 and NFkappaB activity in human hepatoma cells. *Int J Cancer* **2009**, *124* (7), 1526-1534. DOI: 10.1002/ijc.24072.
- (35) Razin, E.; Zhang, Z. C.; Nechushtan, H.; Frenkel, S.; Lee, Y. N.; Arudchandran, R.; Rivera, J. Suppression of microphthalmia transcriptional activity by its association with protein kinase C-interacting protein 1 in mast cells. *J Biol Chem* **1999**, *274* (48), 34272-34276. DOI: 10.1074/jbc.274.48.34272.
- (36) Cortés-Montero, E.; Rodríguez-Muñoz, M.; Sánchez-Blázquez, P.; Garzón, J. The Axonal Motor Neuropathy-Related HINT1 Protein Is a Zinc- and Calmodulin-Regulated Cysteine SUMO Protease. *Antioxid Redox Signal* **2019**, *31* (7), 503-520. DOI: 10.1089/ars.2019.7724.
- (37) Shelton, J.; Lu, X.; Hollenbaugh, J. A.; Cho, J. H.; Amblard, F.; Schinazi, R. F. Metabolism, Biochemical Actions, and Chemical Synthesis of Anticancer Nucleosides, Nucleotides, and Base Analogs. *Chem Rev* **2016**, *116* (23), 14379-14455. DOI: 10.1021/acs.chemrev.6b00209.
- (38) Abraham, T. W.; Kalman, T. I.; McIntee, E. J.; Wagner, C. R. Synthesis and biological activity of aromatic amino acid phosphoramidates of 5-fluoro-2'-deoxyuridine and 1-beta-arabinofuranosylcytosine: evidence of phosphoramidase activity. *J Med Chem* **1996**, *39* (23), 4569-4575. DOI: 10.1021/jm9603680.
- (39) De Clercq, E.; Li, G. Approved Antiviral Drugs over the Past 50 Years. *Clin Microbiol Rev* **2016**, *29* (3), 695-747. DOI: 10.1128/CMR.00102-15.

- (40) Al-Madhoun, A. S.; Tjarks, W.; Eriksson, S. The role of thymidine kinases in the activation of pyrimidine nucleoside analogues. *Mini Rev Med Chem* **2004**, *4* (4), 341-350. DOI: 10.2174/1389557043403963.
- (41) Johansson, K.; Ramaswamy, S.; Ljungcrantz, C.; Knecht, W.; Piskur, J.; Munch-Petersen, B.; Eriksson, S.; Eklund, H. Structural basis for substrate specificities of cellular deoxyribonucleoside kinases. *Nat Struct Biol* **2001**, *8* (7), 616-620. DOI: 10.1038/89661.
- (42) Van Rompay, A. R.; Johansson, M.; Karlsson, A. Phosphorylation of nucleosides and nucleoside analogs by mammalian nucleoside monophosphate kinases. *Pharmacol Ther* **2000**, *87* (2-3), 189-198. DOI: 10.1016/s0163-7258(00)00048-6.
- (43) Jordheim, L. P.; Dumontet, C. Review of recent studies on resistance to cytotoxic deoxynucleoside analogues. *Biochim Biophys Acta* **2007**, *1776* (2), 138-159. DOI: 10.1016/j.bbcan.2007.07.004.
- (44) Halpern, L. The Transfer of Inorganic Phosphorus Across the Red Blood Cell Membrane. *J. Biol. Chem.* **1936**, (114(3)), 747-770.
- (45) Pradere, U.; Garnier-Amblard, E. C.; Coats, S. J.; Amblard, F.; Schinazi, R. F. Synthesis of nucleoside phosphate and phosphonate prodrugs. *Chem Rev* **2014**, *114* (18), 9154-9218. DOI: 10.1021/cr5002035.
- (46) Wagner, C. R.; Iyer, V. V.; McIntee, E. J. Pronucleotides: toward the in vivo delivery of antiviral and anticancer nucleotides. *Med Res Rev* **2000**, *20* (6), 417-451. DOI: 10.1002/1098-1128(200011)20:6<417::aid-med1>3.0.co;2-z.

- (47) Mackman, R. L. Phosphoramidate Prodrugs Continue to Deliver, The Journey of Remdesivir (GS-5734) from RSV to SARS-CoV-2. *ACS Med Chem Lett* **2022**, *13* (3), 338-347. DOI: 10.1021/acsmchemlett.1c00624.
- (48) Mehellou, Y.; Rattan, H. S.; Balzarini, J. The ProTide Prodrug Technology: From the Concept to the Clinic. *J Med Chem* **2018**, *61* (6), 2211-2226. DOI: 10.1021/acs.jmedchem.7b00734.
- (49) McGuigan, C.; Pathirana, R. N.; Mahmood, N.; Devine, K. G.; Hay, A. J. Aryl phosphate derivatives of AZT retain activity against HIV1 in cell lines which are resistant to the action of AZT. *Antiviral Res* **1992**, *17* (4), 311-321. DOI: 10.1016/0166-3542(92)90026-2.
- (50) Navia, M. A.; Fitzgerald, P. M.; McKeever, B. M.; Leu, C. T.; Heimbach, J. C.; Herber, W. K.; Sigal, I. S.; Darke, P. L.; Springer, J. P. Three-dimensional structure of aspartyl protease from human immunodeficiency virus HIV-1. *Nature* **1989**, *337* (6208), 615-620. DOI: 10.1038/337615a0.
- (51) Devine, K. G.; McGuigan, C.; O'Connor, T. J.; Nicholls, S. R.; Kinchington, D. Novel phosphate derivatives of zidovudine as anti-HIV compounds. *AIDS* **1990**, *4* (4), 371-373.
- (52) Curley, D.; McGuigan, C.; Devine, K. G.; O'Connor, T. J.; Jeffries, D. J.; Kinchington, D. Synthesis and anti-HIV evaluation of some phosphoramidate derivatives of AZT: studies on the effect of chain elongation on biological activity. *Antiviral Res* **1990**, *14* (6), 345-356. DOI: 10.1016/0166-3542(90)90053-a.
- (53) Chang, S.; Griesgraber, G. W.; Southern, P. J.; Wagner, C. R. Amino acid phosphoramidate monoesters of 3'-azido-3'-deoxythymidine: relationship between antiviral potency and intracellular metabolism. *J Med Chem* **2001**, *44* (2), 223-231. DOI: 10.1021/jm000260r.

- (54) Kim, J.; Chou, T. F.; Griesgraber, G. W.; Wagner, C. R. Direct measurement of nucleoside monophosphate delivery from a phosphoramidate pronucleotide by stable isotope labeling and LC-ESI(-)-MS/MS. *Mol Pharm* **2004**, *1* (2), 102-111. DOI: 10.1021/mp0340338.
- (55) Cheng, J.; Zhou, X.; Chou, T. F.; Ghosh, B.; Liu, B.; Wagner, C. R. Identification of the amino acid-AZT-phosphoramidase by affinity T7 phage display selection. *Bioorg Med Chem Lett* **2009**, *19* (22), 6379-6381. DOI: 10.1016/j.bmcl.2009.09.067.
- (56) Murakami, E.; Tolstykh, T.; Bao, H.; Niu, C.; Steuer, H. M.; Bao, D.; Chang, W.; Espiritu, C.; Bansal, S.; Lam, A. M.; et al. Mechanism of activation of PSI-7851 and its diastereoisomer PSI-7977. *J Biol Chem* **2010**, *285* (45), 34337-34347. DOI: 10.1074/jbc.M110.161802.
- (57) Li, R.; Licican, A.; Xu, Y.; Pitts, J.; Niu, C.; Zhang, J.; Kim, C.; Zhao, X.; Soohoo, D.; Babusis, D.; et al. Key Metabolic Enzymes Involved in Remdesivir Activation in Human Lung Cells. *Antimicrob Agents Chemother* **2021**, *65* (9), e0060221. DOI: 10.1128/AAC.00602-21.
- (58) Birkus, G.; Wang, R.; Liu, X.; Kutty, N.; MacArthur, H.; Cihlar, T.; Gibbs, C.; Swaminathan, S.; Lee, W.; McDermott, M. Cathepsin A is the major hydrolase catalyzing the intracellular hydrolysis of the antiretroviral nucleotide phosphonoamidate prodrugs GS-7340 and GS-9131. *Antimicrob Agents Chemother* **2007**, *51* (2), 543-550. DOI: 10.1128/AAC.00968-06.
- (59) Saboulard, D.; Naesens, L.; Cahard, D.; Salgado, A.; Pathirana, R.; Velazquez, S.; McGuigan, C.; De Clercq, E.; Balzarini, J. Characterization of the activation pathway of phosphoramidate triester prodrugs of stavudine and zidovudine. *Mol Pharmacol* **1999**, *56* (4), 693-704.
- (60) Wagner, C. R.; McIntee, E. J.; Schinazi, R. F.; Abraham, T. W. Aromatic amino acid phosphoramidate di- and triesters of 3'-azido-3'-deoxythymidine (AZT) are non-toxic inhibitors of HIV-1 replication. *Bioorganic & Medicinal Chemistry Letters* **1995**, *5* (16), 1819-1824.



(61) Li, S.; Jia, Y.; Jacobson, B.; McCauley, J.; Kratzke, R.; Bitterman, P. B.; Wagner, C. R. Treatment of breast and lung cancer cells with a N-7 benzyl guanosine monophosphate tryptamine phosphoramidate pronucleotide (4Ei-1) results in chemosensitization to gemcitabine and induced eIF4E proteasomal degradation. *Mol Pharm* **2013**, *10* (2), 523-531. DOI: 10.1021/mp300699d.

(62) Guang, W.; Wang, H.; Su, T.; Weinstein, I. B.; Wang, J. B. Role of mPKCl, a novel mu-opioid receptor interactive protein, in receptor desensitization, phosphorylation, and morphine-induced analgesia. *Mol Pharmacol* **2004**, *66* (5), 1285-1292. DOI: 10.1124/mol.66.5.

(63) Rodríguez-Muñoz, M.; Sánchez-Blázquez, P.; Vicente-Sánchez, A.; Bailón, C.; Martín-Aznar, B.; Garzón, J. The histidine triad nucleotide-binding protein 1 supports mu-opioid receptor-glutamate NMDA receptor cross-regulation. *Cell Mol Life Sci* **2011**, *68* (17), 2933-2949. DOI: 10.1007/s00018-010-0598-x.

(64) Rodríguez-Muñoz, M.; de la Torre-Madrid, E.; Sánchez-Blázquez, P.; Wang, J. B.; Garzón, J. NMDAR-nNOS generated zinc recruits PKC $\gamma$  to the HINT1-RGS17 complex bound to the C terminus of Mu-opioid receptors. *Cell Signal* **2008**, *20* (10), 1855-1864. DOI: 10.1016/j.cellsig.2008.06.015.

(65) Rodríguez-Muñoz, M.; Sánchez-Blázquez, P.; Vicente-Sánchez, A.; Berrocoso, E.; Garzón, J. The mu-opioid receptor and the NMDA receptor associate in PAG neurons: implications in pain control. *Neuropsychopharmacology* **2012**, *37* (2), 338-349. DOI: 10.1038/npp.2011.155.

(66) Sánchez-Blázquez, P.; Rodríguez-Muñoz, M.; Vicente-Sánchez, A.; Garzón, J. Cannabinoid receptors couple to NMDA receptors to reduce the production of NO and the mobilization of zinc

induced by glutamate. *Antioxid Redox Signal* **2013**, *19* (15), 1766-1782. DOI: 10.1089/ars.2012.5100.

(67) Rodríguez-Muñoz, M.; Cortés-Montero, E.; Pozo-Rodrigálvarez, A.; Sánchez-Blázquez, P.; Garzón-Niño, J. The ON:OFF switch,  $\sigma$ 1R-HINT1 protein, controls GPCR-NMDA receptor cross-regulation: implications in neurological disorders. *Oncotarget* **2015**, *6* (34), 35458-35477. DOI: 10.18632/oncotarget.6064.

(68) Rodríguez-Muñoz, M.; Sánchez-Blázquez, P.; Merlos, M.; Garzón-Niño, J. Endocannabinoid control of glutamate NMDA receptors: the therapeutic potential and consequences of dysfunction. *Oncotarget* **2016**, *7* (34), 55840-55862. DOI: 10.18632/oncotarget.10095.

(69) Cortés-Montero, E.; Sánchez-Blázquez, P.; Onetti, Y.; Merlos, M.; Garzón, J. Ligands Exert Biased Activity to Regulate Sigma 1 Receptor Interactions With Cationic TRPA1, TRPV1, and TRPM8 Channels. *Front Pharmacol* **2019**, *10*, 634. DOI: 10.3389/fphar.2019.00634.

(70) Liu, Q.; Puche, A. C.; Wang, J. B. Distribution and expression of protein kinase C interactive protein (PKCI/HINT1) in mouse central nervous system (CNS). *Neurochem Res* **2008**, *33* (7), 1263-1276. DOI: 10.1007/s11064-007-9578-4.

(71) Zimoń, M.; Baets, J.; Almeida-Souza, L.; De Vriendt, E.; Nikodinovic, J.; Parman, Y.; Battaloglu, E.; Matur, Z.; Guergueltcheva, V.; Tournev, I.; et al. Loss-of-function mutations in HINT1 cause axonal neuropathy with neuromyotonia. *Nat Genet* **2012**, *44* (10), 1080-1083. DOI: 10.1038/ng.2406.

(72) Varadarajulu, J.; Lebar, M.; Krishnamoorthy, G.; Habelt, S.; Lu, J.; Bernard Weinstein, I.; Li, H.; Holsboer, F.; Turck, C. W.; Touma, C. Increased anxiety-related behaviour in Hint1 knockout mice. *Behav Brain Res* **2011**, *220* (2), 305-311. DOI: 10.1016/j.bbr.2011.02.012.

- (73) Barbier, E.; Wang, J. B. Anti-depressant and anxiolytic like behaviors in PKC $\beta$ /HINT1 knockout mice associated with elevated plasma corticosterone level. *BMC Neurosci* **2009**, *10*, 132. DOI: 10.1186/1471-2202-10-132.
- (74) Zhou, Y.; Li, S. F.; Deng, L. S.; Ma, Y. K.; Lei, G.; Dang, Y. H. HINT1 deficiency in aged mice reduces anxiety-like and depression-like behaviours and enhances cognitive performances. *Exp Gerontol* **2022**, *159*, 111683. DOI: 10.1016/j.exger.2021.111683.
- (75) Chen, Q.; Wang, X.; O'Neill, F. A.; Walsh, D.; Kendler, K. S.; Chen, X. Is the histidine triad nucleotide-binding protein 1 (HINT1) gene a candidate for schizophrenia? *Schizophr Res* **2008**, *106* (2-3), 200-207. DOI: 10.1016/j.schres.2008.08.006.
- (76) Varadarajulu, J.; Schmitt, A.; Falkai, P.; Alsaif, M.; Turck, C. W.; Martins-de-Souza, D. Differential expression of HINT1 in schizophrenia brain tissue. *Eur Arch Psychiatry Clin Neurosci* **2012**, *262* (2), 167-172. DOI: 10.1007/s00406-011-0216-4.
- (77) Straub, R. E.; MacLean, C. J.; O'Neill, F. A.; Walsh, D.; Kendler, K. S. Support for a possible schizophrenia vulnerability locus in region 5q22-31 in Irish families. *Mol Psychiatry* **1997**, *2* (2), 148-155. DOI: 10.1038/sj.mp.4000258.
- (78) Barbier, E.; Zapata, A.; Oh, E.; Liu, Q.; Zhu, F.; Undie, A.; Shippenberg, T.; Wang, J. B. Supersensitivity to amphetamine in protein kinase-C interacting protein/HINT1 knockout mice. *Neuropsychopharmacology* **2007**, *32* (8), 1774-1782. DOI: 10.1038/sj.npp.1301301.
- (79) Ding, J. B.; Hu, K. Cigarette Smoking and Schizophrenia: Etiology, Clinical, Pharmacological, and Treatment Implications. *Schizophr Res Treatment* **2021**, *2021*, 7698030. DOI: 10.1155/2021/7698030.

- (80) Jackson, K. J.; Chen, Q.; Chen, J.; Aggen, S. H.; Kendler, K. S.; Chen, X. Association of the histidine-triad nucleotide-binding protein-1 (HINT1) gene variants with nicotine dependence. *Pharmacogenomics J* **2011**, *11* (4), 251-257. DOI: 10.1038/tpj.2010.41.
- (81) Jackson, K. J.; Wang, J. B.; Barbier, E.; Chen, X.; Damaj, M. I. Acute behavioral effects of nicotine in male and female HINT1 knockout mice. *Genes Brain Behav* **2012**, *11* (8), 993-1000. DOI: 10.1111/j.1601-183X.2012.00827.x.
- (82) Jackson, K. J.; Wang, J. B.; Barbier, E.; Damaj, M. I.; Chen, X. The histidine triad nucleotide binding 1 protein is involved in nicotine reward and physical nicotine withdrawal in mice. *Neurosci Lett* **2013**, *550*, 129-133. DOI: 10.1016/j.neulet.2013.06.027.
- (83) Veltsista, D.; Chroni, E. A first case report of HINT1-related axonal neuropathy with neuromyotonia in a Greek family. *Clin Neurol Neurosurg* **2016**, *148*, 85-87. DOI: 10.1016/j.clineuro.2016.07.012.
- (84) Caetano, J. S.; Costa, C.; Baets, J.; Zimon Phd, M.; Venâncio Phd, M.; Saraiva Phd, J.; Negrão, L.; Fineza, I. Autosomal recessive axonal neuropathy with neuromyotonia: a rare entity. *Pediatr Neurol* **2014**, *50* (1), 104-107. DOI: 10.1016/j.pediatrneurol.2013.08.028.
- (85) Jerath, N. U.; Shy, M. E.; Grider, T.; Gutmann, L. A case of neuromyotonia and axonal motor neuropathy: A report of a HINT1 mutation in the United States. *Muscle Nerve* **2015**, *52* (6), 1110-1113. DOI: 10.1002/mus.24774.
- (86) Laššuthová, P.; Brožková, D.; Krůtová, M.; Neupauerová, J.; Haberlová, J.; Mazanec, R.; Dvořáčková, N.; Goldenberg, Z.; Seeman, P. Mutations in HINT1 are one of the most frequent causes of hereditary neuropathy among Czech patients and neuromyotonia is rather an underdiagnosed symptom. *Neurogenetics* **2015**, *16* (1), 43-54. DOI: 10.1007/s10048-014-0427-8.

- (87) Shchagina, O. A.; Milovidova, T. B.; Murtazina, A. F.; Rudenskaya, G. E.; Nikitin, S. S.; Dadali, E. L.; Polyakov, A. V. HINT1 gene pathogenic variants: the most common cause of recessive hereditary motor and sensory neuropathies in Russian patients. *Mol Biol Rep* **2020**, *47* (2), 1331-1337. DOI: 10.1007/s11033-019-05238-z.
- (88) Shah, R. M.; Maize, K. M.; West, H. T.; Strom, A. M.; Finzel, B. C.; Wagner, C. R. Structure and Functional Characterization of Human Histidine Triad Nucleotide-Binding Protein 1 Mutations Associated with Inherited Axonal Neuropathy with Neuromyotonia. *J Mol Biol* **2018**, *430* (17), 2709-2721. DOI: 10.1016/j.jmb.2018.05.028.
- (89) Seburn, K. L.; Morelli, K. H.; Jordanova, A.; Burgess, R. W. Lack of neuropathy-related phenotypes in hint1 knockout mice. *J Neuropathol Exp Neurol* **2014**, *73* (7), 693-701. DOI: 10.1097/NEN.0000000000000085.
- (90) Bardaweel, S. K.; Ghosh, B.; Wagner, C. R. Synthesis and evaluation of potential inhibitors of human and Escherichia coli histidine triad nucleotide binding proteins. *Bioorg Med Chem Lett* **2012**, *22* (1), 558-560. DOI: 10.1016/j.bmcl.2011.10.082.
- (91) Garzón, J.; Herrero-Labrador, R.; Rodríguez-Muñoz, M.; Shah, R.; Vicente-Sánchez, A.; Wagner, C. R.; Sánchez-Blázquez, P. HINT1 protein: a new therapeutic target to enhance opioid antinociception and block mechanical allodynia. *Neuropharmacology* **2015**, *89*, 412-423. DOI: 10.1016/j.neuropharm.2014.10.022.
- (92) Su, T.; Suzui, M.; Wang, L.; Lin, C. S.; Xing, W. Q.; Weinstein, I. B. Deletion of histidine triad nucleotide-binding protein 1/PKC-interacting protein in mice enhances cell growth and carcinogenesis. *Proc Natl Acad Sci U S A* **2003**, *100* (13), 7824-7829. DOI: 10.1073/pnas.1332160100.

- (93) Li, H.; Zhang, Y.; Su, T.; Santella, R. M.; Weinstein, I. B. Hint1 is a haplo-insufficient tumor suppressor in mice. *Oncogene* **2006**, *25* (5), 713-721. DOI: 10.1038/sj.onc.1209111.
- (94) Wang, L.; Zhang, Y.; Li, H.; Xu, Z.; Santella, R. M.; Weinstein, I. B. Hint1 inhibits growth and activator protein-1 activity in human colon cancer cells. *Cancer Res* **2007**, *67* (10), 4700-4708. DOI: 10.1158/0008-5472.CAN-06-4645.
- (95) Yuan, B. Z.; Jefferson, A. M.; Popescu, N. C.; Reynolds, S. H. Aberrant gene expression in human non small cell lung carcinoma cells exposed to demethylating agent 5-aza-2'-deoxycytidine. *Neoplasia* **2004**, *6* (4), 412-419. DOI: 10.1593/neo.03490.
- (96) Zhang, Y. J.; Li, H.; Wu, H. C.; Shen, J.; Wang, L.; Yu, M. W.; Lee, P. H.; Bernard Weinstein, I.; Santella, R. M. Silencing of Hint1, a novel tumor suppressor gene, by promoter hypermethylation in hepatocellular carcinoma. *Cancer Lett* **2009**, *275* (2), 277-284. DOI: 10.1016/j.canlet.2008.10.042.
- (97) Alanazi, A. S.; Miccoli, A.; Mehellou, Y. Aryloxy Pivaloyloxymethyl Prodrugs as Nucleoside Monophosphate Prodrugs. *J Med Chem* **2021**, *64* (22), 16703-16710. DOI: 10.1021/acs.jmedchem.1c01490.
- (98) Weiske, J.; Huber, O. The histidine triad protein Hint1 triggers apoptosis independent of its enzymatic activity. *J Biol Chem* **2006**, *281* (37), 27356-27366. DOI: 10.1074/jbc.M513452200.
- (99) Zhan, T.; Rindtorff, N.; Boutros, M. Wnt signaling in cancer. *Oncogene* **2017**, *36* (11), 1461-1473. DOI: 10.1038/onc.2016.304.
- (100) Duan, D. D.; Xie, H.; Shi, H. F.; Huang, W. W.; Ding, F.; Hong, J. K.; Fan, J. S.; Hu, S. Y.; Wang, Q. W.; Zhou, M. Q. Hint1 Overexpression Inhibits the Cell Cycle and Induces Cell Apoptosis in Human Osteosarcoma Cells. *Onco Targets Ther* **2020**, *13*, 8223-8232. DOI: 10.2147/OTT.S242344.

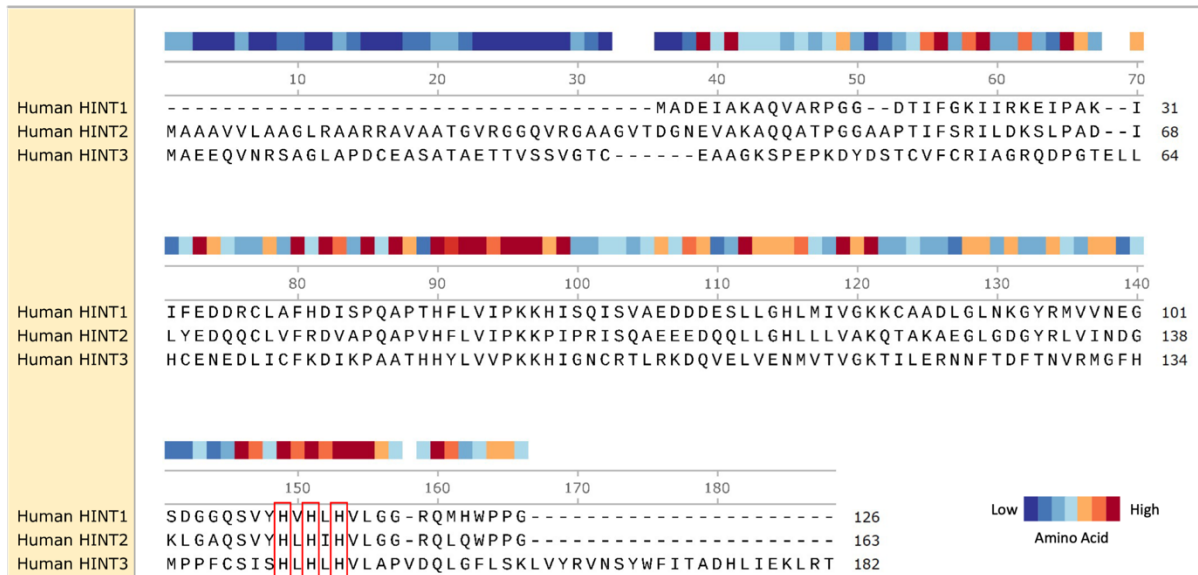
- (101) Bao, T.; Ke, Y.; Wang, Y.; Wang, W.; Li, Y.; Kui, X.; Zhou, Q.; Zhou, H.; Zhang, C.; Zhou, D.; et al. Taraxasterol suppresses the growth of human liver cancer by upregulating Hint1 expression. *J Mol Med (Berl)* **2018**, *96* (7), 661-672. DOI: 10.1007/s00109-018-1652-7.
- (102) Abraham, S. N.; St John, A. L. Mast cell-orchestrated immunity to pathogens. *Nat Rev Immunol* **2010**, *10* (6), 440-452. DOI: 10.1038/nri2782.
- (103) Steingrímsson, E.; Moore, K. J.; Lamoreux, M. L.; Ferré-D'Amaré, A. R.; Burley, S. K.; Zimring, D. C.; Skow, L. C.; Hodgkinson, C. A.; Arnheiter, H.; Copeland, N. G. Molecular basis of mouse microphthalmia (mi) mutations helps explain their developmental and phenotypic consequences. *Nat Genet* **1994**, *8* (3), 256-263. DOI: 10.1038/ng1194-256.
- (104) Nechushtan, H.; Razin, E. The function of MITF and associated proteins in mast cells. *Mol Immunol* **2002**, *38* (16-18), 1177-1180. DOI: 10.1016/s0161-5890(02)00059-7.
- (105) Dwyer, D. F.; Barrett, N. A.; Austen, K. F.; Consortium, I. G. P. Expression profiling of constitutive mast cells reveals a unique identity within the immune system. *Nat Immunol* **2016**, *17* (7), 878-887. DOI: 10.1038/ni.3445.
- (106) Dolot, R.; Kaczmarek, R.; Sęda, A.; Krakowiak, A.; Baraniak, J.; Nawrot, B. Crystallographic studies of the complex of human HINT1 protein with a non-hydrolyzable analog of Ap4A. *Int J Biol Macromol* **2016**, *87*, 62-69. DOI: 10.1016/j.ijbiomac.2016.02.047.
- (107) Strom, A.; Tong, C. L.; Wagner, C. R. Histidine triad nucleotide-binding proteins HINT1 and HINT2 share similar substrate specificities and little affinity for the signaling dinucleotide Ap4A. *FEBS Lett* **2020**, *594* (10), 1497-1505. DOI: 10.1002/1873-3468.13745.
- (108) Rodríguez-Muñoz, M.; de la Torre-Madrid, E.; Sánchez-Blázquez, P.; Garzón, J. NO-released zinc supports the simultaneous binding of Raf-1 and PKC $\gamma$  cysteine-rich domains to HINT1 protein

at the mu-opioid receptor. *Antioxid Redox Signal* **2011**, *14* (12), 2413-2425. DOI:  
10.1089/ars.2010.3511.



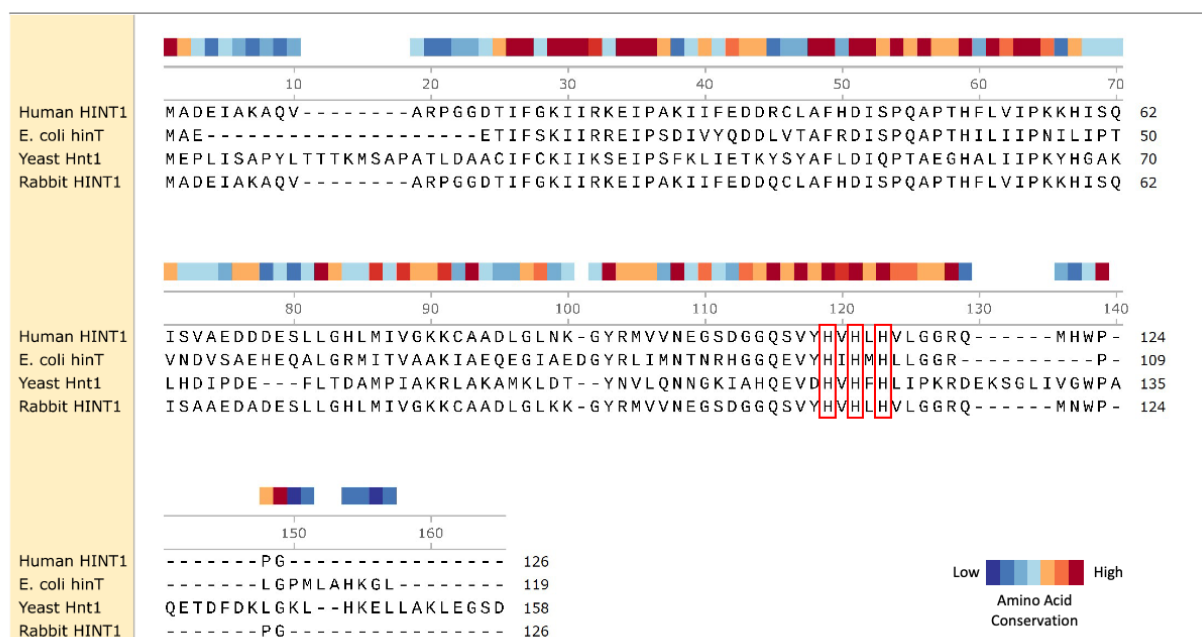
## Supplemental Information

**Figure S1**



**Amino acid sequence alignment of human HINT isoforms (HINT1, HINT2, HINT3).** Alignment highlights the conserved residues across human HINT isoforms. The residues of the conserved catalytic triad of histidine residues (His110, His112 and His114 for HINT1) are marked in a red box.

**Figure S2**



**Amino Acid Sequence Alignment of HINT1 homologs (Human, *E. coli*, Yeast and Rabbit).**

Comparison of relevant HINTs used to study HINT catalysis and substrate specificity. Conservation of specific amino acids are color coded. The residues of the conserved catalytic histidine triad are marked in a red box.

## **Chapter II**

### **Inhibition of Hint1 Modulates Spinal Nociception and NMDA Evoked Behavior in Mice**

## **Abstract**

The interactions between the mu-opioid (MOR) and N-methyl-D-aspartate receptor (NMDAR) constitute an area of intense investigation due to their contributions to maladaptive neuroplasticity. Recent evidence suggests that their association requires the involvement of histidine triad nucleotide-binding protein (HINT1) with the enzyme's active site being critical in its regulatory role. Since it is known that spinal blockade of NMDA receptors prevents the development of opioid analgesic tolerance, we hypothesized that spinal inhibition of the HINT1 enzyme may similarly inhibit opioid tolerance. To address these questions, we evaluated novel HINT1 active site inhibitors in two models of NMDAR and MOR interaction, namely MOR inhibition of spinal NMDA activation and acute endomorphin-2 tolerance. These studies revealed that while the tryptamine carbamate of guanosine inhibitor, TrpGc, blocked both the development of opioid tolerance and the inhibitory effect of opioids on NMDA activation of NMDA receptor, acyl-sulfamate analogs only inhibited the development of opioid tolerance. Thermodynamic binding and x-ray crystallographic studies suggested that there are key differences between the bound HINT1-inhibitor surfaces that may be responsible for their differential ability to probe the ability of HINT1 to regulate cross talk between the mu-opioid receptor and NMDA receptor in the spinal cord.

**Keywords:** Histidine triad nucleotide binding protein1 (HINT1), Neuropathic pain, opioid analgesia, mechanical allodynia, mu-opioid receptors and N-Methyl-D-Aspartate-Receptors.

## Introduction

Transition of nociceptive signals into development of chronic pain is dependent on the key cellular events modulating synaptic plasticity in the central nervous system.<sup>1-3</sup> In addition, duration or frequency of the input signal is critical in mediating long-term cellular fate. To mediate such neuronal processes, an upstream rapid activation of transient signals filters for high-frequency signals that ultimately transmits to downstream signaling processes leading to stable alterations.<sup>4</sup> These include receptor localization, gene expression, morphological changes and synaptic remodeling.<sup>4, 5</sup> Such changes are described as long-term synaptic potentiation (LTP), which often relies on the activation of postsynaptic N-methyl-D-aspartate (NMDA) receptors by neurotransmitters such as glutamate.<sup>6</sup> Development of neuropathic pain is induced primarily via sensitization of the primary sensory neurons (peripheral sensitization) with subsequent sensitization of the spinal cord neurons (central sensitization).<sup>1, 2</sup> Activation of NMDA receptors in spinal dorsal horn nociceptive neurons plays an essential role in developing hypersensitivity to the spinal cord pain circuit.<sup>7, 8</sup> In mouse behavioral assays, administration of the NMDAR agonist NMDA intrathecally exhibits nociceptive biting, scratching, and licking behavior and opioids such as morphine are known to alleviate such responses.<sup>9-11</sup>

According to “control gate theory” nociceptive signals originating in the peripheral nervous system encounter “nerve gates” before reaching the cortical region of the brain. Certain discrete regions of the brain, including PAG, negatively regulate nerve gates.<sup>1</sup> Studies have demonstrated that direct electric stimulation of PAG region inhibits opening of the nerve gates and hence produces an analgesic effect. Most clinically used opioids act by activating MOR (possibly in the PAG region, where they are densely expressed) to produce the analgesic effect. It

is also known that repeated exposure of opioids leads to the development of acute tolerance via activation of NMDAR signaling pathways in both the PAG and the dorsal horn of the spinal cord.<sup>12</sup>  
<sup>13</sup> Such events have been described to be essential for the transition of an acute pain into chronic pain. Although this phenomenon is well known, the molecular mechanism regulating the crosstalk between MOR and NMDAR involved in the transition to chronic pain has remained unclear.

Human HINT1 belongs to the histidine triad (HIT) superfamily which is characterized by their conserved sequence motif, His-X-His-X-His-XX, where X is a hydrophobic residue. Human HINT1 exists as a homodimer and possesses nucleoside phosphoramidase and acyl-AMP hydrolase activity, with a substrate preference for purine over pyrimidine nucleosides.<sup>14</sup> HINT proteins are highly conserved across all the kingdoms of life, suggesting that they have an important biological function. Despite this, their specific cellular substrate and thus their particular regulatory role as an enzyme remains largely unknown. Of what little is known, lysyl-AMP has been shown to be a substrate of HINT1 which supports a body of immunological evidence demonstrating the enzyme's ability to regulate lysyl-tRNA synthetase and MITF mediated mast cell activation.<sup>15-18</sup>

We've previously reported that active site inhibition of HINT1 with our nucleoside carbamate (**TrpGc**) results in an increased morphine analgesic response and pretreatment with the compound prevents the development of morphine tolerance in mice.<sup>19</sup> It has been speculated and shown that upon morphine challenge, the interplay of different protein assemblies (including HINT1, PKC $\gamma$ ,  $\sigma$ 1R, RGS22) at MOR results in the activation of NMDAR, leading to the development of acute morphine tolerance.<sup>20-22</sup> In a recent study we also

developed and characterized the first submicromolar water-soluble inhibitors for HINT1 *in vitro* in order to probe HINT1's role, exchanging the inhibitor's carbamate for an acyl-sulfamate.<sup>23</sup>

With such striking effects observed on the pharmacology of the MOR under the regulation of NMDAR, we hypothesize that similar dramatic effects on the pharmacology of NMDAR via this crosstalk with MOR could be observed by disrupting HINT1's interaction between the receptors using our active site inhibitors. Additionally, we performed structure-activity relationship studies on our previously reported and pharmacologically active carbamate HINT1 inhibitor (**TrpGc**) as well as evaluated the pharmacology of the NMDA receptor for our recently reported, water-soluble submicromolar binding acyl-sulfamate HINT1 inhibitors. Our SAR studies are supported with x-ray crystallographic analysis of the nucleoside carbamate and sulfamate inhibitors. To our knowledge, these are the first studies demonstrating the SAR of HINT1 inhibition as well as the dramatic role it plays on the spinal nociceptive processes induced through NMDAR agonism and endomorphin-2 tolerance prevention.

## Results

### Preference of non-polar side chains in the molecular recognition of nucleoside carbamates by hHint1

We began by investigating the importance of the tryptamine side chain in the molecular recognition ( $K_d$ ) of **TrpGc** by human histidine triad nucleotide binding protein (hHint1) (**Table 1**). To assess the structure activity relationship surrounding (**TrpGc**) we began by designing an analog in which the indole side chain of (**TrpGc**) was removed. Compound (**1**), with an ethylamine side chain, was synthesized using the previously described procedure.<sup>24</sup> The coupling reaction of the

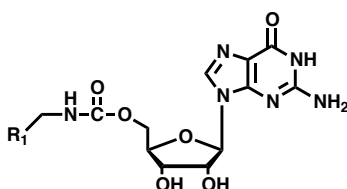
nucleoside carbamates typically takes around 24 hours. The same coupling reaction proceeded very quickly and completed within a few minutes in a microwave synthesizer. The yields of the coupling reactions in the microwave for different amine side chains are reported in **Table 1**. Next, we investigated the binding affinity of (**1**) for hHint1 using isothermal titration calorimetry (ITC). Removal of the indole side chain did not significantly alter the binding affinity for hHint1 when compared to (**TrpGc**).

Next, we wanted to ask if the ethylene linker between the carbamate backbone and the bulky indole ring in (**TrpGc**) was of optimum length and steric character. Hence, we synthesized analogs with phenethylamine (**2**) and benzylamine (**3**) side chains. Replacing tryptamine with a phenethylamine substitution improved the binding affinity by two-fold, while incorporating the shorter benzylamine hampered the binding affinity by two-fold. The increase in the  $K_d$  of (**3**) appears to reflect that shortened linker length and thus increasing the rigidity of the moiety has a negative impact on the binding to hHint1. One of the key features in the structure of hHint1 is that it contains its only tryptophan residue (W123) in the shallow binding pocket S2. In addition to addressing questions surrounding the sterics of binding, we asked if we could gain an increase in the binding affinity by incorporating polar or positively charged groups in the side chain to form additional cation- $\pi$  interactions with the W123. With this aim in mind, we designed compounds with an imidazole side chain (**4**) and a primary amine (**5**), which would be partially positive and fully positively charged respectively at neutral pH.

The synthesis of compound (**5**) was achieved by coupling of the mono boc-protected diethylamine under similar fashion to (**TrpGc**), whereas coupling of the histamine of (**4**) was



**Table 1: Dissociation constants and yields in the microwave-assisted synthesis of nucleoside carbamates**



Compound	R <sub>1</sub>	K <sub>d</sub> (μM)	Yield (%) <sup>a</sup>	
			Ambient	Microwave
TrpGc		3.65 ± 1.00	75	72
<b>1</b>	<b>CH<sub>3</sub></b>	2.45 ± 0.59	67	75
<b>2</b>		1.56 ± 0.01	83	60
<b>3</b>		8.09 ± 0.09	65	56
<b>4</b>		3.19 ± 0.41	34	-
<b>5</b>		12.0 ± 3.10	62	58

<sup>a</sup> Yields reported for the coupling between 2' 3'-OH acetonide protected nucleoside and amine to form carbamate

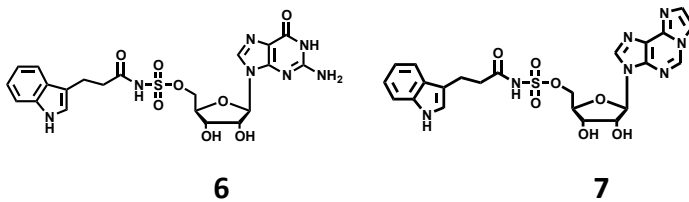
achieved in DMF instead of pyridine due to insolubility of the starting material. Deprotection of the 2' 3'-OH and amine groups was achieved using aqueous trifluoroacetic acid (TFA) in the final step. ITC analysis revealed that modification with an imidazole side chain in **(4)** was well tolerated as little change to the  $K_d$  was found. In contrast, a primary amine in compound **(5)** reduced the binding affinity by four-fold. Taken together these results indicate hHint1 does not prefer a positive and polar side chain in this position. Based on published crystal structures, we hypothesize this could be due to residue Arg95 which, while somewhat buried in the tertiary structure of the protein, could very likely supply a partial positive charge near the site of S2 pocket side-chain binding.

Interestingly, the compounds in this current carbamate inhibitor series have poorer binding affinities than previously reported nucleoside sulfamate inhibitor compounds **(6)** and **(7)** (**Table 2**).<sup>23</sup> Compound **(7)** binding was previously observed to benefit greatly from its larger hydrophobic tricyclic nucleobase, and compound **(6)** strongly mimics our original carbamate (**TrpGc**), highlighting the importance of the acyl-sulfamate functional group over the carbamate for binding *in vitro*. Despite this known improvement in binding for acyl-sulfamates, we hypothesized this series of carbamates would be a better starting point for *in vivo* studies as they are non-ionic, unlike the acyl-sulfamates.

### **X-ray crystal structures reveal key interactions driving the molecular recognition of hHint1 binding**

To identify the critical interactions driving molecular recognition of hHint1 inhibitors, we obtained high-resolution x-ray crystal structures of **(1)**, **(2)**, **(3)**, and (**TrpGc**) bound to hHint1

**Table 2: Dissociation constants of the previously reported nucleoside acyl-sulfamate inhibitors of Hint1.<sup>23</sup>**



Compound	$K_d$ ( $\mu\text{M}$ )
TrpGc	$3.65 \pm 1.00$
<b>6</b>	$0.81 \pm 0.11$
<b>7</b>	$0.23 \pm 0.01$

**(Figure 1)**. These results along with our previously published hHint1 structure with **(7)** provide a strong initial overview of the structural biology of hHint1 active site inhibition.<sup>23</sup> First, all crystalized Hint1 inhibitors engage in hallmark interactions revealed in previous nucleotide bound hHint1 structures. These include hydrogen bonding between the 2',3'-OH of each inhibitor's ribose and Asp43 (2.4-2.6Å), as well as non-bonded interactions between the nucleobase and hydrophobic pocket comprised of Ile18, Ile22, Ile44 (**Figure 1a**). This base binding site also contains a sandwiched face-to-edge-to-face pi-stacking complex with Phe19 between His112 and the inhibitor's nucleobase. Unique to these guanosine derived compounds is a H-bond between the nitrogen at the 2-position of the nucleobase and the backbone oxygen of His42. The ribose and guanine of all four guanosine-carbamate inhibitor structures (**1-3, TrpGc**) are in near perfect alignment but their 5'-carbamate moieties, which coordinate with the catalytic His112 of the protein, appear in slightly different poses (**Figure 1a-d**).

The angle of the carbamate group and distance between its central carbon and the nucleophilic nitrogen of His112 (3.2-3.5Å) appears to be driven by how well the neighboring sidechains of each ligand are able to interact with the shallow shelf like S2 pocket adjacent to Trp123. As predicted in the original molecular design, compound **(2)** is able to occupy this space more comfortably than **(3)** due to the added flexibility the longer linker to its phenyl group affords, but at the cost of losing beneficial pi-stacking interactions with Trp123 that **(3)** maintains (**Figure 1b and 1c**). A comparison of the  $K_{ds}$  demonstrates that the added pi-pi interaction does not outweigh the conformational strain **(3)** must undergo to access this binding pose. In turn, compound **(1)**, lacking a phenyl group altogether, fits well but lacks the potential for anything beyond a simple hydrophobic interaction with Trp123.

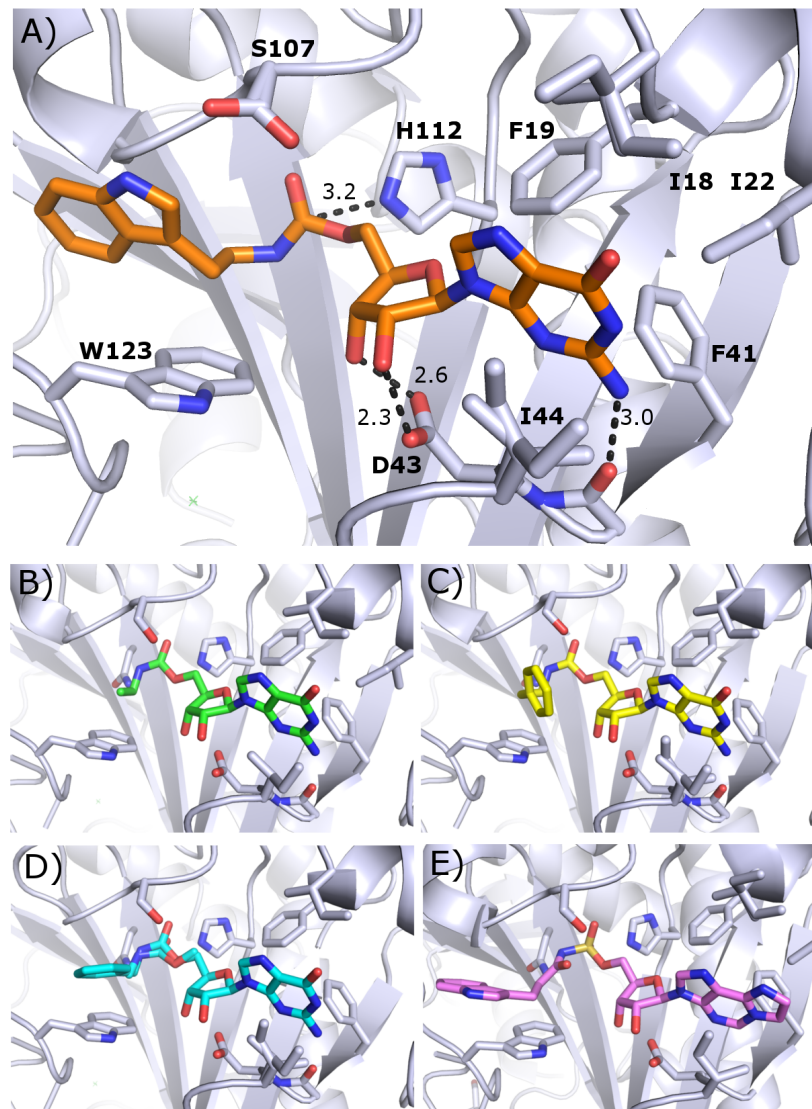


**Figure 1:** Crystal structures of HINT1 inhibitors bound to the enzyme's active site (PDB IDs: 6N3V, 6N3W, 6N3X, 6N3Y, 5I2E). **A)** (**TrpGc**) in orange bound to HINT1 depicted in a grey cartoon and stick format with key interacting residues and important H-bonds and distances (Å) labeled in black. S107 is not close enough to the carbamate to make a significant H-bond and was determined to be in two conformations. **B)** Compound (**1**) in green bound to the HINT1. **C)** Compound (**2**) in yellow bound to the HINT1. **D)** Compound (**3**) in cyan bound to HINT1. **E)** Compound (**7**) in magenta bound to HINT1.

In an important comparison between (**TrpGc**) and our previously published structure of (**7**), we were able to observe the difference between binding of the carbamate and acyl-sulfamate functional groups within these inhibitors (**Figure 2**). As a point of similarity, the partially positive sulfur in the acyl-sulfamate of (**7**) and the carbamate carbon of (**TrpGc**) are both 3.2Å from the nucleophilic nitrogen of His112, however the difference in electrophilicity of the inhibitor's functional groups likely thermodynamically favors (**7**) for binding despite their identical distance. Additionally, the sidechain acyl group of (**7**) is able to form an H-bond with Ser107 (2.7Å) whereas (**TrpGc**) lacks this acyl H-bond acceptor (**Figure 2**). Consequently, two conformations of Ser107 were observed in the (**TrpGc**) bound structure, with neither able to participate in a strong H-bond with the ligand (**Figures 1a and 2**). Despite (**7**) having a longer linker by one carbon to the indole group, the indole moieties of (**7**) and (**TrpGc**) appear in a similar bound location, but at different angles. In light of the pharmacologic SAR these compounds provide (*vide infra*), the observed differences in positioning of the indole between (**7**) and (**TrpGc**) as well as their differential anionic character are may play a role in their differential biological activity.

### **TrpGc and TrpGc analogs inhibit morphine's inhibition of NMDA-evoked behaviors**

Spinal activation of NMDA receptors has been shown to play an important role in the nociceptive processes at the spinal level.<sup>7, 8</sup> Previously, we have shown that inhibition of HINT1 with (**TrpGc**) prevents the development of morphine tolerance by modulating the crosstalk between MOR and NMDA receptors *in vivo*.<sup>19</sup> The bidirectionality of this crosstalk is unclear, thus we wanted to explore whether HINT1 inhibition could also disrupt MOR mediated analgesic relief from noxious NMDAR agonism.

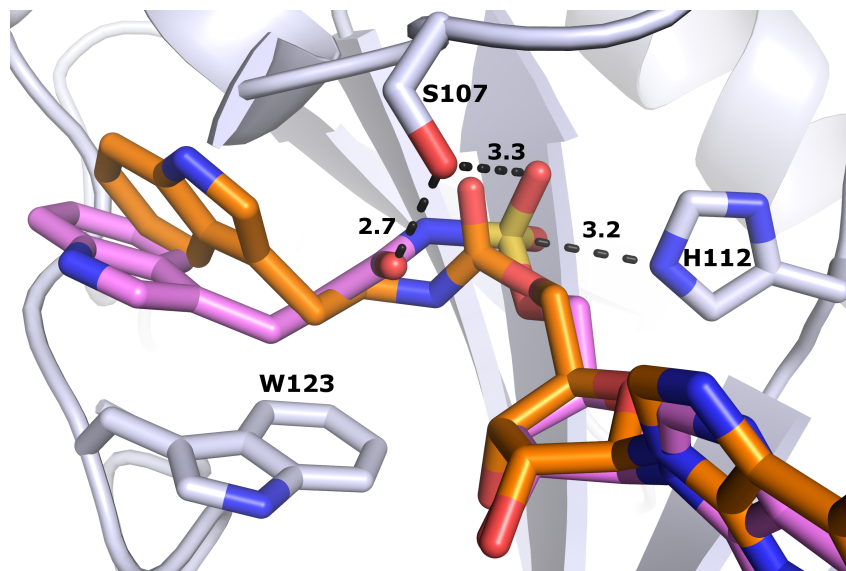


**Figure 2.** Comparison of carbamate and acyl-sulfamate HINT1 nucleoside inhibitor active site binding, observed in the aligned crystal structures of compound (**TrpGc**) in orange onto the compound (**7**) bound structure with (**7**) in pink and protein in grey (PDB IDs: 6N3Y, 5I2E). Both compound's indole side chains align over W123 at slightly different angles through hydrophobic interactions but miss the opportunity to pi-stack. S107 makes a tight H-bond with the acyl group of compound (**7**), which (**TrpGc**) lacks. H112 aligns equidistant (3.2Å) to the sulfur and carbon core of the sulfamate and carbamate respectively.

As described previously, intrathecally delivered NMDA produces a characteristic nociceptive behavior in mice, namely transient scratching and biting directed towards abdominal and tail areas and a transient thermal hypersensitivity as measured by the 49°C tail flick assay<sup>25</sup>. This transient thermal hypersensitivity produced by intrathecal NMDA is reduced by pre-treatment with morphine in a dose-related manner due to morphine's agonism at MORs. This response is presented as the percent maximum possible effect (%MPE, **Figure 3** red diamond). We sought to characterize the ability of the HINT1 inhibitor compounds to reduce morphine's efficacy at reducing NMDA-induced transient thermal hypersensitivity. The HINT1 inhibitor compounds (**6**) and (**7**) showed similar ED<sub>50</sub> values to that of the parent compound, (**TrpGc**) (**Table 3**). However, compound (**2**) showed an increased ED<sub>50</sub> value indicating decreased potency as compared to (**TrpGc**), and compound (**1**) did not demonstrate a dose-related effect at the highest dose tested.

### **TrpGc but not TrpGc analogs inhibit the rapid development of MOR tolerance**

Endomorphin-2, an endogenous and selective MOR agonist, produces an acute spinal tolerance when delivered intrathecally<sup>26</sup>. Male and female mice were pre-treated with either vehicle or an acute tolerance-inducing dose of endomorphin-2 (**Figure 4**). After tail-flick latencies had returned to baseline values (30 minutes following the initial injection), a second probe injection of endomorphin-2 was administered and tail flick latencies were measured again 2.5 minutes following this second injection. Mice treated with vehicle (white bar) demonstrated full antinociception following the probe dose of endomorphin-2, whereas the mice that received both the initial and probe doses of endomorphin-2 (red bar) showed a significant reduction in



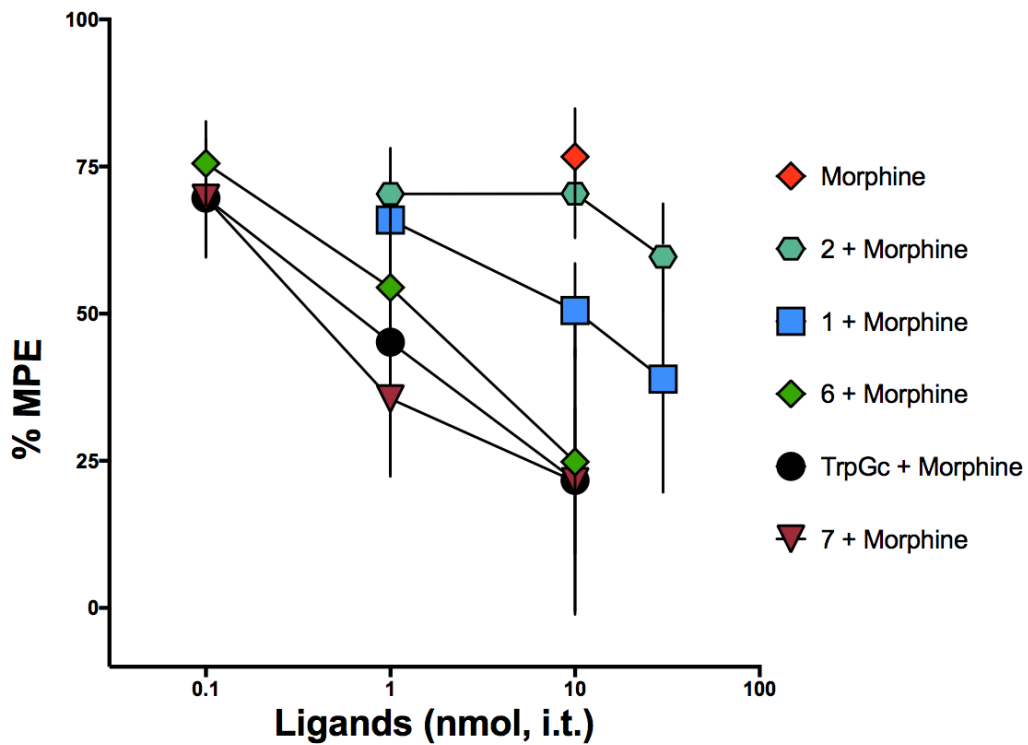


**Figure 3. TrpGc and TrpGc analogs inhibit morphine's inhibition of NMDA-evoked behaviors .** Male mice were given intrathecal treatment of either morphine or morphine + a HINT1 inhibitor. They were then given an intrathecal injection of NMDA and scratching and transient thermal hypersensitivity was measured by tail flick assay. Pretreatment with either TrpGc (black circles) or a TrpGc analog attenuated morphine's inhibition of NMDA-evoked transient thermal hypersensitivity. ED<sub>50</sub> values and 95% CIs were calculated and are reported in **Table 3**.

Pre-Treatment	TrpGc	1	2	6	7
ED <sub>50</sub> (nmol) (95% CI)	<b>0.61</b> (0.28, 1.4)	<b>* 8.4</b> (2.8, 25)	Unable to be calculated	<b>1.2</b> (0.49, 1.8)	<b>0.47</b> (0.20, 1.1)

**Table 3.** Calculated ED<sub>50</sub> values for TrpGc and TrpGc analogues from Figure 1. \*indicates non-overlapping 95% CIs compared to TrpGc and are thus considered a statistically significant difference.

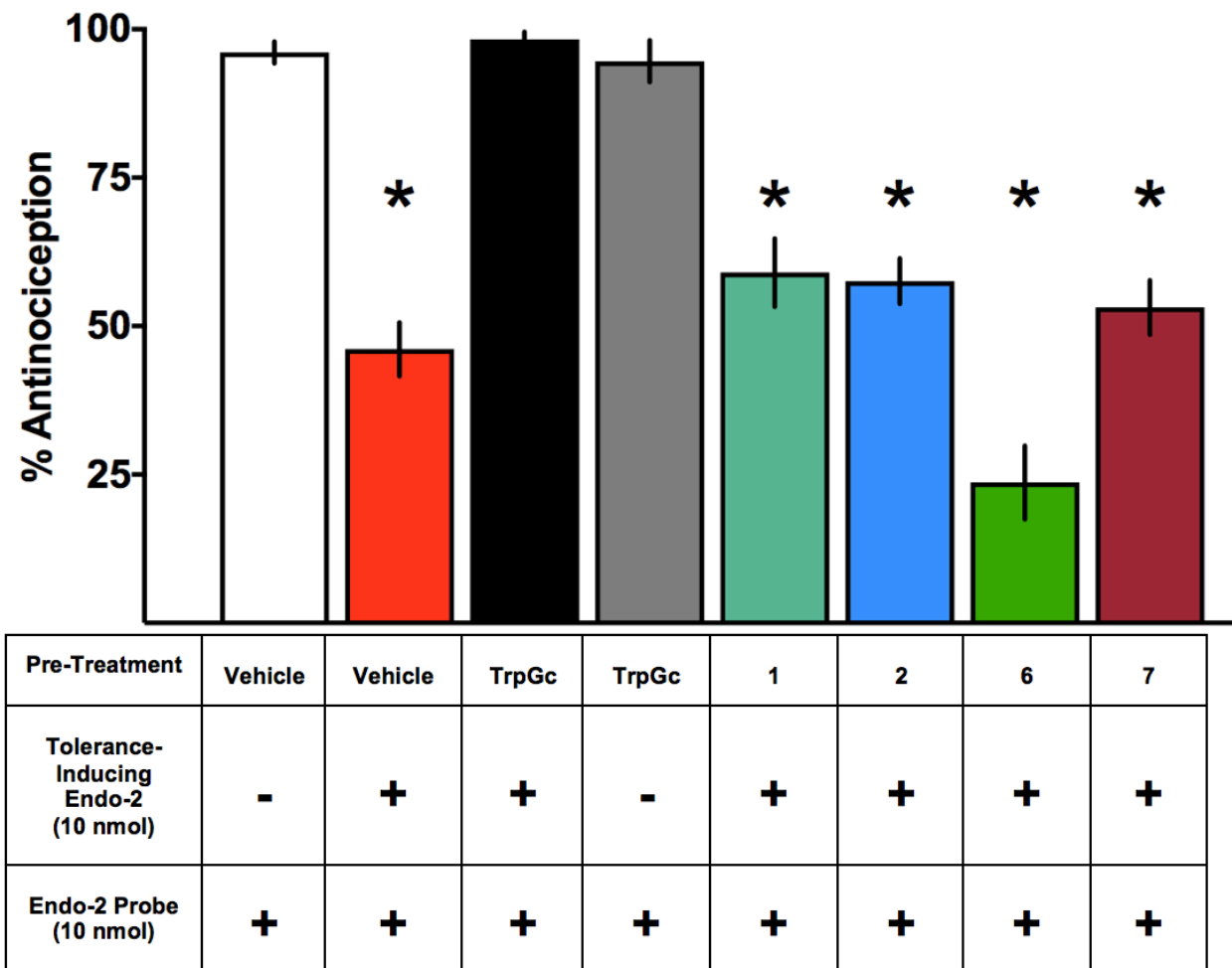


**Figure 4.** TrpGc but not TrpGc analogs inhibit the development of endomorphin-2 tolerance. The spinal antinociceptive effect of endomorphin-2 is significantly greater in male and female mice pre-treated with vehicle (white) as compared to mice pre-treated with endomorphin-2 (red), indicating an ultra-rapid development of tolerance. Treatment with TrpGc prior to the first endo-2 injection is able to prevent this development of tolerance (black), while pre-treatment of TrpGc alone (lacking a tolerance-inducing endo-2 injection) does not itself produce tolerance (grey). The TrpGc analogs (1), (2), (6), and (7) were not able to prevent the development of endo-2 tolerance (teal, blue, green, maroon). \*indicates significant difference from saline-endo-2 control (white) by one-way ANOVA,  $p < 0.05$  with Dunnett's post-hoc analysis.

antinociception following the probe dose of endomorphin-2. This loss of antinociception can be prevented with a pre-treatment of the HINT1 inhibitor TrpGc prior to the first injection of endomorphin-2 (black bar). (**TrpGc**) analogs 1, 2, 6, and 7 (teal, blue, green, and maroon bars) were not able to prevent the loss of antinociception in this assay. Importantly, the parent compound (**TrpGc**) does not itself produce antinociceptive tolerance (grey bar).

## Conclusions

From an *in vitro* binding perspective for HINT1 inhibitor design, changes to the side-chain of (**TrpGc**) revealed the effects of altering the steric constraint and cationic character of the S2 binding pocket portion of the molecule. Specifically, the side chain is adversely sensitive to a shorter bulkier linker as well as side chains with explicit cationic charge. Both substitution of the indole of (**TrpGc**) to a phenethyl group (compound **2**) and truncation of the side chain down to a simple but flexible ethyl group (compound **1**) showed minor improvements in binding affinity *in vitro*. Also summarized in our previous work, the substitution of an acyl-sulfamate instead of a carbamate helps drive the  $K_d$  down by approximately four-fold seen in the comparison of (**TrpGc**) and (**6**). The substitution for the tricyclic adenine like nucleobase used in (**7**) also improves binding and notably also confers the ability to monitor the compound by fluorescence in other *in vitro* analyses.<sup>27</sup>

*In vivo*, the role HINT1 has on the interplay between the MOR and NMDAR was explored. These studies indicate to us that disruption of HINT1 via the enzymatic inhibitor **TrpGc**, but not the reported **TrpGc** analogs, is a viable strategy to target maladaptive plasticity involving MOR and NMDAR-mediated signaling as seen in endomorphin-2 tolerance tests. Delivery of **TrpGc** as

well as select **TrpGc** analogs (**6** and **7**) however interestingly do interrupt morphine's inhibition of NMDA-evoked transient thermal hypersensitivity (**Figure 4, Table 3**). But again, only (**TrpGc**) and none of the analogs were able to prevent the development of short term endomorphin-2-induced tolerance.

Comparing the *in vitro* and *in vivo* SAR, compounds (**1**) and (**2**) had identical or enhanced binding affinity to the parent compound (**TrpGc**) but exhibited a significant reduction in both measures of *in vivo* efficacy. Counter to our hypothesis that the greater hydrophobicity of these novel carbamates would enhance their activity relative to the more water-soluble anionic acyl-sulfamates, we observed that compounds (**6**), (**7**) and (**TrpGc**) had a similar ability to suppress the effect of morphine on NMDA receptor activation (Figure 3). Thus, the SAR emphasizes the importance of indole bearing side-chains for this specific biological activity. Nevertheless, these higher affinity acyl-sulfamates, (**6**) and (**7**), failed to prevent tolerance to endomorphin-2. Thus, while (**TrpGc**) is able to potently potentiate endomorphine-2 tolerance and morphine suppression of NMDA receptor activation, the incorporation of the highly polar acyl-sulfamate group results in differentiation between these activities *in vivo*.

Again, loss of the indolyl moiety, as demonstrated by the carbamate analogs (**1**) and (**2**) resulted in a loss of potency for both biological processes. Consequently, simple occupation of the active site appears to be insufficient to affect either endomorphin-2 tolerance or morphine suppression of NMDA receptor activation. As can be seen from the co-crystal structures of (**1-3**) and (**TrpGc**) with HINT1, the specific steric and potential N-H hydrogen bonding ability of the indolyl moiety of (**TrpGc**) suggests a role for these molecular descriptors in defining the interaction of HINT1 with molecular constituents governing its biological activity (**Figure 1**).

Additionally, as can be seen from an electrostatic potential surface map of the co-crystal structures of **(7)** and **(TrpGc) (Figure 5)**, the substitution of a highly polar anionic acyl-sulfamate moiety instead of the carbamate moiety results in a loss of the ability to modulate opioid tolerance while maintaining the ability to disrupt MOR mediated alleviation of noxious NMDAR agonism. Therefore, subtle changes in the molecular surface of the HINT1-inhibitor surface are likely responsible for differentially affecting the interactions of HINT1 with molecular constituents responsible for HINT1's role on these biological processes in the spinal cord.

Taken together, the results of this study demonstrate functionally for the first time that HINT1 governs the interaction of MOR with the NMDA receptor in the spinal cord and thus highlights the importance of the HINT1 active site in their regulatory crosstalk. Moreover, these studies demonstrate that the role of HINT1 on opioid tolerance is not limited to the brain, but is manifest in the spinal cord as well.<sup>24</sup> Importantly, subtle differences in the molecular surface of the inhibitor-HINT1 surface can dramatically and differentially affect the biological role of HINT1 in the CNS, implying that the molecular partners and events governing these activities have a defined uniqueness. Ongoing studies further exploring the governing role of HINT1 inhibitor structure on the biological role HINT1 plays in both opioid tolerance, NMDA receptor activation and neuropathic pain should provide insights into the molecular mechanisms governing HINT1's role in the CNS. Furthermore, with SAR and x-ray crystal structures as guiding tools, a wider array of HINT1 inhibitors should be synthesized and further studied to interrogate the differences in these pain-modulating pathways.

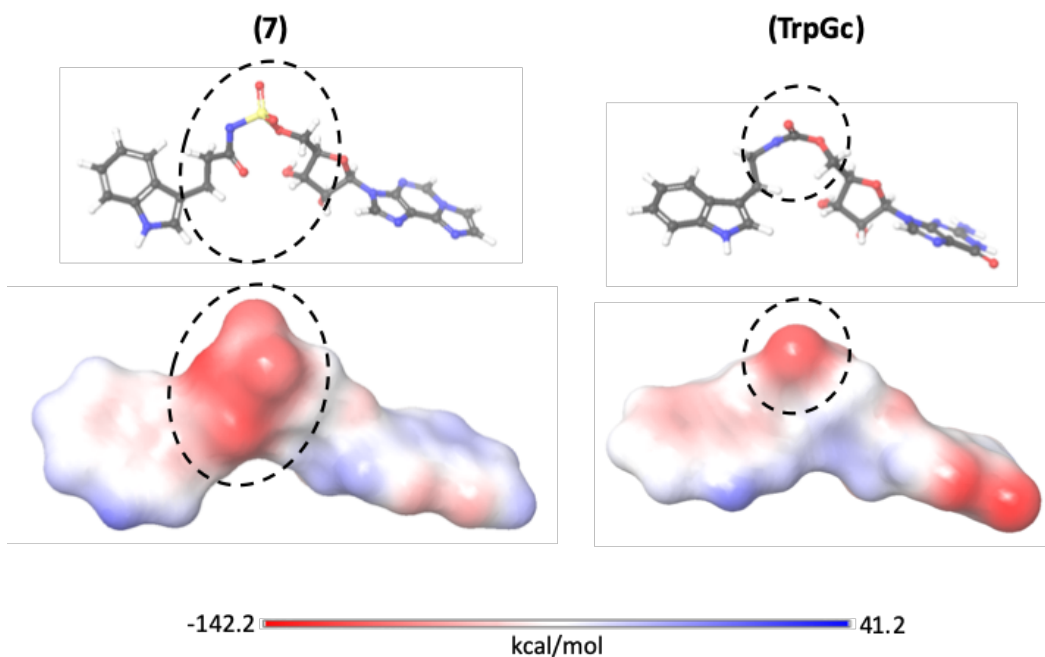


**Figure 5:** Ball and stick representation of compounds (7) and (TrpGc) extracted from their HINT1 bound crystal structures, along with calculated electrostatic potential surface maps of both molecules. The acyl-sulfamate of compound (7) imparts a much broader negative electrostatic surface potential to this central region of the inhibitor compared to the carbamate found in (TrpGc).

## **Abbreviations**

HINT1, histidine triad nucleotide binding protein 1; hHINT1, human histidine triad nucleotide binding protein 1; CNS, Central nervous system; GPCR, G-protein coupled receptors; NMDAR, N-methyl-D-aspartate receptor; MOR, Mu-opioid receptor; NMDA, N-methyl-D-aspartate, i.c.v, intracerebroventricular injection and i.t., intrathecal injection.

## **Acknowledgment**

The studies were generously supported with Wallin Discovery Fund for Neuroscience at University of Minnesota. We also thankfully acknowledge funding from the University of Minnesota Endowment and Funding from the University of Minnesota Foundation. Use of the IMCA-CAT beamline 17-ID at the Advanced Photon Source was supported by the companies of the Industrial Macromolecular Crystallography Association through a contract with Hauptman-Woodward Medical Research Institute. This research used resources of the Advanced Photon Source, a U.S. Department of Energy (DOE) Office of Science User Facility operated for the DOE Office of Science by Argonne National Laboratory under Contract No. DE-AC02-06CH11357. Thank you to Rachit Shah for the initial compound design and contributions to synthesis, Cristina Peterson for performing the animal experiments, and Alex Strom for performing the X-Ray crystallography.



## **Materials and Methods**

### **Isothermal Titration Calorimetry**

ITC experiments were conducted on a MicroCal Auto-ITC200 system (GE Healthcare life sciences). All titration experiments were performed at 25 °C in ITC buffer (10 mM Tris, 150 mM NaCl, pH 7.5). hHint1 was exchanged into ITC buffer using Micro biospin6 columns (BioRad, USA). Final protein concentrations were determined via NanoDrop absorbance using an extinction coefficient from the ExPASy ProtParam web tool. To determine the dissociation constant of stock concentration (100-500  $\mu$ M) of inhibitors were titrated with 10-50  $\mu$ M of Hint1. Twenty injections of ligand were injected (injection volume 2  $\mu$ l) into the protein cell. The resulting change in enthalpy was measured and the background heat of dilution was subtracted by performing similar experiments in the absence of protein. The background heat of dilution was subtracted from the resulting data and was fitted into one-site binding model using the ITC200 microcal software. The resulting association constant obtained by fitting the curve was converted into  $K_d$  using the  $K_a = 1/K_d$  relationship.

### **Protein Crystallography**

Crystals were grown via hanging drop vapor diffusion, with drops comprised of 2  $\mu$ L of protein (A280 = 6-10, in 50mM HEPES, 250 mM NaCl, 10% glycerol v/v, pH 7.5 buffer) and 2  $\mu$ L of well solution. Well solutions contained 25-35% PEG 8K, and 100 mM MES at pH 6.1-6.5. Crystals formed after 3 days of incubation at 20 °C. Co-crystals with inhibitors were prepared by soaking pre-formed crystals in mother liquor containing 25 mM of each ligand for 15-60 minutes. In addition to the mother liquor was 10% DMSO to adequately dissolve the hydrophobic carbamate-

based inhibitors which came at a cost to soaking crystal's structural integrity and thus the ability to soak the crystals for long. After soaking, crystals were cryoprotected using 20% PEG 400 and flash vitrified with liquid nitrogen. Diffraction data were collected at 100K at beamline 17-ID (IMCA-CAT) using a Dectris Pilatus 6M Pixel Array Detector at the Advanced Photon Source of Argonne National Laboratories in Argonne, IL. Molecular replacement was conducted with hHint1 coordinates (PDB ID 3TW2) using Phaser<sup>28</sup> within PHENIX.<sup>29</sup> Modeling and molecular visualization were performed in Coot.<sup>30</sup> Ligand restraints were calculated using JLigand,<sup>31</sup> and refinement was performed using PHENIX.

### **Electrostatic Potential Maps**

Electrostatic potential surface maps were calculated in the Schrodinger-Maestro software suite, utilizing Jaguar single point energy calculations for surface mapping data. The density functional B3LYP and basis set 6-31G\*\*++ were used, including diffuse functions to better model the anionic acyl-sulfamate compound (**7**).

### **Animals**

ICR-CD-1 mice (male and female, 21-30 grams) were maintained on a 12-hour light/dark cycle with unrestricted access to water and food. All experiments were approved by the Institutional Animal Care and Use Committee of the University of Minnesota.

### **Drug Preparation for Behavioral Assays**

Morphine sulfate (NIDA) and endomorphin-2 (endo-2) were dissolved in 0.9% saline. Endomorphin-2 was prepared as previously described<sup>26</sup>. Briefly, endo-2 was synthesized using

solid-state methods and HPLC-purified by the Microchemical Facility of the University of Minnesota and was dissolved for intrathecal injection in 0.9% normal saline. All stocks of TrpGc and TrpGc analogs were dissolved in 5% DMSO, 10% EtOH, and 10% cremophor, and diluted with diH<sub>2</sub>O to a final concentration of 0.5% DMSO, 1% cremophor, and 1% ethanol. From this stock, a final concentration was reached by diluting the stock solution with 0.9% normal saline into the injection concentration.

### **Intrathecal Injections**

All drugs were delivered in 5  $\mu$ L volumes via intrathecal injection in conscious mice <sup>32</sup>. Briefly, the mice were held by the iliac crest and drugs were injected into the intrathecal space by a 30-gauge, 0.5-inch needle attached to a 50  $\mu$ L Luer-hub Hamilton syringe.

### **Warm Water Tail Immersion Assay**

Antinociception was measured using a warm water tail immersion assay. Mice were wrapped in a soft cloth with their tails exposed and approximately 3/4 of the tail was dipped into a warm water bath (49 or 52.5°C). The latency for the mouse to flick its tail was recorded before and after intrathecal administration of drug. In order to avoid tissue damage, a maximum cutoff of 12 seconds was set. A minimum of 4 mice were used for each drug, and each subject received only one HINT1 inhibitor compound.

## Morphine Inhibition of NMDA-evoked Behavior

Intrathecal injection of NMDA gives rise to both a transient thermal hypersensitivity that can be measured by a warm water tail immersion assay, and a caudally-directed scratching and biting behavior lasting for 1-5 minutes. For this initial screen of the TrpGc analog compounds, we measured the impact of each inhibitor on morphine's inhibition of NMDA-evoked transient thermal hypersensitivity. A baseline tail flick latency (pre-NMDA tail flick latency) was recorded at 49°C. TrpGc or a TrpGc analog was intrathecally injected (0.1-30 nmol/5 µL) into male ICR mice (25-30g) 10 minutes prior to an intrathecal injection of morphine sulfate (10 nmol/5 µL). After a period of 10 minutes, NMDA was injected intrathecally and another tail flick latency was recorded (post-NMDA tail flick latency). The percent maximum possible effect (%MPE) was calculated according to the following equation:

$$MPE\% = -100 * \frac{(Experimental\ Value) - (Control)}{(Control)}$$

where the Control value is the average reduction of tail flick latency within the cohort of subjects receiving only NMDA treatment:

$$(Control) = (post\ NMDA\ tail\ flick\ latency - pre\ NMDA\ tail\ flick\ latency)$$

and the Experimental Value is the change in tail flick latency in the presence of NMDA + morphine or NMDA + morphine + HINT1 inhibitor.

## Endomorphin-2 tolerance

Baseline thermal responsiveness was assessed in a 52.5°C water bath tail-immersion assay with a cutoff time of 12 seconds. TrpGc, TrpGc analog or vehicle was injected intrathecally, followed 5 minutes later by an intrathecal injection of endomorphin-2 (endo-2) at a dose of 10 nmol/5 µL into male and female ICR mice. Observation of a Straub tail for each subject was used as an indication of a successful intrathecal injection of an opioid agonist. Thirty minutes following this injection, an additional tail flick was assessed in order to confirm a return to baseline responsiveness and a lack of continued analgesia (predrug latency). A probe dose of endo-2 (10 nmol/5 µL, i.t.) was injected, and a final tail flick latency (postdrug latency) was assessed 2.5 minutes following this probe endo-2 injection.

The results are expressed as a percentage maximum possible effect (%MPE) according to the following equation:

$$\%MPE = 100 * \frac{(postdrug\ latency - predrug\ latency)}{(12\ second\ cut\ off - predrug\ latency)}$$

## Behavioral Data Analysis

For behavioral assays, data were calculated as described above. The data are represented as mean +/- SEM for each assay. A minimum of three doses were used for dose-response analysis. The ED<sub>50</sub> values were calculated using the graded dose-response curve method of Tallarida et al.<sup>33, 34</sup>. Non-overlapping 95% confidence intervals (CI)s of ED<sub>50</sub> values were considered to be statistically significant between treatment groups.

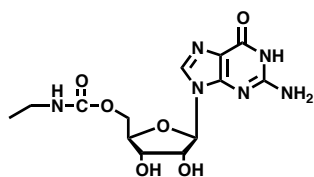
### **General procedure for the synthesis of carbamates**

To a cold, stirred solution of 2',3'-O-isopropylidene guanosine (1.0 eqvi, 0.309 mmol) in pyridine (5 mL), p-Cl phenyl chloroformate was added (1.2 eqvi 0.3708 mmol) dropwise over a period of 30 minutes. The solution was stirred at room temperature until TLC and ESI MS analyses showed complete consumption of the starting material (2.5 hours). The respective amine (2 eqvi, 0.618 mmol in pyridine) was then added to the solution of activated carbonate ester of nucleoside forming the nucleoside carbamate in one-pot. At the end of 24 hours the reaction mixture was evaporated to dryness under vacuum. The resulting crude mixture was dissolved in ethyl acetate and washed with NaHCO<sub>3</sub> (2 x 15 ml) and brine (1 x 10 ml). The organic layer was dried over Na<sub>2</sub>SO<sub>4</sub> (anhydrous) and evaporated. Purification by normal phase flash chromatography (CH<sub>2</sub>Cl<sub>2</sub>/MeOH) afforded the respective compounds. The isolated product from the above step was deprotected using a solution of TFA/H<sub>2</sub>O (4:1, 2.5 ml) at rt. The reaction was completed in 20 minutes as indicated by TLC. The reaction mixture was evaporated and the product was purified by reverse phase flash chromatography (ACN/Water).

### **General procedure for the synthesis of using microwave**

To a cold, stirred solution of 2',3'-O-isopropylidene guanosine (1.0 eqvi, 0.309 mmol) in pyridine (5 mL), was added p-Cl phenyl chloroformate (1.2 eqvi 0.3708 mmol) dropwise over a period of 30 minutes. To the solution of an activated carbonate ester of nucleoside was added a respective amine (2 eqvi, 0.618 mmol in pyridine) to form nucleoside carbamate. The reaction vessel was sealed and pre-stirred for 30 sec. Next with high stirring; the vessel was heated at temperature of 50 °C, with power of 200 watt for 10 min in the microwave synthesizer. The resulting crude

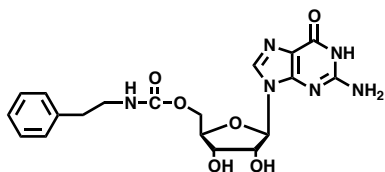
mixture was dissolved in ethyl acetate and washed with  $\text{NaHCO}_3$  (2 x 15 ml) and brine (1 x 10 ml). The organic layer was dried over  $\text{Na}_2\text{SO}_4$  (anhydrous) and evaporated. Purification by normal phase flash chromatography ( $\text{CH}_2\text{Cl}_2$ / MeOH) afforded the respective compounds in yields reported over two-steps. The yields for each carbamate inhibitor are reported in Table 1.



### Synthesis of 5'-O-[1-Ethyl]Carbamoyl Guanosine (1)

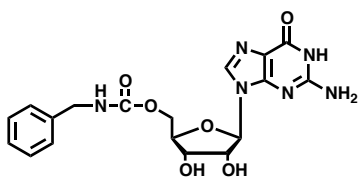
Here ethylamine was commercially available in the gaseous form and was transferred in three neck flask under anhydrous condition and cooled under  $-78\text{ }^{\circ}\text{C}$  to form liquid. The  $^1\text{H}$  NMR spectrum was (DMSO- $d_6$ ): 1.01 (t, 3H), 2.99 (q, 2H), 3.99-4.05 (m, 3H), 4.17 (m, 1H), 4.46 (m, 1H), 5.27 (t, 1H), 5.45 (t, 1H), 5.69 (t, 1H), 6.47 (s, 2H), 7.28 (m, 1H), 7.91 (s, 1H) and 10.63 (s, 1H).  $^{13}\text{C}$ -DMSO- $d_6$ : 157.21, 156.26, 154.20, 152.04, 135.93, 117.12, 86.43, 82.80, 73.46, 71.07, 64.37, 35.52 and 15.52 ppm. Low resolution ESI-MS [M+H] 355.1, HRMS (ESI+) calcd for  $\text{C}_{13}\text{H}_{18}\text{N}_5\text{O}_5$  [(M+H)+] 355.1366 found 355.1367





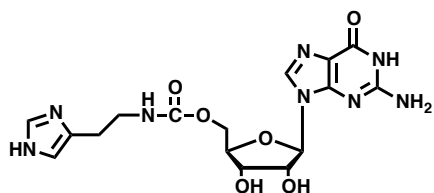
### Synthesis of 5'-O-[3-Phenyl-1-Ethyl]Carbamoyl Guanosine (2)

The  $^1\text{H}$  NMR spectrum was (DMSO- $d_6$ ): 2.69 (t, 2H), 3.19 (q, 2H), 4.00 (s, 1H), 4.01 (m, 2H), 4.01 (m, 2H), 4.17 (m, 1H), 4.48 (m, 1H), 5.28 (d, 1H), 5.44 (d, 1H), 5.70 (d, 1H), 6.47 (s, 2H), 7.20 (d, 3H), 7.26-7.28 (m, 2H), 7.41 (t, 1H), 7.91 (s, 1H) and 10.62 (s, 1H).  $^{13}\text{C}$ - DMSO- $d_6$ : 157.19, 156.38, 154.19, 152.03, 139.75, 135.95, 129.11, 128.81, 126.56, 117.15, 86.43, 82.77, 73.45, 71.05, 64.47, 42.5 and 36.0 ppm. Low resolution ESI-MS [M+H] 431.1, HRMS (ESI+) calcd for  $\text{C}_{13}\text{H}_{18}\text{N}_5\text{O}_5$  [(M+H)+] 431.1679 found 431.1675



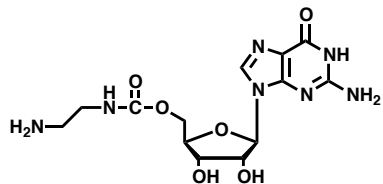
### Synthesis of 5'-O-[1-Benzyl]Carbamoyl Guanosine (3)

The  $^1\text{H}$  NMR spectrum was (DMSO- $d_6$ ): 4.08 (m, 3H), 4.20 (m, 3H), 4.48 (m, 1H), 5.28 (d, 1H), 5.45 (d, 1H), 5.70 (d, 1H), 6.47 (s, 2H), 7.24-7.26 (m, 3H), 7.31-7.33 (m, 3H), 7.88 (t, 1H) and 7.91 (s, 1H).  $^{13}\text{C}$ - DMSO- $d_6$ : 157.20, 156.72, 154.19, 152.04, 140.09, 135.95, 128.77, 127.49, 127.28, 117.12, 86.42, 82.74, 73.45, 71.04, 64.69 and 40.26. Low resolution ESI-MS [M+H] 416.9 HRMS (ESI+) calcd for  $\text{C}_{13}\text{H}_{18}\text{N}_5\text{O}_5$  [(M+H)+] 417.1523 found 417.1519



### Synthesis of 5'-O-[3-Imidazolyl-1-Ethyl]Carbamoyl Guanosine (4)

The  $^1\text{H}$  NMR spectrum was (DMSO- $d_6$ ): 2.75 (t, 3H), 3.99 (m, 1H), 4.05 (m, 2H), 4.18-4.21 (m, 1H), 4.46 (m, 1H), 5.30 (m, 1H), 5.48 (m, 1H), 5.71 (d, 1H), 6.5 (s, 2H), 7.41 (s, 1H), 7.47 (t, 1H), 7.86 (s, 1H), 8.90 (s, 1H), 10.66 (s, 1H) and 14.06.  $^{13}\text{C}$ - DMSO- $d_6$ : 157.20, 156.46, 154.22, 135.84, 134.38, 131.52, 129.14, 117.12, 116.71, 86.52, 82.64, 73.51, 71.02, 64.26, 60.92 and 25.40 ppm. Low resolution ESI-MS  $[\text{M}+\text{H}]$  421.2 HRMS (ESI+) calcd for  $\text{C}_{13}\text{H}_{18}\text{N}_5\text{O}_5$   $[(\text{M}+\text{H})^+]$  421.1584 found 421.1519



### Synthesis of 5'-O-[3-amino-1-Ethyl]Carbamoyl Guanosine (5)

The  $^1\text{H}$  NMR spectrum was (DMSO- $d_6$ ): 2.86 (t, 2H), 3.30 (q, 2H), 4.02 (m, 1H), 4.09-4.13 (m, 2H), 4.25 (d, 1H), 4.45 (q, 1H), 5.31 (d, 1H), 5.51 (d, 1H), 5.70 (d, 1H), 6.50 (s, 2H), 7.46 (t, 1H), 7.74 (s, 2H), 7.88 (s, 1H) and 10.66 (s, 1H).  $^{13}\text{C}$ - DMSO- $d_6$ : 157.20, 156.46, 154.23, 151.98, 135.86, 117.10, 86.62, 82.49, 73.53, 70.98, 64.95, 39.22 and 38.51 ppm. Low resolution ESI-MS [M+H] 370.2 HRMS (ESI+) calcd for  $\text{C}_{13}\text{H}_{18}\text{N}_5\text{O}_5$  [(M+H)+] 370.1475 found 370.1472

## References:

1. Basbaum, A. I.; Bautista, D. M.; Scherrer, G.; Julius, D., Cellular and molecular mechanisms of pain. *Cell* **2009**, *139* (2), 267-84.
2. Hucho, T.; Levine, J. D., Signaling pathways in sensitization: toward a nociceptor cell biology. *Neuron* **2007**, *55* (3), 365-76.
3. Woolf, C. J.; Salter, M. W., Neuronal plasticity: increasing the gain in pain. *Science* **2000**, *288* (5472), 1765-9.
4. Kandel, E. R.; Dudai, Y.; Mayford, M. R., The molecular and systems biology of memory. *Cell* **2014**, *157* (1), 163-86.
5. Gordley, R. M.; Williams, R. E.; Bashor, C. J.; Toettcher, J. E.; Yan, S.; Lim, W. A., Engineering dynamical control of cell fate switching using synthetic phospho-regulons. *Proc Natl Acad Sci U S A* **2016**, *113* (47), 13528-13533.
6. Ji, R. R.; Kohno, T.; Moore, K. A.; Woolf, C. J., Central sensitization and LTP: do pain and memory share similar mechanisms? *Trends Neurosci* **2003**, *26* (12), 696-705.
7. Liu, X. J.; Salter, M. W., Glutamate receptor phosphorylation and trafficking in pain plasticity in spinal cord dorsal horn. *Eur J Neurosci* **2010**, *32* (2), 278-89.
8. Chen, G.; Xie, R. G.; Gao, Y. J.; Xu, Z. Z.; Zhao, L. X.; Bang, S.; Berta, T.; Park, C. K.; Lay, M.; Chen, W.; Ji, R. R.,  $\beta$ -arrestin-2 regulates NMDA receptor function in spinal lamina II neurons and duration of persistent pain. *Nat Commun* **2016**, *7*, 12531.

9. Sakurada, T.; Manome, Y.; Tan-No, K.; Sakurada, S.; Kisara, K., The effects of substance P analogues on the scratching, biting and licking response induced by intrathecal injection of N-methyl-D-aspartate in mice. *Br J Pharmacol* **1990**, *101* (2), 307-10.
10. Aanonsen, L. M.; Wilcox, G. L., Phencyclidine selectively blocks a spinal action of N-methyl-D-aspartate in mice. *Neurosci Lett* **1986**, *67* (2), 191-7.
11. Masuyama, T.; Shimizu, T.; Iwashita, T.; Yoshimura, N.; Fukuda, T., Spinal antinociceptive effect of substance P on the responses induced by intrathecally injected NMDA in mice. *Brain Res* **1996**, *722* (1-2), 200-2.
12. Corder, G.; Doolen, S.; Donahue, R. R.; Winter, M. K.; Jutras, B. L.; He, Y.; Hu, X.; Wieskopf, J. S.; Mogil, J. S.; Storm, D. R.; Wang, Z. J.; McCarson, K. E.; Taylor, B. K., Constitutive  $\mu$ -opioid receptor activity leads to long-term endogenous analgesia and dependence. *Science* **2013**, *341* (6152), 1394-9.
13. Garzón, J.; Rodríguez-Muñoz, M.; Sánchez-Blázquez, P., Direct association of Mu-opioid and NMDA glutamate receptors supports their cross-regulation: molecular implications for opioid tolerance. *Curr Drug Abuse Rev* **2012**, *5* (3), 199-226.
14. Chou, T. F.; Baraniak, J.; Kaczmarek, R.; Zhou, X.; Cheng, J.; Ghosh, B.; Wagner, C. R., Phosphoramidate pronucleotides: a comparison of the phosphoramidase substrate specificity of human and Escherichia coli histidine triad nucleotide binding proteins. *Mol Pharm* **2007**, *4* (2), 208-17.
15. Lee, Y. N.; Nechushtan, H.; Figov, N.; Razin, E., The function of lysyl-tRNA synthetase and Ap4A as signaling regulators of MITF activity in FcepsilonRI-activated mast cells. *Immunity* **2004**, *20* (2), 145-51.

16. Genovese, G.; Ghosh, P.; Li, H.; Rettino, A.; Sioletic, S.; Cittadini, A.; Sgambato, A., The tumor suppressor HINT1 regulates MITF and  $\beta$ -catenin transcriptional activity in melanoma cells. *Cell Cycle* **2012**, *11* (11), 2206-15.
17. Motzik, A.; Amir, E.; Erlich, T.; Wang, J.; Kim, B. G.; Han, J. M.; Kim, J. H.; Nechushtan, H.; Guo, M.; Razin, E.; Tshori, S., Post-translational modification of HINT1 mediates activation of MITF transcriptional activity in human melanoma cells. *Oncogene* **2017**, *36* (33), 4732-4738.
18. Chou, T. F.; Wagner, C. R., Lysyl-tRNA synthetase-generated lysyl-adenylate is a substrate for histidine triad nucleotide binding proteins. *J Biol Chem* **2007**, *282* (7), 4719-27.
19. Guang, W.; Wang, H.; Su, T.; Weinstein, I. B.; Wang, J. B., Role of mPKCI, a novel mu-opioid receptor interactive protein, in receptor desensitization, phosphorylation, and morphine-induced analgesia. *Mol Pharmacol* **2004**, *66* (5), 1285-92.
20. Rodríguez-Muñoz, M.; Sánchez-Blázquez, P.; Vicente-Sánchez, A.; Bailón, C.; Martín-Aznar, B.; Garzón, J., The histidine triad nucleotide-binding protein 1 supports mu-opioid receptor-glutamate NMDA receptor cross-regulation. *Cell Mol Life Sci* **2011**, *68* (17), 2933-49.
21. Rodríguez-Muñoz, M.; Garzón, J., Nitric oxide and zinc-mediated protein assemblies involved in mu opioid receptor signaling. *Mol Neurobiol* **2013**, *48* (3), 769-82.
22. Sánchez-Blázquez, P.; Rodríguez-Muñoz, M.; Berrocoso, E.; Garzón, J., The plasticity of the association between mu-opioid receptor and glutamate ionotropic receptor N in opioid analgesic tolerance and neuropathic pain. *Eur J Pharmacol* **2013**, *716* (1-3), 94-105.
23. Shah, R.; Strom, A.; Zhou, A.; Maize, K. M.; Finzel, B. C.; Wagner, C. R., Design, Synthesis, and Characterization of Sulfamide and Sulfamate Nucleotidomimetic Inhibitors of hHint1. *ACS Med Chem Lett* **2016**, *7* (8), 780-4.

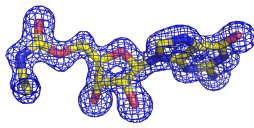
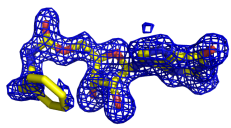
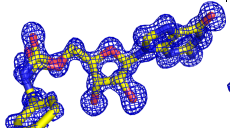
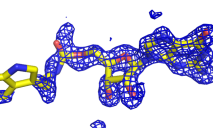
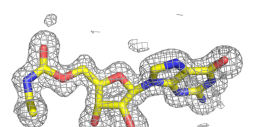
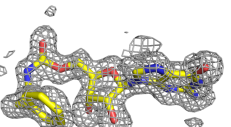
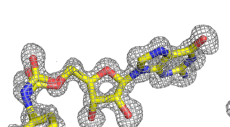
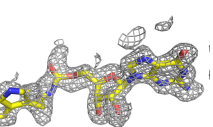
24. Garzón, J.; Herrero-Labrador, R.; Rodríguez-Muñoz, M.; Shah, R.; Vicente-Sánchez, A.; Wagner, C. R.; Sánchez-Blázquez, P., HINT1 protein: a new therapeutic target to enhance opioid antinociception and block mechanical allodynia. *Neuropharmacology* **2015**, *89*, 412-23.
25. Aanonsen, L. M.; Wilcox, G. L., Nociceptive action of excitatory amino acids in the mouse: effects of spinally administered opioids, phencyclidine and sigma agonists. *J Pharmacol Exp Ther* **1987**, *243* (1), 9-19.
26. Stone, L. S.; Fairbanks, C. A.; Laughlin, T. M.; Nguyen, H. O.; Bushy, T. M.; Wessendorf, M. W.; Wilcox, G. L., Spinal analgesic actions of the new endogenous opioid peptides endomorphin-1 and -2. *Neuroreport* **1997**, *8* (14), 3131-5.
27. Shah, R.; Zhou, A.; Wagner, C. R., Switch-on fluorescent/FRET probes to study human histidine triad nucleotide binding protein 1 (hHint1), a novel target for opioid tolerance and neuropathic pain. *Org Biomol Chem* **2017**, *15* (48), 10230-10237.
28. McCoy, A. J.; Grosse-Kunstleve, R. W.; Adams, P. D.; Winn, M. D.; Storoni, L. C.; Read, R. J., Phaser crystallographic software. *J Appl Crystallogr* **2007**, *40* (Pt 4), 658-674.
29. Adams, P. D.; Afonine, P. V.; Bunkóczi, G.; Chen, V. B.; Davis, I. W.; Echols, N.; Headd, J. J.; Hung, L. W.; Kapral, G. J.; Grosse-Kunstleve, R. W.; McCoy, A. J.; Moriarty, N. W.; Oeffner, R.; Read, R. J.; Richardson, D. C.; Richardson, J. S.; Terwilliger, T. C.; Zwart, P. H., PHENIX: a comprehensive Python-based system for macromolecular structure solution. *Acta Crystallogr D Biol Crystallogr* **2010**, *66* (Pt 2), 213-21.
30. Emsley, P.; Cowtan, K., Coot: model-building tools for molecular graphics. *Acta Crystallogr D Biol Crystallogr* **2004**, *60* (Pt 12 Pt 1), 2126-32.



31. Lebedev, A. A.; Young, P.; Isupov, M. N.; Moroz, O. V.; Vagin, A. A.; Murshudov, G. N., Jligand: a graphical tool for the CCP4 template-restraint library. *Acta Crystallogr D Biol Crystallogr* **2012**, *68* (Pt 4), 431-40.
32. Hylden, J. L.; Wilcox, G. L., Intrathecal morphine in mice: a new technique. *Eur J Pharmacol* **1980**, *67* (2-3), 313-6.
33. Tallarida, R. J.; Murray, R. B., Manual of pharmacological calculations with computer programs. *Springer Verlag:New York* **1987**, 26-31.
34. Tallarida, R. J.; Porreca, F.; Cowan, A., Statistical analysis of drug-drug and site-site interactions with isobolograms. *Life Sci* **1986**, *45*, 947-61.

## Supplemental Information:

### Supplemental Table 1: X-ray Crystallography Statistics

Ligand OMIT Map (mFo-DFc) Contoured at $3\sigma$ (Chain A)				
Ligand OMIT Map (mFo-DFc) Contoured at $2\sigma$ (Chain A)				
PDB ID Code	6N3V	6N3W	6N3X	6N3Y
Ligand ID	KB7	KBJ	KBD	HHJ
Resolution (Å)	1.45	1.75	1.10	1.80
Space group	C121	C121	C121	C121
a	77.92	77.97	77.87	78.16
b cell edges (Å)	46.30	46.21	46.41	46.33
c	63.96	63.84	64.03	63.90
Cell axis angle (°)	90.00 94.96 90.00	90.00 94.74 90.00	90.00 94.46 90.00	90.00 94.32 90.00
<b>Data Processing</b>				
Resolution range (Å) (high shell)	39.77-1.450 (1.530-1.450)	63.620-1.750 (1.840-1.750)	39.91-1.100 (1.160-1.100)	63.71-1.800 (1.806-1.800)
Observations measured (high shell)	145241 (19748)	81842 (11136)	316410 (43008)	67651 (578)
Unique reflections (high shell)	40242 (5836)	22184 (3330)	90215 (12885)	21005 (202)
Average multiplicity (high shell)	3.6 (3.4)	3.6 (3.3)	3.5 (3.3)	3.2 (2.9)
Completeness (%) (high shell)	99.7 (99.8)	99.2 (99.8)	97.7 (96.0)	98.5 (100.0)
$R_{merge}$ (high shell)	0.049 (0.374)	0.080 (0.335)	0.051 (0.333)	0.050 (0.141)
Mean $\langle I/\sigma I \rangle$ (high shell)	17.0 (3.2)	13.8 (3.5)	15.7 (3.2)	13.9 (5.5)
<b>Refinement statistics</b>				
Resolution range (Å) (high shell)	39.78-1.45 (1.484-1.450)	63.63-1.750 (1.83-1.75)	31.91-1.100 (1.112-1.100)	34.42-1.800 (1.895-1.800)

Working set reflections (high shell)	38138 (2514)	21666 (2666)	85576 (2710)	19939 (2854)
$R_{free}$ reflections (high shell)	2050 (124)	1108 (156)	4568 (159)	1038 (167)
$R$ (%) (high shell)	0.1568 (0.2251)	0.1532 (0.1736)	0.1617 (0.2386)	0.2048 (0.2202)
$R_{free}$ (%) (high shell)	0.1745 (0.2464)	0.1895 (0.2252)	0.1729 (0.2321)	0.2475 (0.2929)
No. of non-hydrogen atoms	2075	1870	2246	2120
No. of solvent waters	190	192	288	55
<i>Mean B-factors (<math>\text{\AA}^2</math>)</i>				
Protein atoms	13.23	11.19	8.88	16.56
Solvent atoms	23.76	19.73	19.41	18.49
Ligand atoms	13.38	15.19	9.25	29.22
<hr/> <i>RMS deviations From Ideal Geometry</i> <hr/>				
Bond lengths ( $\text{\AA}$ )	0.005	0.006	0.005	0.006
Bond angles ( $^\circ$ )	0.84	0.847	0.882	0.895
Ramachandran plot outliers (%)	0.00	0.00	0.00	0.00
MolProbity score	0.99	1.19	1.12	1.3

## **Chapter 3**

### **Development of HINT1 Inhibitors to Selectively Modulate MOR-NMDAR Cross Regulation**

## Abstract

The Human Histidine Triad Nucleotide Binding Protein 1 (HINT1) has recently become a protein of interest due to its involvement in several CNS processes, including neuroplasticity and the development of several neuropsychiatric disorders. Crucially, HINT1 behaves as a mediator for the cross regulation of the mu opioid receptor (MOR) and *N*-methyl-D-aspartate receptor (NMDAR). Active site inhibition of HINT1 using small molecule inhibitors has been demonstrated to have a significant impact on this cross-regulatory relationship *in vivo*. Herein, we describe the development of a series of ethenoadenosine HINT1 inhibitors to further evaluate the effect of HINT1 inhibition on morphine's blockade of NMDA-evoked behaviors and the development of acute endomorphin-2 tolerance. X-ray crystallographic analysis and HINT1 binding experiments demonstrate that modifications to the inhibitor nucleobase greatly impact the inhibitor binding interactions with HINT1. Our results reveal a complex structural-activity relationship for HINT1 inhibitors in which minor modifications to the ethenoadenosine scaffold resulted in dramatic changes to their activity in these assays modeling MOR-NMDAR interaction. Specifically, we observed the ability of HINT1 inhibitors to selectively affect individual pathways of MOR-NMDAR crosstalk. These studies highlight the critical role of HINT1 in MOR-NMDAR crosstalk and demonstrate the intriguing potential of using HINT1 active-site inhibitors as tools to probe its role in these biochemical pathways.

## Introduction

HINT1 has recently garnered interest due to its involvement in several CNS processes and its association with the development of multiple neuropsychiatric disorders.<sup>1, 2</sup> Additionally, targeting HINT1 using small molecule HINT1 inhibitors has demonstrated its potential as a target for pain therapy.<sup>3, 4</sup> The histidine triad nucleotide binding protein 1 (HINT1) is a member of the ubiquitously expressed and ancient superfamily of histidine triad (HIT) proteins, which are characterized by their conserved catalytic sequence His-X-His-X-His-X-X, where X is a hydrophobic residue. HINT1 is a 14 kD homodimer that possesses phosphoramidase and acyl-AMP hydrolase activity, with a preference for purine over pyrimidine nucleoside substrates.<sup>5, 6</sup> This catalytic activity is crucial for the activation of several clinically relevant nucleoside phosphoramidate prodrugs, but the endogenous function and substrate of HINT1 are not well understood.<sup>7, 8</sup> While the exact role of HINT1's enzymatic activity still remains a mystery, HINT1 is observed to participate in wide array of biological processes such as tumor suppression, mast cell activation, and apoptosis.<sup>9-11</sup> HINT1 participates in these processes via interaction with transcription factor complexes such as pontin and reptin, LEC/TCF, and MITF/USF2.<sup>9-11</sup> The involvement of HINT1 in such a range of processes makes it an exciting target for further evaluation.

HINT1 has widespread expression in the CNS, with the high levels observed in cerebral cortex, periaqueductal gray area, and nucleus accumbens, which are responsible for motor and sensory functions, modulation of pain, and addiction properties respectively.<sup>12</sup> Alterations to HINT1 expression and HINT1 mutations have been associated with the development of several neuropsychiatric disorders including schizophrenia, addiction, and inherited peripheral neuropathies.<sup>1, 13-16</sup> HINT1<sup>-/-</sup> mice display several behavioral changes compared to their wildtype

counterparts, including decreased nicotine dependence, hypersensitivity to amphetamines, and increased anxiety and depression-like behaviors, demonstrating a crucial role for HINT1 in several CNS processes.<sup>13, 14, 17, 18</sup> Further, HINT1 regulates the signaling of several CNS receptors such as the mu opioid receptor (MOR), cannabinoid receptors, transient receptor potential cation channels, and sigma receptors, making it an extremely interesting target for pharmacological interrogation.<sup>19-22</sup> In the case of MOR, HINT1 is critical in mediating the cross-regulation observed between MOR and the N-methyl-D-aspartate receptor (NMDAR).<sup>22</sup> Following opioid activation of MOR and its subsequent analgesic pathway, HINT1 mediates the formation of several protein assemblies which lead to the activation of NMDAR.<sup>2</sup> The resulting signaling cascade ultimately leads to phosphorylation of MOR and downregulation of its signaling.<sup>22</sup>

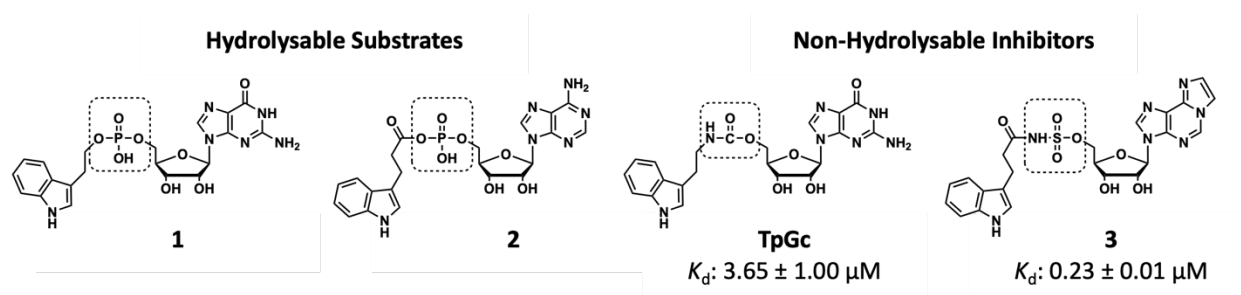
Previously, our lab has developed small molecule HINT1 inhibitors via replacement of hydrolysable phosphoramidate and acyl-monophosphate groups of compounds **1** and **2** with non-hydrolysable bioisosteres such as the carbamates and acyl-sulfamates, as shown by **TrpGc** and **3**, respectively (**Figure 1**). We have demonstrated that active-site inhibition of HINT1 using these nucleoside-based inhibitors has a striking effect on several pain pathways *in vivo*. Treatment of mice with morphine and our HINT1 inhibitor **TrpGc** results in an increased analgesic response and decreased development of morphine tolerance.<sup>3</sup> Crucially, these effects were not observed in HINT1<sup>-/-</sup> mice following treatment with **TrpGc**.<sup>3</sup> Assessment of a series of HINT1 inhibitors in two forms of MOR-NMDAR crosstalk, namely MOR inhibition of NMDAR activation and endomorphin-2 tolerance, demonstrated the first SAR of HINT1 inhibition and continued to establish the stark pharmacological effect of HINT1 inhibition in these processes.<sup>4</sup> Notably, the tryptamine side chain of our HINT1 inhibitors does not contribute significantly to HINT1 binding,

but is crucial to the *in vivo* activity of HINT1 inhibitors.<sup>4</sup> Additionally, both carbamate and acyl-sulfamate based HINT1 inhibitors were capable of blocking MOR inhibition of NMDAR evoked thermal hypersensitivity, but only the carbamate based **TrpGc** blocked the development of endomorphin-2 tolerance.<sup>4</sup> Interestingly, we found that the binding affinity of HINT1 inhibitors did not correlate to their activity *in vivo*. Importantly, we observed that active-site inhibition of HINT1 with small molecules can have selective effects across these assays, though the mechanism behind these effects is not clear.

With the intriguing results from our previous SAR studies, specifically the ability of certain inhibitors to selectively impact individual pathways in MOR-NMDAR crosstalk, we sought expand our arsenal of HINT1 inhibitors and further probe the pharmacological effects of HINT1 inhibition. Due to the high binding affinity and selective activity of our previously reported ethenoadenosine based inhibitor, Compound **3**, we have designed and synthesized a series of substituted ethenoadenosine based inhibitors.<sup>4, 23</sup> Importantly, due to the differential activities of the carbamate and acyl-sulfamate backbones, we have synthesized both analogues for each inhibitor. We have evaluated the binding of each of these inhibitors via their inhibition of HINT1 hydrolysis using our previously reported continuous fluorescence assay.<sup>24</sup> Additionally, we analyzed the binding interactions of these inhibitors via X-ray crystallographic analysis. Finally, we evaluated each of these inhibitors for their ability to block MOR inhibition of NMDAR activation, prevent endomorphin-2 tolerance, and produce an analgesic response following spinal administration. These results highlight the intriguing role of HINT1 in MOR-NMDAR crosstalk and the pharmacological opportunities provided by small molecule inhibition of HINT1.



Figure 1



**HINT1 Substrates and Previously Developed HINT1 Inhibitors.** Notable HINT1 substrates and inhibitors. Dissociation constants for **TpGc** and **3** binding to HINT1 were previously reported.<sup>3,23</sup>

## Results

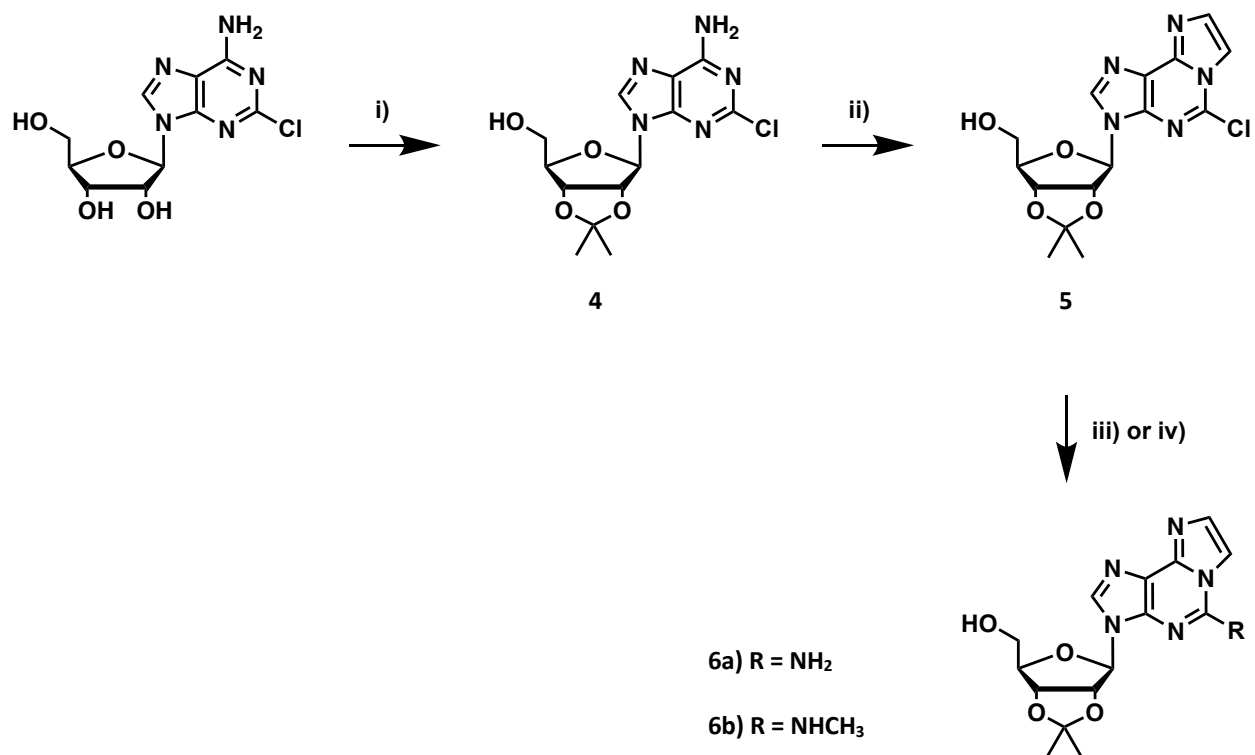
### Modifications to the Ethenoadenosine Base Alter Inhibitor Binding to HINT1

We began by examining the impact of substitution to the ethenoadenosine base for our nucleoside carbamate inhibitors by evaluating their inhibition of HINT1 enzymatic activity. Due to the hydrogen bond observed between the 2-amino group of the guanosine base of HINT1 inhibitors and the backbone carbonyl of His42 of HINT1, we hypothesized that addition of an amine to the 2-position of the ethenoadenosine base could result in a similar hydrogen bond and improved inhibitor binding affinity.<sup>4</sup> To probe the SAR of this position, we designed a series of three ethenoadenosine-based carbamate inhibitors (**Compounds 8-10**) with varying degrees of substitution at the 2-position. Synthesis of **8** and **9** proceeded via the common intermediate **5**. We proceeded beginning with the commercially available 2-chloroadenosine. First, acetonide protection of the 2', 3' – OH was achieved using perchloric acid in acetone followed by neutralization with ammonium hydroxide to yield **4**. Cyclization of the exocyclic amine was achieved with an aqueous solution of chloroacetaldehyde in mildly acidic sodium acetate buffer at 40° C, yielding the fluorescent product and common intermediate **5**. Substitution of the 2-chloro group in compound **5** using the respective amine yielded the nucleoside products **6a** and **6b**. Synthesis of the carbamate inhibitors **8** and **9** proceeded beginning with nucleoside intermediates **6a** and **6b**. The intermediate nucleoside **6c**, lacking any substitution at the two position was synthesized as previously reported and served as the starting point for compound **10**.<sup>23</sup> The carbamate backbone was achieved via a two-step one-pot coupling reaction. Addition of *p*-nitrophenyl chloroformate to **6a-c** in pyridine yielded the activated carbonate ester

intermediate. Dropwise addition of tryptamine in pyridine to this intermediate produces the penultimate products **7a-c**. Treatment of **7a-c** with trifluoroacetic acid in water results in efficient acetonide deprotection, yielding the final products **8-10**. Addition of bulk to the 2-position was detrimental to enzymatic inhibition of hHINT1, as observed via determination of the inhibitor  $K_i$  by our lab's previously reported continuous fluorescence assay (**Table 1**).<sup>24</sup> Specifically, the non-substituted ethenoadenosine carbamate **10**, had the lowest  $K_i$  of the three inhibitors. Addition of the 2-amino group in **8** increased the  $K_i$  10-fold, while the 2-methylamino containing compound **9** resulted in a roughly 60-fold increase compared to compound **10**.

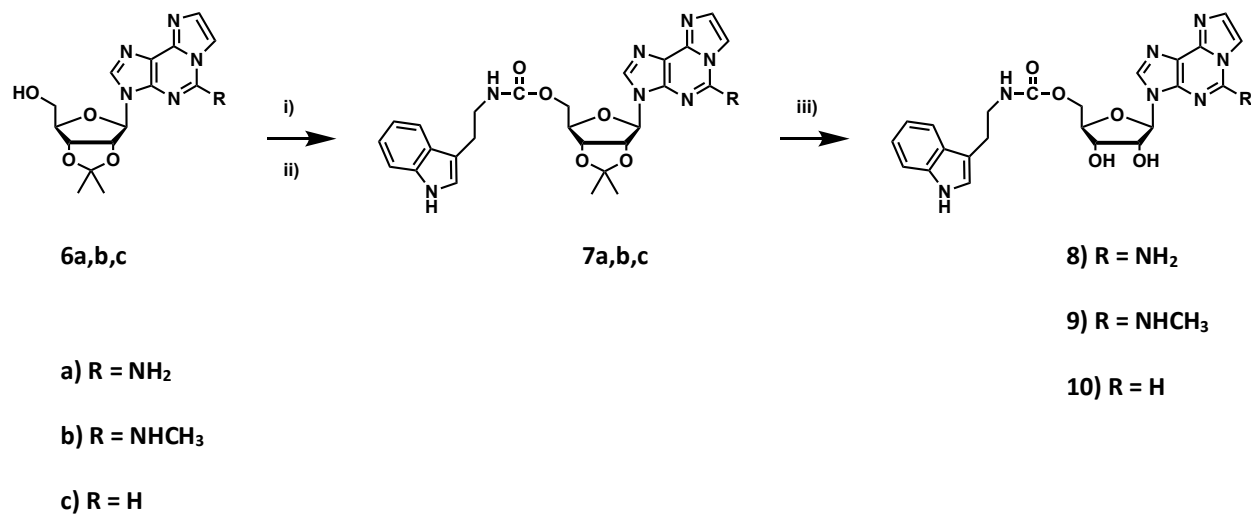
Next, we evaluated the effect of ethenoadenosine modifications to the acyl-sulfamate containing nucleoside inhibitors. Synthesis of the acyl-sulfamate inhibitors was achieved using our lab's previously reported synthetic route beginning with compounds **6a** and **6b**.<sup>23</sup> Treatment of compounds **6a,b** with sulfamoyl chloride and triethylamine in DMA yielded compounds **11a,b**. Coupling of **11a,b** with the *N*-hydroxysuccinic acid ester of 3-indole propionic acid (**15**) in the presence of DBU yielded the penultimate products **12a,b**. Deprotection of the acetonide group with aqueous TFA yielded the final products **13** and **14** in good yield. Substitution at the 2-position did not have the same effect on HINT1 binding for the acyl-sulfamate series as it did for the carbamates. Compound **14**, possessing the  $N^2$ -methyl group, had an inhibition constant roughly half that of **13** (**Table 2**). Replacement of the carbamate backbone of **9**, with the acyl-sulfamate backbone of **14** resulted in a 10-fold improvement in  $K_i$ , a result which we have observed with

Scheme 1



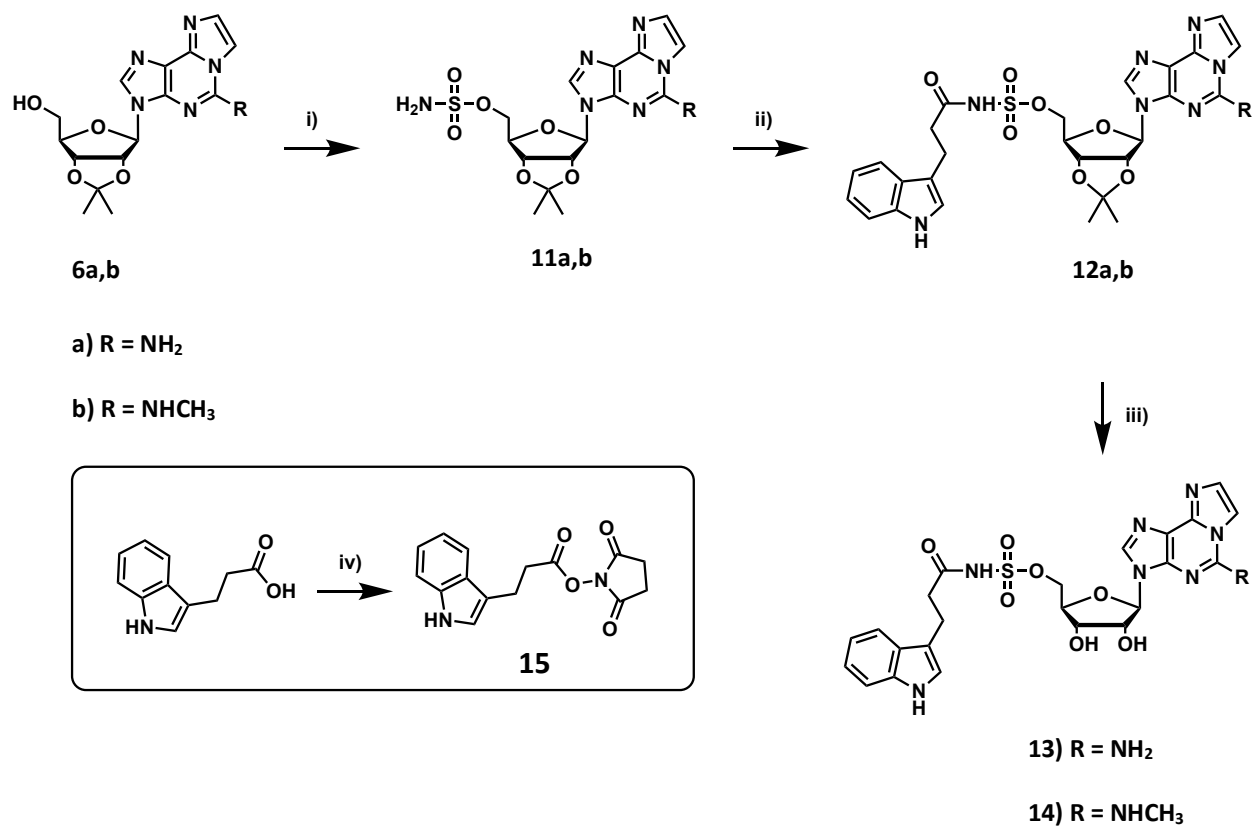
**Synthetic Strategy for Preparation of Nucleoside Precursors 6a and 6b.** Reagents and conditions: (i) Acetone, perchloric acid, rt, 3 h; (ii) chloroacetaldehyde solution in H<sub>2</sub>O 50% wv, 0.1 M sodium acetate buffer pH 6.5, 40° C, 24 h; iii) 2.0 M NH<sub>3</sub>/Isopropanol, 75° C, sealed tube, on; iv) 2.0 M methylamine/THF, rt, on.

## Scheme 2



**Synthetic Scheme for the Preparation of Target Compounds 8-10.** Reagents and conditions: i) p-NO-phenyl chloroformate, pyridine, rt, 3 h; ii) Tryptamine, pyridine, rt, on; iii) 4:1 TFA:H<sub>2</sub>O, rt, 30 min.

**Scheme 3**



**Synthetic Scheme for the Preparation of Target Compounds 13 and 14.** Reagents and conditions:

i) Sulfamoyl chloride, TEA, DMF, 0° C, 1 h; ii) **15**, DBU, DMF, 0° C, 1 h, rt, on; iii) 4:1 TFA:H<sub>2</sub>O, rt, 30 min; iv) NHS, EDC, THF, rt, 21 h.

our previous inhibitors.<sup>4</sup> However, this improvement was not observed for compounds **8** and **13**, which possess the exocyclic amine at the 2-position, but lack the N<sup>2</sup>-methyl modification, as these compounds had similar inhibition constants for HINT1.

### **X-Ray Crystallography Reveals the Impact of Ethenoadenosine Base Modifications on Inhibitor Binding to HINT1**

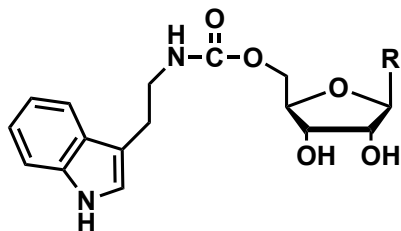
To examine the molecular interactions responsible for inhibitor/HINT1 binding, we obtained high resolution X-ray crystallographic structures for compounds (**8-10, 13, 14**) bound to HINT1 (**Figure 2**). Crucially, each of the new inhibitors displayed the typical HINT1 binding position and interactions observed in our previously obtained crystal structures. Notably, the 2', 3'-OH of each inhibitor ribose forms a tight hydrogen bond with the side chain of Asp43 (2.5-2.7 Å) of HINT1. Further, each inhibitor occupies the hydrophobic binding pocket composed of Ile18, Phe19, Ile22, Phe41, and Ile44. However, substitution of the ethenoadenosine base had a significant impact on the position of each nucleobase for inhibitors **8-10** (**Figure 3A**), with increasing bulk shifting the base further out in the hydrophobic pocket. Compound **10**, lacking any substitution, sat deepest in the binding pocket, while **9**, containing the 2-methylamino substitution was pushed furthest out due the added steric bulk of this modification. Additionally, to accommodate the increased size of **9** its ribose is slightly out of alignment with **8** and **10** (**Figure 3A**), though it still maintains its tight hydrogen bonds with Asp43. In agreement with our hypothesis, the 2-amino group of **8** formed a tight hydrogen bond with the backbone carbonyl of His42 (**Figure 3A,B**). Comparison of the crystal structures of **8** and **TrpGc** reveals that the 2-amino group of each inhibitor participates in a nearly identical hydrogen bonding interaction (**Figure 3B**). Despite this

additional hydrogen bond, **10** still binds favorably to hHINT1 compared **8** when looking at their  $K_i$ s, indicating that the additional H-bond does not outweigh the shift in nucleobase position required to accommodate this modification.

As expected, the position of the carbamate group does not appear to be severely impacted by the alterations made at the ethenoadenosine base, as indicated by both the similar angle of the carbamate groups and the distance between the carbon centers and the nucleophilic nitrogen of His112 (3.1-3.3 Å). However, while the tryptamine side chains of **8** and **10** occupy similar positions, the indole of **9** appears to be rotated roughly 90 degrees, resulting in the indole pointing away from the binding pocket. This is potentially due to the larger size of the nucleobase in **9**. Comparison of the two acyl-sulfamate compounds **13** and **14** reveals a significant change in the backbone geometry between the two inhibitors (**Figure 4**). The acyl sulfamate of **13** displays a similar binding mode to our previously reported **3**, in which the side chain acyl group participates in a hydrogen bond with Ser107 (2.9 Å). By comparison, the side chain acyl group of **14** is rotated roughly 90 degrees away from the side chain of Ser107. As a result, the distance between the acyl group and Ser107 is too far for a potential hydrogen bond (3.8 Å). However, the absence of this hydrogen bond does not appear detrimental to HINT1 binding for **14**, as its  $K_i$  is roughly two-fold lower than **13** (**Table 2**). The sulfamate inhibitors also display differences in tryptamine position, with the indole groups of **13** and **14** flipped 180° from each other (**Figure 4**). The differences in side chain position, especially the solvent accessible indole, could contribute to their unique pharmacology *in vivo*.

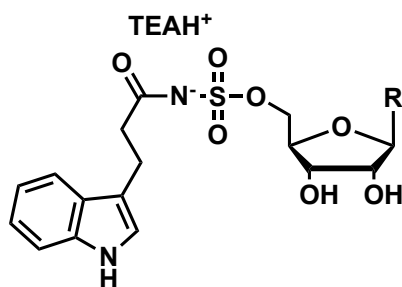


**Table 1**



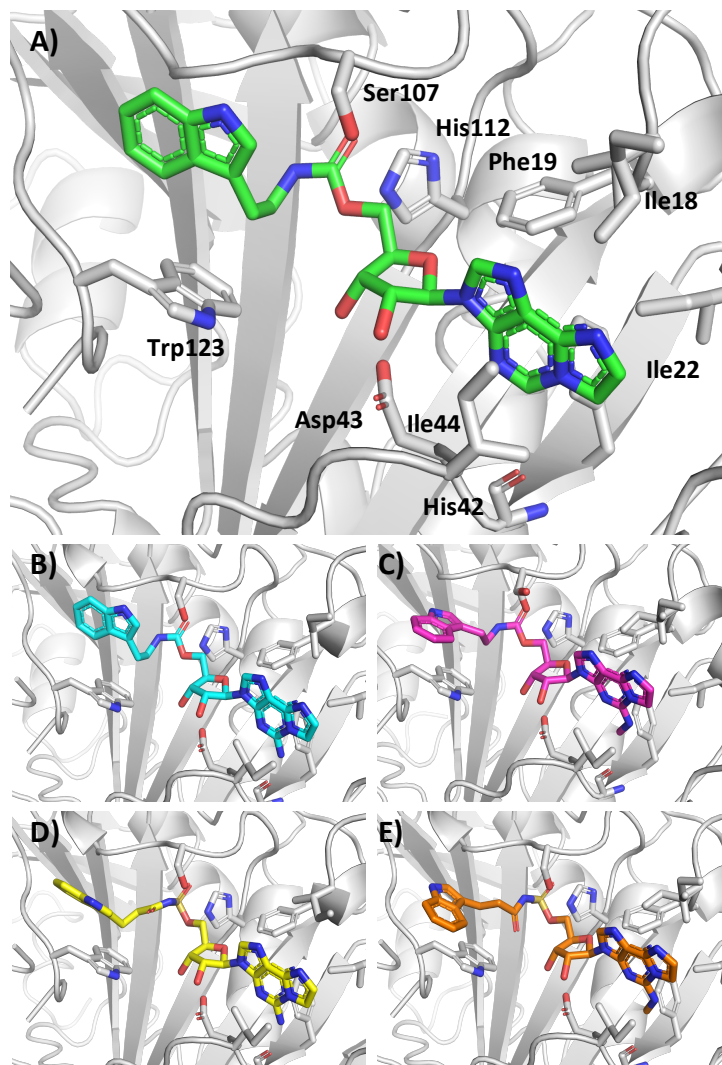
Compound	R	$K_i$ ( $\mu\text{M}$ )
8		$1.14 \pm 0.07$
9		$6.31 \pm 0.09$
10		$0.132 \pm 0.064$

Table 2



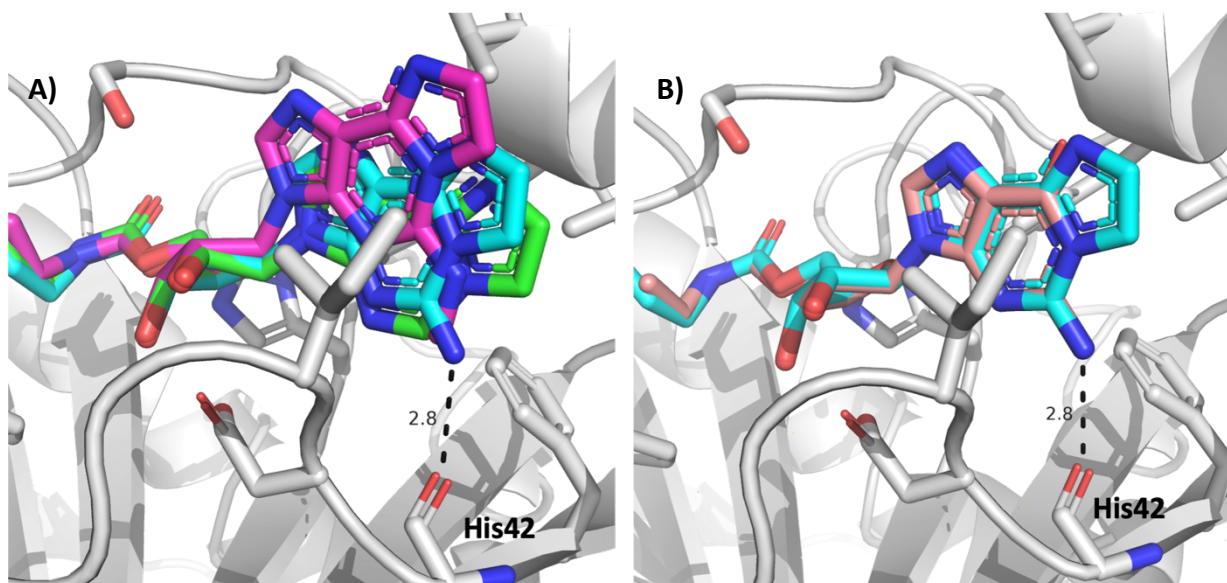
Compound	R	K <sub>i</sub> (μM)
13		1.43 ± 0.08
14		0.730 ± 0.090

Figure 2



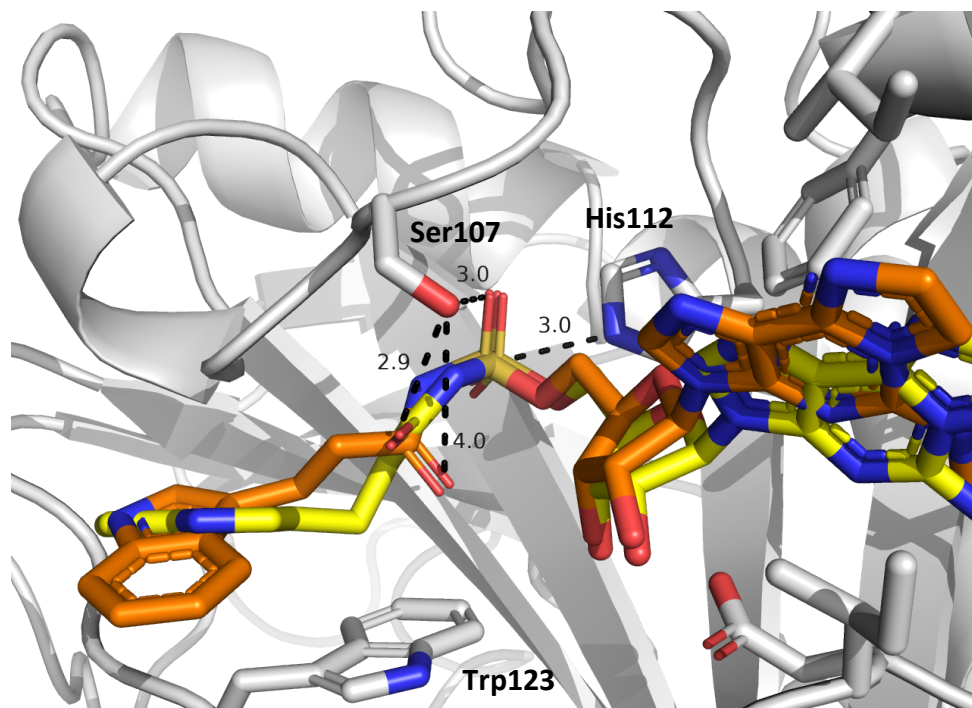
**Co-crystal structures of Compounds 8-10, 13, 14 bound to HINT1.** A) Compound **10** (Green) bound to HINT1 (gray) depicted as a cartoon. Key residues are labeled. A) Compound **10** (Green). B) Compound **8** (Cyan). C) Compound **9** (Magenta). D) Compound **13** (Yellow). E) Compound **14** (Orange).

**Figure 3**



**Comparison of Nucleoside Positioning for HINT1 Inhibitors.** A) Carbamate Series of HINT1 inhibitors bound to HINT1; Compound **8** (Cyan), **9** (Magenta), and **10** (Green). Increasing nucleobase size results in displacement of the ethenoadenosine base. Compound **8** forms a tight hydrogen bond with the backbone carbonyl of His42. B) Compound **8** (Cyan) and **TrpGc** (Light Pink) (PDB: **6N3V**) bound to HINT1. The 2-aminoethenoadenosine and guanosine nucleobases form identical hydrogen bonds to the backbone carbonyl of His42.

Figure 4



**Comparison of Acyl-Sulfamate Side Chains for Compounds 13 and 14 Bound to HINT1.** The acyl-sulfamate side chains of compound **13** (Yellow) and **14** (orange) display different geometries. The acyl-group of **13** makes a tight hydrogen bond to Ser107 (2.9 Å), while the side chain of **14** is rotated 90°, no longer in position to form a hydrogen bond. The indoles of **13** and **14** are rotated 180° from each other. The sulfamate groups of both inhibitors are in similar positions, with the sulfamate group in close position to active site His112 and hydrogen bonding to Ser107.

## **TrpGc Blocks Morphine's Inhibition of NMDA-Evoked Behaviors and Thermal Hyperalgesia**

As previously described, NMDA delivered to the intrathecal space of the spinal cord produces a set of quantifiable nociceptive behaviors in mice: first, a transient, caudally-directed set of scratching and biting behaviors and second, a transient thermal hyperalgesia that is observed using the warm water tail flick assay. Both the behavioral scratching and the thermal hyperalgesia can be inhibited by delivery of morphine prior to NMDA (**Figure 5**). This response is calculated as the percent maximum possible effect (%MPE). We first assessed whether the HINT1 inhibitor compounds were effective at reducing morphine's efficacy at reducing the NMDA-induced scratching and biting behaviors. While **TrpGc** effectively reduced morphine's efficacy in this assay, consistent with previous reports, none of the newly developed compounds showed similar efficacy (**Figure 5A**).<sup>4</sup> The observed ED<sub>50</sub> for TrpGc was 0.56nmol (0.21 – 1.4nmol, CI), consistent with our previous report.<sup>4</sup> The ED<sub>50</sub> could not be calculated for any other tested compound due to the lack of efficacy.

Following assessment of the scratching and biting behaviors, the same subjects were then tested for the presence of transient thermal hyperalgesia in the warm water tail flick assay, and their responses were compared to a pre-NMDA baseline tail flick. While subjects who receive only NMDA show a decrease in their tail flick, termed delta tail flick, subjects pre-treated with morphine do not display this transient thermal hypersensitivity (**Figure 5B**). **TrpGc** again significantly inhibited morphine's efficacy in preventing this thermal hypersensitivity, with **10** showing a similar effect, but the 10 nmol dose was not statistically significant different from morphine alone. Compounds **9** and **14** had little impact on morphine's efficacy in this assay, while compound **8** delivered alongside morphine showed a marked and significant

decrease in thermal hypersensitivity as measured by an increase in tail flick latency as compared to morphine alone, suggesting either enhancement of morphine efficacy or a direct analgesic effect of compound **8** in this assay.

### **Intrathecal Administration of 8, but No Other Inhibitor Leads to the Development of Analgesia**

To assess the analgesic efficacy of the line of Hint1 inhibitor compounds as single agents rather than in combination with morphine, mice were intrathecally injected with increasing doses of the HINT1 inhibitor and their responses in the warm water tail flick assay were evaluated. Once again, **8** showed an analgesic effect whereas the rest of the Hint1 compounds did not show analgesic efficacy in this assay (**Figure 6**).

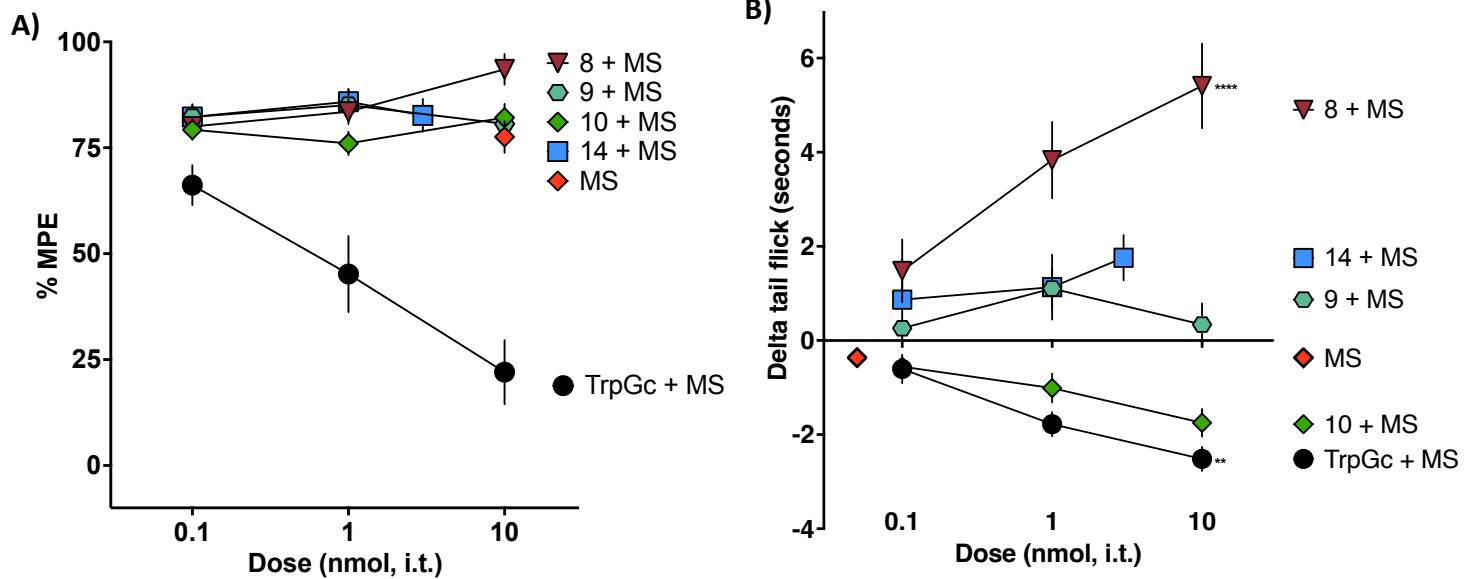
### **TrpGc and 9 Inhibit Endomorphin-2 Tolerance**

Endomorphin-2, an endogenous MOR agonist, produces acute tolerance when delivered to the intrathecal space. Male and female mice were pre-treated with either vehicle control or a tolerance-inducing dose of endomorphin-2. 30 minutes following this first injection, tail flick latencies return to baseline levels and a second injection of endomorphin-2 was administered. Following this second injection, tail flick latencies are again assessed. Mice that receive a vehicle pre-treatment demonstrated full antinociception following the second injection, the probe dose of endomorphin-2. However, mice pre-treated with endomorphin-2 showed reduced antinociception following the probe dose, a demonstration of acute spinal tolerance. To determine whether the inhibitor compounds could effectively inhibit the development of acute

spinal tolerance, mice were pretreated with HINT1 inhibitor. **TrpGc** and **9** reduced the magnitude of acute spinal analgesic tolerance, whereas **13** and **14** displayed potentiated tolerance.

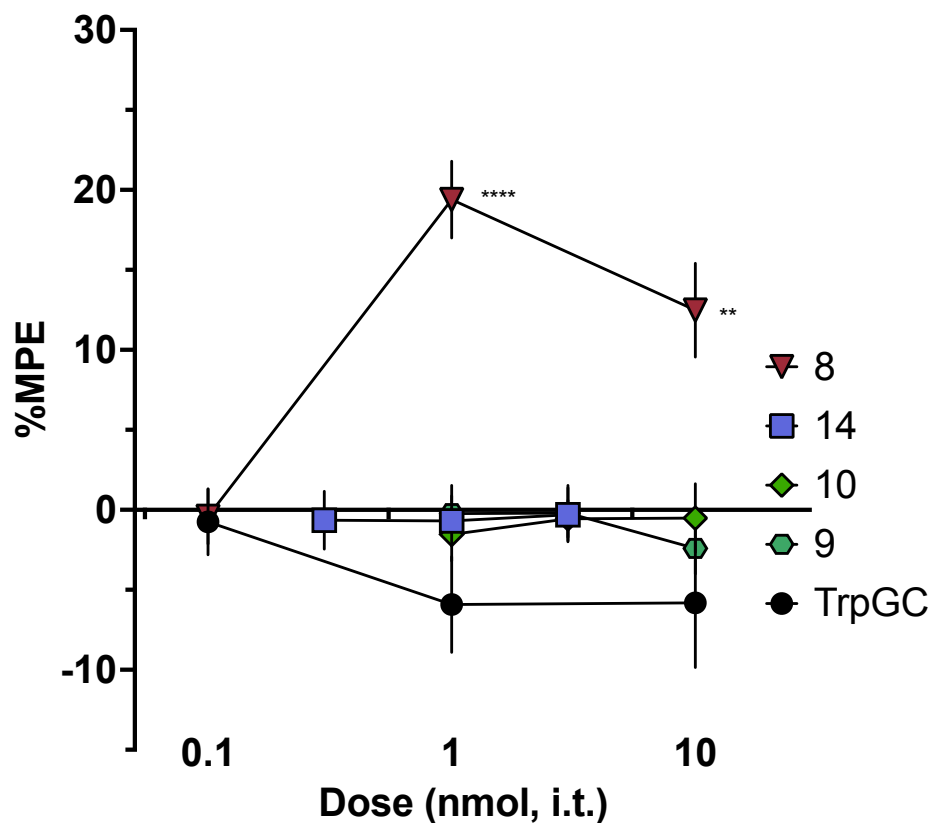


Figure 5



**HINT1 Inhibitors Effect on Morphine's Inhibition of NMDA-Evoked Nociceptive Behaviors.** Male and female mice were given intrathecal treatment of either morphine sulfate (MS) or MS + a HINT1 inhibitor. They were then given an intrathecal injection of NMDA and scratching and biting behaviors were counted and transient thermal hypersensitivity was measured by tail flick assay. (A) TrpGc alone inhibited MS's inhibition of scratching and biting behaviors, with an observed ED50 of 0.56 nmol (0.2-1.4 nmol, CI). ED50s could not be calculated for any other compound due to a lack of a dose-related effect in this assay. (B) Pretreatment with TrpGc (black circles) significantly attenuated MS-mediated inhibition of NMDA-evoked transient thermal hypersensitivity, whereas pretreatment with compound 8 enhanced MS-mediated prevention of the development of thermal hypersensitivity following intrathecally-delivered NMDA. \*\* $p < 0.01$ , \*\*\*\*  $p < 0.0001$ . One-way ANOVA with Dunnett's posthoc test with multiple comparisons to a control (MS delivered alone).

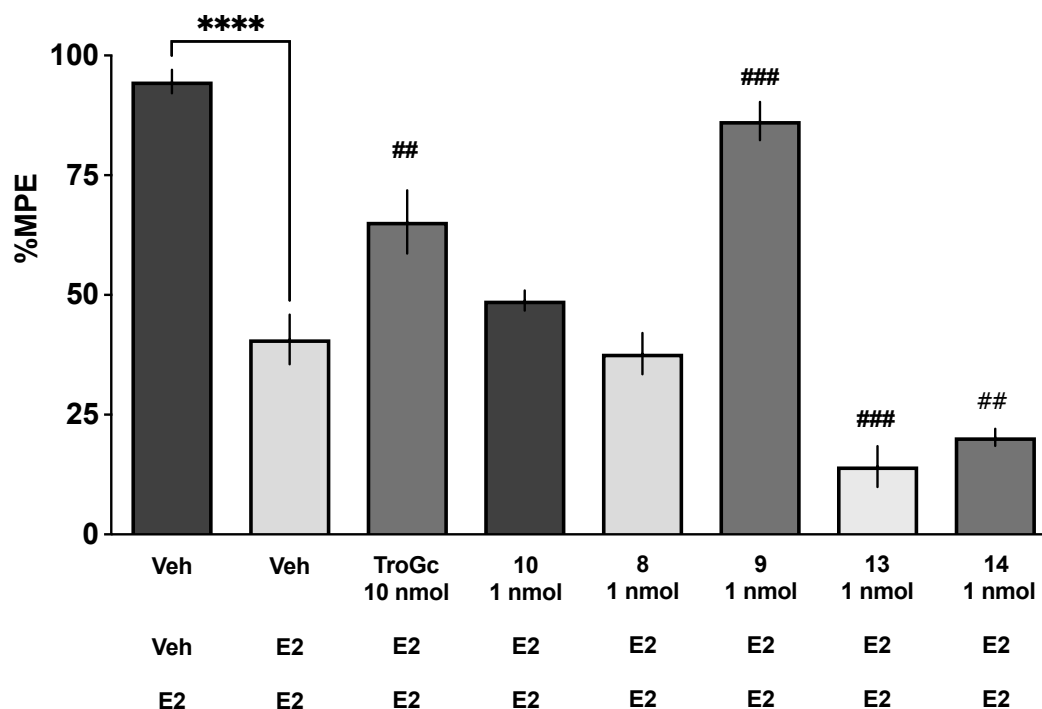
Figure 6



#### Analysis of Analgesia Following Intrathecal Dosing of HINT1 Inhibitors.

Assessment of Hint1 inhibitors in warm water tail immersion assay. Following baseline tail flick assessment, subjects were given intrathecal injections of increasing doses of TrpGc or Hint1 analogue compound, and tail flick latency was again assessed. Responses are reported as %MPE, which was used to generate dose-response curves. Compound 8 showed increasing MPE at 1 and 10 nmol, i.t. doses as compared to 0.1 nmol, while the other compounds did not have a dose-related effect. \*\* $p < 0.01$ , \*\*\*\* $p < 0.0001$ . One-way ANOVA with Dunnett's posthoc test with multiple comparisons to a control (0.1 nmol dose).

Figure 7



**TrpGc and 9 inhibit endomorphin-2 tolerance.** The spinal antinociceptive effect of endomorphin-2 is significantly greater in male and female mice pretreated with vehicle (leftmost column) as compared with mice pretreated with endomorphin-2 (2<sup>nd</sup> column), indicating an ultrarapid development of tolerance, as previously described. Treatment with TrpGc prior to the first endo-2 injection can prevent this development of tolerance. The TrpGc analogues 506.52 and 641.72 were also able to prevent the development of endo-2 tolerance. \*\*\*\*\* indicates significant difference from saline-endo-2 control by Student's t-test,  $p < 0.001$ . # indicates significant difference from pre-treatment with endomorphin-2 alone (2<sup>nd</sup> column) by one-way ANOVA with Dunnett's posthoc test with multiple comparisons to a control.

## Conclusions

Previous works by our lab have demonstrated the exciting potential for small molecule HINT1 inhibitors to affect various pain pathways. Based on the tight binding and unique pharmacological effect of **3**, our lab sought to develop ethenoadenosine based analogues with the goals of improving HINT1 enzymatic inhibition and furthering our understanding of the role of HINT1 in the interplay of MOR and NMDAR. *In vitro*, we confirmed our hypothesis that addition of the 2-amino group to the ethenoadenosine nucleobase (compounds **8** and **13**) results in the formation of a hydrogen bond with the backbone carbonyl of His42, identical to that of the guanosine-based inhibitor **TrpGc**. Despite this, compound **10**, which lacks the amine at the 2-position, was the strongest inhibitor of HINT1 enzymatic activity as observed by our continuous fluorescence assay. Further, addition of the N<sup>2</sup>-methyl group to the exocyclic amine (compounds **9** and **14**) disrupts this hydrogen bond and shifts the nucleobase further up in the hydrophobic pocket. Interestingly, while this modification resulted in decreased binding for the carbamate inhibitors (Compound **8** and **9**), the addition of the N<sup>6</sup>-methyl group improved binding for the acyl-sulfamates (Compounds **13** and **14**).

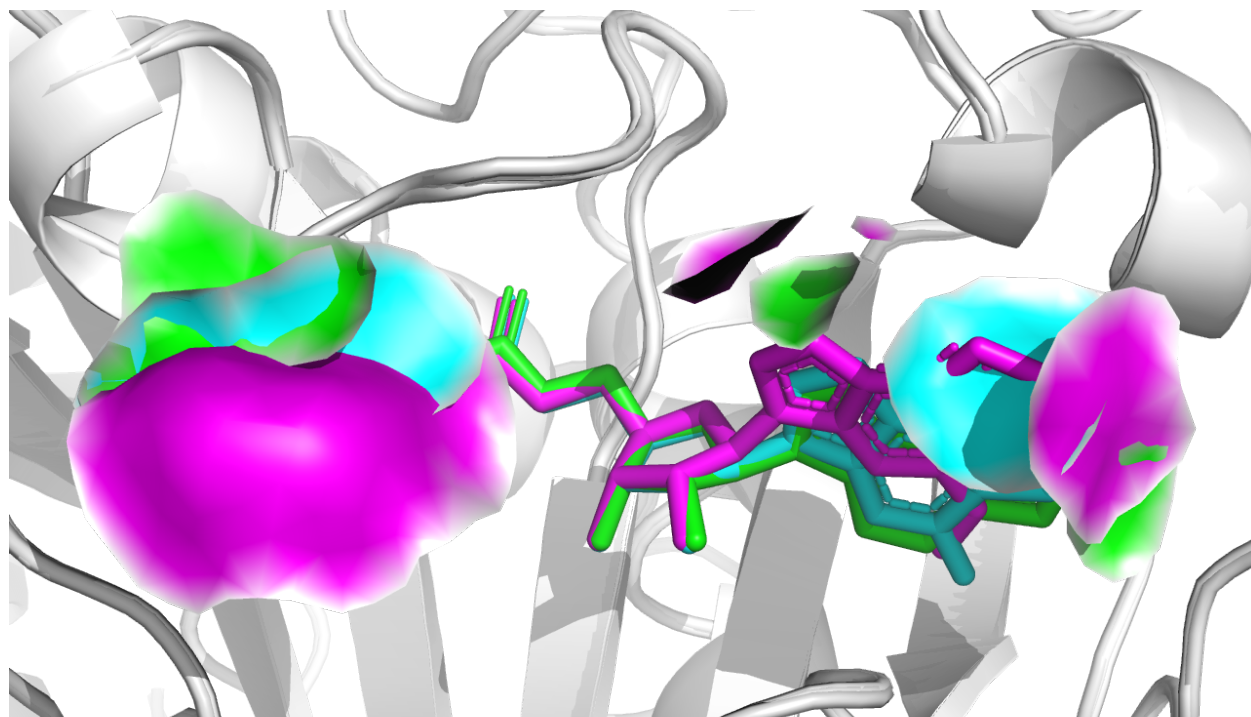
*In vivo*, we evaluated the effect of HINT1 inhibitors on MOR-NMDAR crosstalk via their impact on MOR inhibition of NMDAR activation and the development of acute endomorphin-2 tolerance. We observed that minor modifications to the ethenoadenosine scaffold resulted in major changes their activity. Consistent with our previous results, **TrpGc** displayed broad activity, preventing morphine from blocking NMDA evoked transient thermal hypersensitivity and behaviors as well as preventing the development of endomorphin-2 tolerance. Replacement of the guanosine base with the tricyclic ethenoadenosine base (**10**) abolished activity in all three

assays. Addition of a N<sup>2</sup>-methyl group (**9**) to the ethenoadenosine base resulted in ablation of its activity against MOR inhibition of NMDA evoked transient thermal sensitivity and behaviors but was observed to prevent the development of acute endomorphin-2 tolerance. Perhaps the most intriguing result comes from (**8**), which displayed enhancement of morphine efficacy in the NMDA evoked transient thermal hypersensitivity assay, as opposed to inhibition that we have observed with the other HINT1 inhibitors. Further, (**8**) was observed to induce analgesia following intrathecal injection, something not yet observed with any HINT1 inhibitor. Lastly, replacement of the carbamate backbone of compounds (**8**) and (**9**) with an acyl-sulfamate, compounds (**13**) and (**14**) seems to largely ablate their activity *in vivo*, with no efficacy observed in the NMDA evoked transient thermal hypersensitivity and behavior assays. This could potentially be explained by the large difference in polarity between the two sets of compounds. Interestingly, treatment with these compounds resulted in increased development of endomorphin-2 tolerance, though the mechanism behind this activity is not clear.

The SAR efforts of this work have resulted in a set of HINT1 inhibitors that selectively impact unique pathways of MOR-NMDAR crosstalk *in vivo*. Analysis of the *in vitro* and *in vivo* results has yet to establish a clear connection between these two activities. Consistent with our previous works, HINT1 binding was not correlated with *in vivo* activity. Evaluation of the co-crystal structures for the HINT1 bound inhibitors reveals that despite the presence of similar hallmark interactions, alterations to the nucleobase have a profound effect on the positioning of both the nucleobase and the inhibitor side chain. Due to the solvent accessible nature of these regions, each HINT1 inhibitor alters the molecular surface of the HINT1-Inhibitor complex (**Figure 8**). Because HINT1's involvement in MOR-NMDAR crosstalk relies on its participation in several

protein-protein interactions, alteration to its molecular surface could have a significant impact on its ability to participate in these key interactions. Interestingly, due to the unique pharmacological effects observed for these inhibitors *in vivo*, it appears that small-molecule intervention can potentially alter HINT1's interactions with some specificity, resulting in the selective inhibition of one pathway versus another, though further studies into the specific effects on these protein-protein interactions are needed. Additionally, we observed that **8** produces analgesia following intrathecal administration, though the mechanism behind this activity is not clear. Together, these results highlight the intriguing role of HINT1 in MOR-NMDAR crosstalk and the pharmacological possibilities that small molecule inhibition of HINT1 can afford. Evaluation of the mechanisms behind these pathways at the molecular level represents the crucial next step in advancing our understanding of the role of HINT1 in the CNS.

**Figure 8**



**Comparison of the molecular surface of carbamate-based nucleoside inhibitors.** Compounds 8 (Cyan), 9 (Magenta), and 10 (Green) bound to HINT1. The contributions of the inhibitors to the molecular surface of the bound HINT1/inhibitor complex are displayed in their respective colors. Changes to the molecular surface occur at the nucleobase and tryptamine side-chain.

## **Materials and Methods**

### **Continuous Fluorescence Assay**

Kinetics experiments were conducted on the Cary Eclipse UV spectrophotometer. All experiments were performed in HINT1 assay buffer (20 mM HEPES, 2 mM CaCl<sub>2</sub>, pH 7.4) at ambient temperature. HINT1 was exchanged into HINT1 assay buffer using 10 kD cutoff spin columns. HINT1 concentrations were determined via NanoDrop absorbance using an extinction coefficient determined from ExpASY ProtParam tool. Procedure was adapted from previous work.<sup>24</sup> All assays were performed in a 600 µl tapered quartz cuvette. HINT1 and inhibitor were incubated for 30 sec followed by substrate addition. The cuvette was immediately placed in the fluorimeter following substrate addition. The rate of fluorescence was measured over 5 minutes and the slope was determined. Fluorescence was converted to [Tryptamine] using the slope gathered from a tryptamine standard curve. The inhibition curves were plotted in Graphpad Prism and K<sub>i</sub> values were determined using a nonlinear regression. Values are reported with the standard error of the residual.

### **Protein Crystallography**

Crystals were grown via hanging drop vapor diffusion, with drops composed of 2 µL of protein and 2 µL of well solution. Well solutions contained 10-14 % (w/v) PEG 4000 and 100 mM sodium cacodylate pH 6.0-6.6. Crystals were formed after 4 days of incubation at 8 °C. Co-crystals with inhibitors were prepared by soaking preformed crystals in mother liquor containing 12.5 mM of each ligand for 3-40 min. DMSO was used to adequately dissolve the inhibitors, which came at a cost to soaking crystal's structural integrity and thus the ability to soak the crystals for



long. Soaked crystals did not need cryopreservation, but had to be mounted on a very thin film from the crystallization buffer. The excess liquid was removed by gentle touching of the mounting loop against the plate surface and the crystal was then flash cooled directly in an N<sub>2</sub> stream. Diffraction data were collected using Rigaku XtaLAB Synergy-S diffractometer equipped with a HyPix-6000HE Hybrid Photon Counting (HPC) detector and Cu microfocus sealed X-ray source as well as a low-temperature Oxford Cryostream 800 liquid nitrogen cooling system at 100 K. The data collection strategy was calculated within *CrysAlis PRO* to ensure desired data redundancy and percent completeness. Data were processed, integrated and scaled using *CrysAlis PRO* and AIMLESS. Data acquisition and processing statistics are shown in Table X1.<sup>25</sup>

Molecular replacement was conducted with hHINT1 coordinates (PDB ID: 6yqm [X3]) using *MOLREP* software.<sup>26</sup> Modeling and molecular visualization were performed in *COOT*.<sup>27</sup> Ligand restraints were calculated using *JLigand* [X6] and refinement was performed using *REFMAC5*.<sup>28</sup> All refinement steps were monitored with  $R_{\text{cryst}}$  and  $R_{\text{free}}$  values. The stereochemical quality of the resulting models was assessed using the program *MOLPROBITY* and the validation tools implemented in *COOT*.<sup>29</sup> The values of the mean temperature factors for protein main and side chains, ligands and water molecules were calculated using the program BAVERAGE from CCP4 suite.<sup>30</sup> Superposition of protein structures was performed using the program LSQKAB.<sup>31</sup> The refinement statistics of the described structures are listed in **Table S1**.

## **Animals**

ICR-CD-1 mice (male and female, 21-30 grams) were maintained on a 12-hour light/dark cycle with unrestricted access to water and food. All experiments were approved by the Institutional Animal Care and Use Committee of the University of Minnesota. Animal experiments were adapted from our previous work.<sup>4</sup>

## **Drug Preparation for Behavioral Assays**

Morphine sulfate (NIDA) and endomorphin-2 (endo-2) were dissolved in 0.9% saline. Endomorphin-2 was prepared as previously described.<sup>32</sup> Briefly, endo-2 was synthesized using solid-state methods and HPLC-purified by the Microchemical Facility of the University of Minnesota and was dissolved for intrathecal injection in 0.9% normal saline. All stocks of TrpGc and TrpGc analogues were dissolved in 5% DMSO, 10% EtOH, and 10% cremophor and diluted with diH<sub>2</sub>O to a final concentration of 0.5% DMSO, 1% cremophor, and 1% ethanol. From this stock, a final concentration was reached by diluting the stock solution with 0.9% normal saline into the injection concentration.

## **Intrathecal Injections**

All drugs were delivered in 5  $\mu$ L volumes via intrathecal injection in conscious mice.<sup>33</sup> Briefly, the mice were held by the iliac crest and drugs were injected into the intrathecal space by a 30-gauge, 0.5-inch needle attached to a 50  $\mu$ L Luer-hub Hamilton syringe.

### **Warm Water Tail Immersion Assay**

Antinociception was measured using a warm water tail immersion assay. Mice were wrapped in a soft cloth with their tails exposed and approximately 3/4 of the tail was dipped into a warm water bath (49 or 52.5°C). The latency for the mouse to flick its tail was recorded before and after intrathecal administration of drug. In order to avoid tissue damage, a maximum cutoff of 12 seconds was set. A minimum of 4 mice were used for each drug, and each subject received only one HINT1 inhibitor compound.

### **Morphine Inhibition of NMDA-evoked Behavior**

Intrathecally-injected NMDA gives rise to both a transient thermal hypersensitivity that can be measured by a warm water tail immersion assay, and a caudally-directed scratching and biting behavior lasting for 1-5 minutes. For this initial screen of the TrpGc analog compounds, we measured the impact of each inhibitor on morphine's inhibition of NMDA-evoked transient thermal hypersensitivity. A baseline tail flick latency (pre-NMDA tail flick latency) was recorded at 49°C. TrpGc or a TrpGc analog was intrathecally injected (0.1-30 nmol/5 µL) into male ICR mice (25-30g) 10 minutes prior to an intrathecal injection of morphine sulfate (10 nmol/5 µL). After a period of 10 minutes, NMDA was injected intrathecally and another tail flick latency was recorded (post-NMDA tail flick latency). The percent maximum possible effect (%MPE) was calculated according to the following equation:

$$MPE\% = -100 * \frac{(Experimental\ Value) - (Control)}{(Control)}$$

where the Control value is the average reduction of tail flick latency within the cohort of subjects receiving only NMDA treatment:

$$(Control) = (post\ NMDA\ tail\ flick\ latency - pre\ NMDA\ tail\ flick\ latency)$$

and the Experimental Value is the change in tail flick latency in the presence of NMDA + morphine or NMDA + morphine + HINT1 inhibitor.

### **Endomorphin-2 tolerance**

Baseline thermal responsiveness was assessed in a 52.5°C water bath tail-immersion assay with a cutoff time of 12 seconds. TrpGc, TrpGc analog or vehicle was injected intrathecally, followed 5 minutes later by an intrathecal injection of endomorphin-2 (endo-2) at a dose of 10 nmol/5 µL into male and female ICR mice. Observation of a Straub tail for each subject was used as an indication of a successful intrathecal injection of an opioid agonist. Thirty minutes following this injection, an additional tail flick was assessed in order to confirm a return to baseline responsiveness and a lack of continued analgesia (predrug latency). A probe dose of endo-2 (10 nmol/5 µL, i.t.) was injected, and a final tail flick latency (postdrug latency) was assessed 2.5 minutes following this probe endo-2 injection.

The results are expressed as a percentage maximum possible effect (%MPE) according to the following equation:

$$\%MPE = 100 * \frac{(postdrug\ latency - predrug\ latency)}{(12\ second\ cut\ off - predrug\ latency)}$$

### **Behavioral Data Analysis**

For behavioral assays, data were calculated as described above. The data are represented as mean +/- SEM for each assay. A minimum of three doses were used for dose-response analysis.

## **Acknowledgements**

Financial support is gratefully acknowledged from NIAID (AI146049) and the University of Minnesota Foundation. Thank you to the labs of Carolyn Fairbanks and Rafal Dolot for your fantastic collaboration. Thank you to Cristina Peterson and Kelley Kitto for designing and performing the NMDA evoked behavior, endomorphin-2 tolerance, and analgesia assays and to Rafal Dolot for performing the HINT1 X-ray crystallography experiments.

## References

- (1) Dang, Y. H.; Liu, Z. W.; Liu, P.; Wang, J. B. Emerging Roles of Histidine Triad Nucleotide Binding Protein 1 in Neuropsychiatric Diseases. *Zhongguo Yi Xue Ke Xue Yuan Xue Bao* **2017**, *39* (5), 705-714. DOI: 10.3881/j.issn.1000-503X.2017.05.018.
- (2) Rodríguez-Muñoz, M.; Sánchez-Blázquez, P.; Vicente-Sánchez, A.; Bailón, C.; Martín-Aznar, B.; Garzón, J. The histidine triad nucleotide-binding protein 1 supports mu-opioid receptor-glutamate NMDA receptor cross-regulation. *Cell Mol Life Sci* **2011**, *68* (17), 2933-2949. DOI: 10.1007/s00018-010-0598-x.
- (3) Garzón, J.; Herrero-Labrador, R.; Rodríguez-Muñoz, M.; Shah, R.; Vicente-Sánchez, A.; Wagner, C. R.; Sánchez-Blázquez, P. HINT1 protein: a new therapeutic target to enhance opioid antinociception and block mechanical allodynia. *Neuropharmacology* **2015**, *89*, 412-423. DOI: 10.1016/j.neuropharm.2014.10.022.
- (4) Shah, R. M.; Peterson, C.; Strom, A.; Dillenburg, M.; Finzel, B.; Kitto, K. F.; Fairbanks, C.; Wilcox, G.; Wagner, C. R. Inhibition of HINT1 Modulates Spinal Nociception and NMDA Evoked Behavior in Mice. *ACS Chem Neurosci* **2019**, *10* (10), 4385-4393. DOI: 10.1021/acchemneuro.9b00432.
- (5) Brenner, C. Hint, Fhit, and GalT: function, structure, evolution, and mechanism of three branches of the histidine triad superfamily of nucleotide hydrolases and transferases. *Biochemistry* **2002**, *41* (29), 9003-9014. DOI: 10.1021/bi025942q.
- (6) Maize, K. M.; Shah, R.; Strom, A.; Kumarapperuma, S.; Zhou, A.; Wagner, C. R.; Finzel, B. C. A Crystal Structure Based Guide to the Design of Human Histidine Triad Nucleotide Binding Protein 1 (hHint1) Activated ProTides. *Mol Pharm* **2017**, *14* (11), 3987-3997. DOI: 10.1021/acs.molpharmaceut.7b00664.

- (7) Mehellou, Y.; Rattan, H. S.; Balzarini, J. The ProTide Prodrug Technology: From the Concept to the Clinic. *J Med Chem* **2018**, *61* (6), 2211-2226. DOI: 10.1021/acs.jmedchem.7b00734.
- (8) Murakami, E.; Tolstykh, T.; Bao, H.; Niu, C.; Steuer, H. M.; Bao, D.; Chang, W.; Espiritu, C.; Bansal, S.; Lam, A. M.; et al. Mechanism of activation of PSI-7851 and its diastereoisomer PSI-7977. *J Biol Chem* **2010**, *285* (45), 34337-34347. DOI: 10.1074/jbc.M110.161802.
- (9) Weiske, J.; Huber, O. The histidine triad protein Hint1 interacts with Pontin and Reptin and inhibits TCF-beta-catenin-mediated transcription. *J Cell Sci* **2005**, *118* (Pt 14), 3117-3129. DOI: 10.1242/jcs.02437.
- (10) Genovese, G.; Ghosh, P.; Li, H.; Rettino, A.; Sioletic, S.; Cittadini, A.; Sgambato, A. The tumor suppressor HINT1 regulates MITF and  $\beta$ -catenin transcriptional activity in melanoma cells. *Cell Cycle* **2012**, *11* (11), 2206-2215. DOI: 10.4161/cc.20765.
- (11) Motzik, A.; Amir, E.; Erlich, T.; Wang, J.; Kim, B. G.; Han, J. M.; Kim, J. H.; Nechushtan, H.; Guo, M.; Razin, E.; et al. Post-translational modification of HINT1 mediates activation of MITF transcriptional activity in human melanoma cells. *Oncogene* **2017**, *36* (33), 4732-4738. DOI: 10.1038/onc.2017.81.
- (12) Liu, Q.; Puche, A. C.; Wang, J. B. Distribution and expression of protein kinase C interactive protein (PKCI/HINT1) in mouse central nervous system (CNS). *Neurochem Res* **2008**, *33* (7), 1263-1276. DOI: 10.1007/s11064-007-9578-4.
- (13) Barbier, E.; Zapata, A.; Oh, E.; Liu, Q.; Zhu, F.; Undie, A.; Shippenberg, T.; Wang, J. B. Supersensitivity to amphetamine in protein kinase-C interacting protein/HINT1 knockout mice. *Neuropsychopharmacology* **2007**, *32* (8), 1774-1782. DOI: 10.1038/sj.npp.1301301.



- (14) Barbier, E.; Wang, J. B. Anti-depressant and anxiolytic like behaviors in PKCI/HINT1 knockout mice associated with elevated plasma corticosterone level. *BMC Neurosci* **2009**, *10*, 132. DOI: 10.1186/1471-2202-10-132.
- (15) Shah, R. M.; Maize, K. M.; West, H. T.; Strom, A. M.; Finzel, B. C.; Wagner, C. R. Structure and Functional Characterization of Human Histidine Triad Nucleotide-Binding Protein 1 Mutations Associated with Inherited Axonal Neuropathy with Neuromyotonia. *J Mol Biol* **2018**, *430* (17), 2709-2721. DOI: 10.1016/j.jmb.2018.05.028.
- (16) Zimoń, M.; Baets, J.; Almeida-Souza, L.; De Vriendt, E.; Nikodinovic, J.; Parman, Y.; Battaloğlu, E.; Matur, Z.; Guergueltcheva, V.; Tournev, I.; et al. Loss-of-function mutations in HINT1 cause axonal neuropathy with neuromyotonia. *Nat Genet* **2012**, *44* (10), 1080-1083. DOI: 10.1038/ng.2406.
- (17) Jackson, K. J.; Wang, J. B.; Barbier, E.; Damaj, M. I.; Chen, X. The histidine triad nucleotide binding 1 protein is involved in nicotine reward and physical nicotine withdrawal in mice. *Neurosci Lett* **2013**, *550*, 129-133. DOI: 10.1016/j.neulet.2013.06.027.
- (18) Varadarajulu, J.; Lebar, M.; Krishnamoorthy, G.; Habelt, S.; Lu, J.; Bernard Weinstein, I.; Li, H.; Holsboer, F.; Turck, C. W.; Touma, C. Increased anxiety-related behaviour in Hint1 knockout mice. *Behav Brain Res* **2011**, *220* (2), 305-311. DOI: 10.1016/j.bbr.2011.02.012.
- (19) Cortés-Montero, E.; Sánchez-Blázquez, P.; Onetti, Y.; Merlos, M.; Garzón, J. Ligands Exert Biased Activity to Regulate Sigma 1 Receptor Interactions With Cationic TRPA1, TRPV1, and TRPM8 Channels. *Front Pharmacol* **2019**, *10*, 634. DOI: 10.3389/fphar.2019.00634.

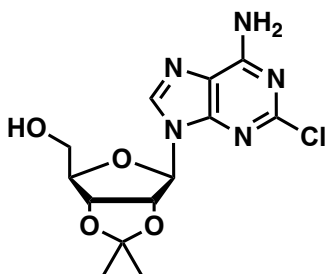
- (20) Vicente-Sánchez, A.; Sánchez-Blázquez, P.; Rodríguez-Muñoz, M.; Garzón, J. HINT1 protein cooperates with cannabinoid 1 receptor to negatively regulate glutamate NMDA receptor activity. *Mol Brain* **2013**, *6*, 42. DOI: 10.1186/1756-6606-6-42.
- (21) Rodríguez-Muñoz, M.; Cortés-Montero, E.; Pozo-Rodríguez, A.; Sánchez-Blázquez, P.; Garzón-Niño, J. The ON:OFF switch,  $\sigma$ 1R-HINT1 protein, controls GPCR-NMDA receptor cross-regulation: implications in neurological disorders. *Oncotarget* **2015**, *6* (34), 35458-35477. DOI: 10.18632/oncotarget.6064.
- (22) Rodríguez-Muñoz, M.; de la Torre-Madrid, E.; Sánchez-Blázquez, P.; Wang, J. B.; Garzón, J. NMDAR-nNOS generated zinc recruits PKC $\gamma$  to the HINT1-RGS17 complex bound to the C terminus of Mu-opioid receptors. *Cell Signal* **2008**, *20* (10), 1855-1864. DOI: 10.1016/j.cellsig.2008.06.015.
- (23) Shah, R.; Strom, A.; Zhou, A.; Maize, K. M.; Finzel, B. C.; Wagner, C. R. Design, Synthesis, and Characterization of Sulfamide and Sulfamate Nucleotidomimetic Inhibitors of hHint1. *ACS Med Chem Lett* **2016**, *7* (8), 780-784. DOI: 10.1021/acsmchemlett.6b00169.
- (24) Chou, T. F.; Baraniak, J.; Kaczmarek, R.; Zhou, X.; Cheng, J.; Ghosh, B.; Wagner, C. R. Phosphoramidate pronucleotides: a comparison of the phosphoramidase substrate specificity of human and Escherichia coli histidine triad nucleotide binding proteins. *Mol Pharm* **2007**, *4* (2), 208-217. DOI: 10.1021/mp060070y.
- (25) Evans, P. R.; Murshudov, G. N. How good are my data and what is the resolution? *Acta Crystallogr D Biol Crystallogr* **2013**, *69* (Pt 7), 1204-1214. DOI: 10.1107/S0907444913000061.
- (26) Vagin, A.; Teplyakov, A. MOLREP: An automated program for molecular replacement. *J. Appl. Crystallogr* **1997**, *30*, 1022-1025.

- (27) Emsley, P.; Cowtan, K. Coot: model-building tools for molecular graphics. *Acta Crystallogr D Biol Crystallogr* **2004**, *60* (Pt 12 Pt 1), 2126-2132. DOI: 10.1107/S0907444904019158.
- (28) Kovalevskiy, O.; Nicholls, R. A.; Long, F.; Carlon, A.; Murshudov, G. N. Overview of refinement procedures within REFMAC5: utilizing data from different sources. *Acta Crystallogr D Struct Biol* **2018**, *74* (Pt 3), 215-227. DOI: 10.1107/S2059798318000979.
- (29) Chen, V. B.; Arendall, W. B.; Headd, J. J.; Keedy, D. A.; Immormino, R. M.; Kapral, G. J.; Murray, L. W.; Richardson, J. S.; Richardson, D. C. MolProbity: all-atom structure validation for macromolecular crystallography. *Acta Crystallogr D Biol Crystallogr* **2010**, *66* (Pt 1), 12-21. DOI: 10.1107/S0907444909042073.
- (30) Winn, M. D.; Ballard, C. C.; Cowtan, K. D.; Dodson, E. J.; Emsley, P.; Evans, P. R.; Keegan, R. M.; Krissinel, E. B.; Leslie, A. G.; McCoy, A.; et al. Overview of the CCP4 suite and current developments. *Acta Crystallogr D Biol Crystallogr* **2011**, *67* (Pt 4), 235-242. DOI: 10.1107/S0907444910045749.
- (31) Kabsch, W.; Sander, C. Dictionary of protein secondary structure: pattern recognition of hydrogen-bonded and geometrical features. *Biopolymers* **1983**, *22* (12), 2577-2637. DOI: 10.1002/bip.360221211.
- (32) Stone, L. S.; Fairbanks, C. A.; Laughlin, T. M.; Nguyen, H. O.; Bushy, T. M.; Wessendorf, M. W.; Wilcox, G. L. Spinal analgesic actions of the new endogenous opioid peptides endomorphin-1 and -2. *Neuroreport* **1997**, *8* (14), 3131-3135. DOI: 10.1097/00001756-199709290-00025.
- (33) Hylden, J. L.; Wilcox, G. L. Intrathecal morphine in mice: a new technique. *Eur J Pharmacol* **1980**, *67* (2-3), 313-316.

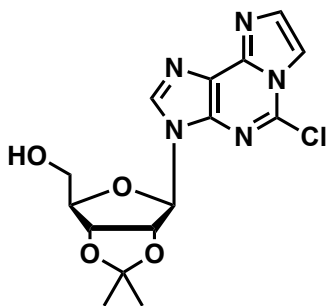
(34) Tallarida, R. J.; Murray, R. B. Manual of pharmacological calculations with computer programs. *Springer Verlag:New York* **1987**, 26-31.

(35) Tallarida, R. J.; Porreca, F.; Cowan, A. Statistical analysis of drug-drug and site-site interactions with isobolograms. *Life Sci* **1986**, *45*, 947-961.

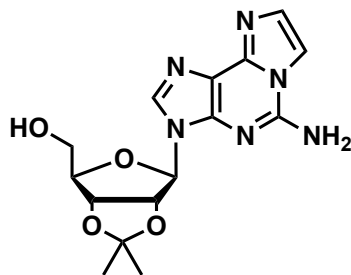
## Supplemental Information



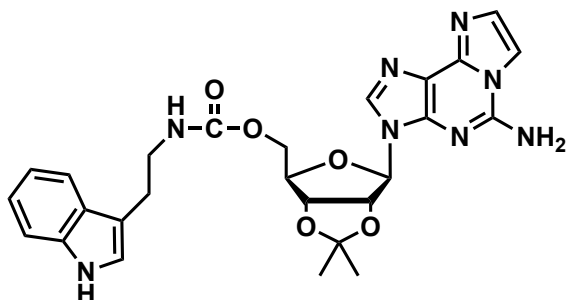
**Synthesis of 2',3'-Isopropylidene 2-chloroadenosine.** To a round bottom flask was added 2-chloroadenosine with acetone. To the flask was added perchloric acid dropwise. The reaction stirred at room temperature for 3 hours. The reaction was neutralized with ammonium hydroxide ~5 ml. The reaction was concentrated under reduced pressure and purified using normal phase chromatography (0-15% MeOH/DCM). Relevant fractions were pooled and concentrated under reduced pressure. Yield: quant. The  $^1\text{H}$  NMR spectrum was (DMSO- $d_6$ ): 1.34 (s, 3H), 1.55 (s, 3H), 3.54 (td, 2H), 4.22 (td, 1H), 4.94 (dd, 1H), 5.08 (d, 1H), 5.29 (dd, 1H), 6.06 (d, 1H), 7.86 (s, 2H), 8.36 (s, 1H).  $^{13}\text{C}$ -DMSO- $d_6$ :  $^{13}\text{C}$  NMR (126 MHz, DMSO)  $\delta$  25.68, 27.51, 61.95, 81.73, 83.92, 87.16, 89.84, 113.57, 118.58, 140.42, 150.44, 153.56, 157.29. ESI-MS [M+H] 342.2.



**Synthesis of 2',3'-Isopropylidene 2-Chloroethenoadenosine.** MD-3-17 (2.00 g, 5.85 mmol) was added to a round bottom flask with 50% w/v chloroacetaldehyde/H<sub>2</sub>O (36.00 ml, and 0.1 M NaOAc. The pH was adjusted to 6.5 using 1 M HCl. The reaction was stirred at 40°C for 48 hours. The reaction was concentrated under reduced pressure, then extracted with ethyl acetate and bicarb. The organic layer was collected and purified using normal phase flash chromatography (0-7% MeOH/DCM). The relevant fractions were pooled and concentrated under reduced pressure. Yield: 871 mg, 40.7%. The <sup>1</sup>H NMR spectrum was (DMSO-d<sub>6</sub>): 1.35 (s, 3H), 1.57 (s, 3H), 3.57 (td, 2H), 4.27 (m, 1H), 5.00 (dd, 1H), 5.09 (t, 1H), 5.36 (dd, 1H), 6.24 (d, 1H), 7.69 (d, 1H), 8.09 (d, 1H), 8.59 (s, 1H). <sup>13</sup>C-DMSO-d<sub>6</sub>: δ 141.77, 140.79, 138.19, 133.63, 133.52, 123.00, 113.65, 113.34, 90.36, 87.44, 84.33, 81.79, 61.88, 27.48, 25.67. ESI-MS [M+H] 366.2.

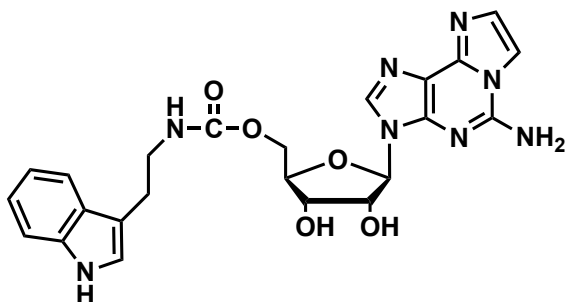


**Synthesis of 2',3'-Isopropylidene 2-aminoethenoadenosine.** To a sealed tube was added MD-3-29 (300 mg, 0.82 mmol) and 2.0 M NH<sub>3</sub>/isopropanol (6.72 ml, 13.44 mmol). The flask was sealed and heated to 75°C overnight. The crude mixture was transferred to a round bottom flask and concentrated under reduced pressure. The product was purified using normal phase chromatography (0-15% MeOH/DCM). Relevant fractions were pooled and concentrated under reduced pressure. Yield: 190 mg, 67%. The <sup>1</sup>H NMR spectrum was (DMSO-d<sub>6</sub>): δ 1.35 (s, 3H), 1.55 (s, 3H), 3.55 (qt, 2H), 4.16 (td, 1H), 5.05 (m, 2H), 5.32 (dd, 1H), 6.12 (d, 1H), 7.43 (d, 1H), 7.62 (s, 2H), 7.94 (d, 1H), 8.12 (s, 1H). <sup>13</sup>C-DMSO-d<sub>6</sub>: δ 25.76, 27.57, 62.14, 81.78, 84.19, 87.30, 89.21, 110.08, 113.53, 116.47, 132.14, 136.42, 140.70, 142.34, 145.48. ESI-MS [M+H] 347.2.

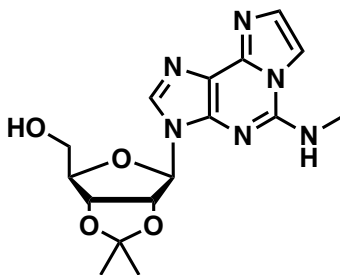


**2',3'-Isopropylidene-5'-O-[(3-Indolyl)-1-Ethyl]Carbamoyl 2-aminoethenoadenosine.** MD-3-39 (200 mg, 0.58 mmol) and 4-nitrophenyl chloroformate (186 mg, 0.92 mmol) were added to a round bottom flask and dissolved in pyridine (8 ml). The reaction was stirred for 2.5 hr at room temperature. To the reaction mixture was added tryptamine (185 mg, 1.15 mmol) dissolved in pyridine (2 ml). The reaction was stirred overnight at RT. The reaction was concentrated under reduced pressure. The crude mixture was taken up in ethyl acetate and sodium bicarbonate. The organic layer was extracted twice and combined. The organic layer was washed with bicarb, brine and water. The organic layer was collected, dried over MgSO<sub>4</sub>, filtered, and dried under reduced pressure. The product was purified using flash chromatography (0-15% DCM/MeOH). The relevant fractions were pooled and concentrated under reduced pressure. Yield: 74.5 mg, 24.2%. The <sup>1</sup>H NMR spectrum was (DMSO-d<sub>6</sub>): 1.35 (s, 3H), 1.56 (s, 3H), 2.81 (t, 2H), 3.18 (d, 1H), 3.23 (dd, 2H), 4.30 (m, 2H), 5.18 (dd, 1H), 5.38 (dd, 1H), 6.18 (d, 1H), 6.97 (m, 1H), 7.05 (m, 1H), 7.14 (d, 1H), 7.32 (d, 2H), 7.37 (t, 1H), 7.44 (d, 1H), 7.50 (d, 1H), 7.66 (s, 2H), 7.95 (d, 1H), and 8.09 (s, 1H). <sup>13</sup>C- DMSO-d<sub>6</sub>: 156.24, 145.52, 142.32, 140.54, 136.67, 136.61, 132.16, 127.65, 123.10, 121.35, 118.68, 118.64, 116.62, 113.79, 112.03, 118.81, 110.11, 89.14, 84.81, 84.08, 81.79, 64.61, 49.07, 27.57, 25.89, and 25.80. ESI-MS [M+H] 533.3.

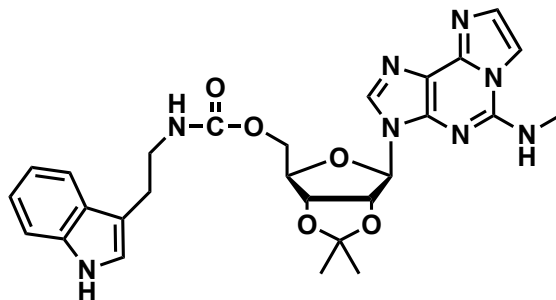




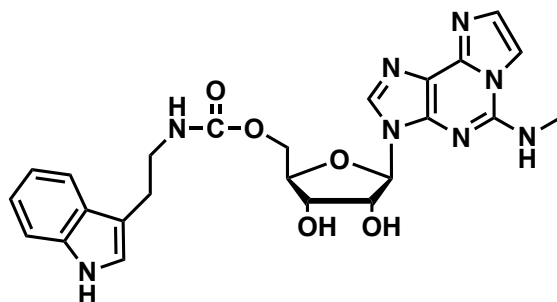
**5'-O-[(3-Indolyl)-1-Ethyl]Carbamoyl 2-aminoethenoadenosine.** MD-3-45 (74 mg, 0.14 mmol) was added to a scintillation vial with 4:1 TFA/H<sub>2</sub>O (2 ml). The reaction stirred at RT for 30 min. The reaction was transferred to a round bottomed flask with 0.1% TEA/Ethanol and subsequently concentrated under reduced pressure. 3 rounds of 50 ml of 0.1% TEA/Ethanol were used to quench the reaction. The crude product was purified using reverse phase flash chromatography 85-0% H<sub>2</sub>O/ACN). The relevant fractions were concentrated under reduced pressure to remove any acetonitrile, then flash frozen and lyophilized to yield the product as a white powder. Yield: 56.5 mg, 83%. The <sup>1</sup>H NMR spectrum was (DMSO-d<sub>6</sub>): δ 2.76 (t, 2H), 3.20 (m, 2H), 4.05 (m, 3H), 4.19 (dd, 1H), 4.55 (t, 1H), 5.30 (m, 1H), 5.47 (s, 1H), 5.85 (d, 1H), 6.90 (t, 1H), 6.99 (t, 1H), 7.08 (d, 1H), 7.26 (d, 1H), 7.39 (t, 1H), 7.45 (d, 1H), 7.52 (s, 1H), 7.73 (d, 2H), 7.95 (t, 1H), 8.16 (s, 1H), 10.73 (s, 1H). <sup>13</sup>C-DMSO-d<sub>6</sub>: <sup>13</sup>C NMR (126 MHz, DMSO) δ 9.08, 26.00, 41.68, 46.21, 64.52, 71.12, 73.58, 82.94, 87.04, 110.60, 111.84, 112.05, 115.17, 118.65, 118.71, 121.38, 123.11, 127.65, 136.69, 137.12, 141.50, 145.59, 156.47. ESI-MS [M+H] 492.3.



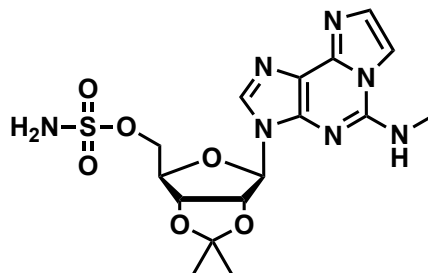
**2',3'-Isopropylidene N<sup>2</sup>-methyl-2-aminoethenoadenosine.** To a dry round bottom flask was added MD-3-9 (300 mg, 0.56 mmol) and 2.0 M methylamine/THF (7 ml, 14.00 mmol). The flask was purged under nitrogen gas/vacuum and stirred at room temperature overnight. The product crashed out as a white precipitate, the reaction mixture becoming thick. Volatiles were removed under reduced pressure. The product was purified by normal phase chromatography (0-15% MeOH/DCM). The relevant fractions were pooled and concentrated under reduced pressure. Yield: 223 mg, 75% The <sup>1</sup>H NMR spectrum was (DMSO-d<sub>6</sub>): 1.35 (s, 3H), 1.56 (s, 3H), 3.06 (d, 3H), 3.55 (m, 2H), 4.16 (m, 1H), 4.98 (t, 1H), 5.05 (dd, 1H), 5.47 (dd, 1H), 6.19 (d, 1H), 7.44 (d, 1H), 7.87 (q, 1H), 7.95 (d, 1H), 8.10 (s, 1H). <sup>13</sup>C-DMSO-d<sub>6</sub>: 144.96, 142.22, 140.39, 137.13, 132.19, 116.55, 113.49, 109.53, 89.48, 87.15, 83.84, 81.93, 62.02, 28.68, 27.51, and 25.16. ESI-MS [M+H] 361.3.



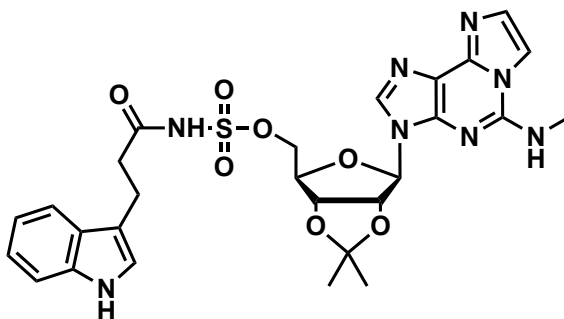
**Synthesis of 2',3'-Isopropylidene-5'-O-[(3-Indolyl)-1-Ethyl]Carbamoyl N<sup>2</sup>-methyl-2-aminoethenoadenosine.** MD-3-41 (250 mg, 0.69 mmol) and 4-nitrophenyl chloroformate (220 mg, 1.10mmol) were added to a round bottom flask and dissolved in pyridine (10 ml). The reaction was stirred for 2.5 hr at room temperature. To the reaction mixture was added tryptamine (221 mg, 1.38 mmol) dissolved in pyridine (2 ml). The reaction was stirred overnight at RT. The reaction was concentrated under reduced pressure. The crude mixture was taken up in ethyl acetate and sodium bicarbonate. The organic layer was extracted twice and combined. The organic layer was washed with sodium bicarbonate, brine and water. The organic layer was collected, dried over MgSO<sub>4</sub>, filtered, and dried under reduced pressure. The product was purified using flash chromatography (0-15% DCM/MeOH). The relevant fractions were pooled and concentrated under reduced pressure. Yield: 142 mg, 38%. The <sup>1</sup>H NMR spectrum was (DMSO-d<sub>6</sub>): δ 1.36 (s, 3H), 1.57 (s, 3H), 2.80 (t, 2H), 3.07 (d, 3H), 3.22 (m, 4H), 4.08 (m, 2H), 4.25 (dd, 1H), 4.35 (td, 1H), 5.10 (dd, 1H), 5.54 (dd, 1H), 6.26 (d, 1H), 6.96 (t, 1H), 7.06 (m, 1H), 7.14 (d, 1H), 7.33 (d, 1H), 7.39 (t, 1H), 7.45 (d, 1H), 7.50 (d, 1H), 7.90 (q, 1H), 7.96 (d, 1H), 8.09 (s, 1H), 10.79 (m, 1H). <sup>13</sup>C-DMSO-d<sub>6</sub>: δ 25.63, 25.89, 27.47, 28.72, 41.68, 49.07, 64.35, 81.99, 83.76, 84.48, 89.52, 109.61, 111.81, 112.02, 113.77, 116.67, 118.64, 118.67, 121.35, 123.09, 127.65, 132.23, 136.67, 137.24, 140.24, 142.17, 145.04, 156.18. ESI-MS [M+H] 547.4.



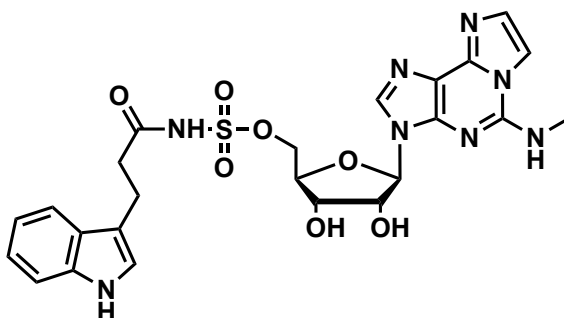
**Synthesis of 5'-O-[(3-Indolyl)-1-Ethyl]Carbamoyl N<sup>2</sup>-methyl-2-aminoethenoadenosine.** MD-3-47 was added to a scintillation vial with 4:1 TFA/H<sub>2</sub>O. The reaction stirred at RT for 30 min. The reaction was transferred to a round bottomed flask with 0.1% TEA/Ethanol and subsequently concentrated under reduced pressure. 3 rounds of 50 ml of 0.1% TEA/Ethanol were used to quench the reaction. The crude product was purified using reverse phase flash chromatography (85-0% H<sub>2</sub>O/ACN). The relevant fractions were concentrated under reduced pressure to remove any ACN, then flash frozen and lyophilized to yield the product as a white powder. Yield: 64.5 mg, 69%. The <sup>1</sup>H NMR spectrum was (DMSO-d<sub>6</sub>): δ 2.75 (dd, 2H), 2.99 (d, 3H), 3.19 (m, 2H), 4.02 (dt, 1H), 4.06 (dd, 1H), 4.16 (q, 1H), 4.23 (dd, 1H), 4.68 (q, 1H), 5.32 (d, 1H), 5.43 (d, 1H), 5.87 (d, 1H), 6.90 (t, 1H), 6.99 (m, 1H), 7.07 (d, 1H), 7.25 (d, 1H), 7.37 (m, 2H), 7.45 (d, 1H), 7.76 (q, 1H), 7.88 (d, 1H), 8.05 (s, 1H), 10.72 (d, 1H). <sup>13</sup>C-DMSO-d<sub>6</sub>: δ 25.98, 28.71, 41.68, 64.72, 71.26, 73.30, 82.73, 87.82, 109.52, 111.82, 112.06, 116.49, 118.65, 118.69, 121.36, 123.09, 127.66, 132.05, 136.68, 136.97, 141.19, 142.25, 145.00, 156.44. ESI-MS [M+H] 506.3.



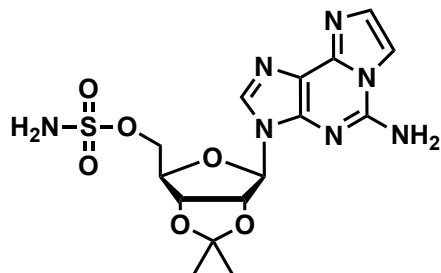
**Synthesis of 2',3'-Isopropylidene-5'-O-(Sulfamoyl) N<sup>2</sup>-methyl-2-aminoethenoadenosine.** MD-3-49 (200 mg, 0.56 mmol) was added to a dry round bottom flask with DMF (2 ml), purged with nitrogen gas, and cooled to 0°C. to the flask was added MD-3-1 (259 mg, 2.24 mmol). TEA (78  $\mu$ l, 0.56 mmol) was added dropwise to the flask. The reaction was stirred at 0°C for 10 minutes, then RT for 1 h. The crude mixture was concentrated under reduced pressure and then purified by reverse phase chromatography (95-0% H<sub>2</sub>O). The relevant fractions were pooled and acetonitrile was removed under reduced pressure. The resulting solution was lyophilized producing the product as a white powder. Yield: 91 mg, 38%. The <sup>1</sup>H NMR spectrum was (DMSO-d<sub>6</sub>): 1.30 (s, 3H), 1.50 (s, 3H), 2.47 (s, 1H), 3.00 (d, 3H), 4.07 (dd, 1H), 4.17 (dd, 1H), 4.32 (m, 1H), 5.09 (dd, 1H), 5.49 (dd, 1H), 6.22 (d, 1H), 7.38 (d, 1H), 7.50 (s, 2H), 7.83 (q, 1H), 7.88 (d, 1H), and 8.01 (s, 1H). <sup>13</sup>C-DMSO-d<sub>6</sub>: 145.08, 142.15, 140.11, 137.38, 132.23, 116.72, 113.98, 109.62, 89.59, 84.13, 83.81, 81.73, 68.51, 28.78, 27.39, and 25.59 ppm. ESI-MS [M+H] 426.3.



**Synthesis of 2',3'-Isopropylidene-5'-O-[N-(3-Indolepropionic acid)sulfamoyl] N<sup>2</sup>-methyl-2-aminoethenoadenosine.** MD-3-53 (160 mg, 0.36 mmol) and MD-3-17 (155 mg, 0.54 mmol) were added to a dry round bottom flask with DMF (2 ml). The flask was purged with nitrogen gas/vacuum and cooled to 0°C. To the flask was added DBU (59  $\mu$ l, 0.40 mmol). The reaction stirred for 1 hour at 0°C and then overnight at room temperature. The crude mixture was concentrated under reduced pressure and then purified by reverse phase chromatography (95-0%, 1% TEA in H<sub>2</sub>O/ACN). The relevant fractions were pooled and concentrated under reduced pressure. Yield: 167 mg, 66%. The <sup>1</sup>H NMR spectrum was (DMSO-d<sub>6</sub>):  $\delta$  1.35 (s, 3H), 1.57 (s, 3H), 2.34 (m, 2H), 2.83 (m, 2H), 3.07 (d, 3H), 4.02 (dd, 1H), 4.08 (dd, 1H), 4.37 (td, 1H), 5.12 (dd, 1H), 5.48 (dd, 1H), 6.22 (d, 1H), 6.93 (m, 1H), 7.04 (m, 2H), 7.30 (d, 1H), 7.45 (m, 2H), 7.87 (q, 1H), 7.95 (d, 1H), 8.14 (s, 1H), 10.68 (m, 1H). <sup>13</sup>C-DMSO-d<sub>6</sub>: <sup>13</sup>C NMR (126 MHz, DMSO)  $\delta$  12.25, 22.01, 28.78, 46.18, 67.73, 71.62, 73.48, 83.19, 87.80, 109.43, 111.66, 115.34, 116.46, 118.46, 118.72, 121.14, 122.36, 127.69, 132.08, 136.67, 137.04, 141.19, 142.33, 144.94, 177.92. ESI-MS [M+H] 597.4.

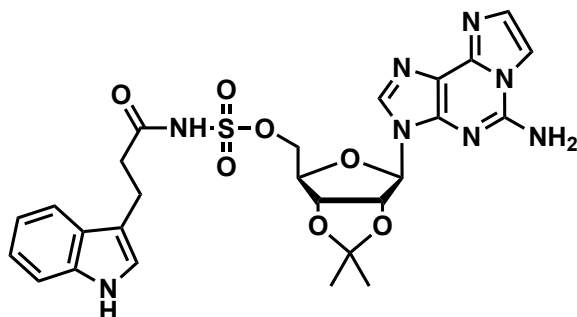


**5'-O-[N-(3-Indolepropionic acid)sulfamoyl] N<sup>2</sup>-methyl-2-aminoethenoadenosine.** MD-3-69 (100 mg, 0.14 mmol) was added to a scintillation vial with 4:1 TFA/H<sub>2</sub>O. The reaction stirred at RT for 30 min. The reaction was transferred to a round bottomed flask with 0.1% TEA/Ethanol and subsequently concentrated under reduced pressure. 3 rounds of 50 ml of 0.1% TEA/Ethanol were used to quench the reaction. The crude product was purified using reverse phase flash chromatography 95-0% 0.1% in H<sub>2</sub>O/ACN). The relevant fractions were concentrated under reduced pressure to remove any ACN, then flash frozen and lyophilized to yield the product as a white powder. Yield: 73 mg, 77%. The <sup>1</sup>H NMR spectrum was (DMSO-d<sub>6</sub>): δ 2.29 (m, 1H), 2.30 (d, 1H), 2.78 (m, 2H), 3.97 (dd, 1H), 4.02 (td, 1H), 4.08 (dd, 1H), 4.19 (td, 1H), 4.70 (q, 1H), 5.29 (d, 1H), 5.35 (d, 1H), 5.85 (d, 1H), 6.86 (t, 1H), 6.96 (m, 1H), 7.00 (d, 1H), 7.23 (d, 1H), 7.35 (d, 1H), 7.41 (d, 1H), 7.71 (q, 1H), 7.86 (d, 1H), 8.07 (s, 1H), 8.80 (s, 1H), 10.60 (d, 1H). <sup>13</sup>C-DMSO-d<sub>6</sub>: δ 12.25, 22.01, 28.78, 46.18, 67.73, 71.62, 73.48, 83.19, 87.80, 109.43, 111.66, 115.34, 116.46, 118.46, 118.72, 121.14, 122.36, 127.69, 132.08, 136.67, 137.04, 141.19, 142.33, 144.94, 177.92. ESI-MS [M+H] 556.3.



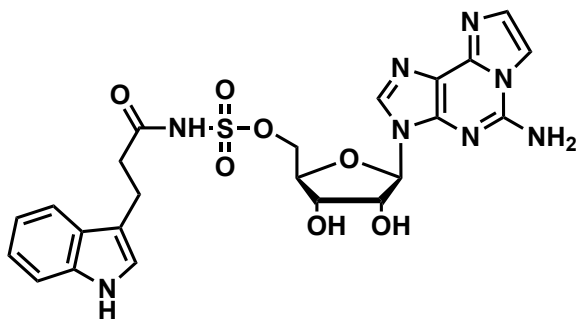
**Synthesis of 2',3'-Isopropylidene-5'-O-(Sulfamoyl) 2-aminoethenoadenosine MD-3-49** was added to a dry round bottom flask, purged with nitrogen gas, and cooled to 0°C. to the flask was added MD-3-1. TEA was added dropwise to the flask. The reaction was stirred at 0°C for 10 minutes, then RT for hour. The crude mixture was concentrated under reduced pressure and then purified by reverse phase chromatography (95-0% H<sub>2</sub>O). The relevant fractions were pooled and acetonitrile was removed under reduced pressure. The resulting solution was lyophilized producing the product as a white powder. Yield: 123 mg, 50%. The <sup>1</sup>H NMR spectrum was (DMSO-d<sub>6</sub>): 1.29 (s, 3H), 1.49 (s, 3H), 2.47 (s, 3H), 4.06 (dd, 1H), 4.18 (dd, 1H), 4.31 (m, 1H), 5.22 (dd, 1H), 5.31 (dd, 1H), 6.17 (d, 1H), 7.37 (d, 1H), 7.49 (s, 2H), 7.55 (s, 2H), 7.87 (d, 1H), and 7.99 (s, 1H). <sup>13</sup>C-DMSO-d<sub>6</sub>: 145.56, 142.30, 140.30, 136.83, 132.14, 116.70, 113.87, 110.14, 89.30, 84.68, 84.26, 81.74, 68.96, 40.90, 40.58, 40.49, 40.41, 40.32, 40.25, 40.16, 40.08, 39.99, 39.91, 39.82, 39.66, 39.49, 27.47, 25.77. ESI-MS [M+H] 440.3.





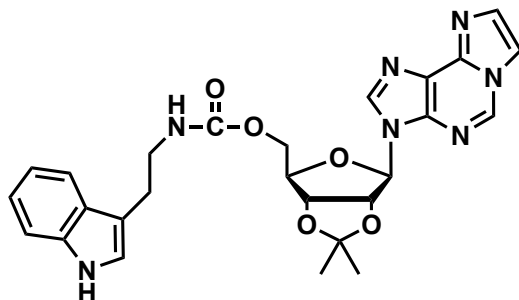
**2',3'-Isopropylidene-5'-O-[N-(3-Indolepropionic acid)sulfamoyl] 2-aminoethenoadenosine**

**Triethylammonium salt.** MD-3-53 (120 mg, 0.37 mmol) and MD-3-17 (160 mg, 0.56 mmol) were added to a dry round bottom flask with DMF (2 ml). The flask was purged with nitrogen gas/vacuum and cooled to 0°C. To the flask was added DBU (70  $\mu$ l, 0.47 mmol). The reaction stirred for 1 hour at 0°C and then overnight at room temperature. The crude mixture was concentrated under reduced pressure and then purified by reverse phase chromatography (95-0%, 1% TEA in H<sub>2</sub>O/ACN). The relevant fractions were pooled and concentrated under reduced pressure. Yield: 190 mg, 74%. The <sup>1</sup>H NMR spectrum was (DMSO-d<sub>6</sub>): <sup>1</sup>H NMR (500 MHz, DMSO)  $\delta$  1.31 (s, 3H), 1.53 (s, 3H), 2.38 (td, 2H), 2.85 (t, 2H), 3.90 (dd, 1H), 4.35 (td, 1H), 4.43 (dd, 1H), 5.21 (dd, 1H), 5.32 (dd, 1H), 6.14 (d, 1H), 6.87 (m, 1H), 7.00 (ddd, 1H), 7.04 (d, 1H), 7.28 (d, 1H), 7.42 (m, 2H), 7.79 (s, 2H), 7.93 (d, 1H), 8.11 (s, 1H), 9.47 (s, 0H), 10.66 (d, 1H). <sup>13</sup>C-DMSO-d<sub>6</sub>: <sup>13</sup>C NMR (126 MHz, DMSO)  $\delta$  9.42, 19.31, 21.98, 23.76, 25.68, 26.35, 27.56, 28.68, 32.17, 38.08, 46.22, 48.34, 53.85, 67.09, 82.20, 84.02, 84.50, 90.17, 110.07, 111.68, 113.39, 115.18, 116.60, 118.41, 118.64, 118.66, 121.15, 122.35, 127.63, 132.10, 136.67, 136.76, 136.91, 140.42, 142.36, 145.54, 165.86, 178.16. ESI-MS [M+H] 611.4.

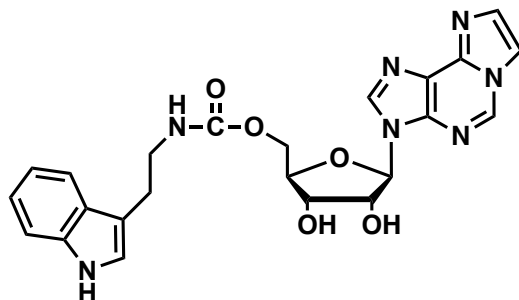


### Synthesis of 5'-O-[N-(3-Indolepropionic acid)sulfamoyl] 2-aminoethenoadenosine

**Triethylammonium salt.** MD-3-69 (100 mg, 0.14 mmol) was added to a scintillation vial with 4:1 TFA/H<sub>2</sub>O. The reaction stirred at RT for 30 min. The reaction was transferred to a round bottomed flask with 0.1% TEA/Ethanol and subsequently concentrated under reduced pressure. 3 rounds of 50 ml of 0.1% TEA/Ethanol were used to quench the reaction. The crude product was purified using reverse phase flash chromatography 95-0% 0.1% in H<sub>2</sub>O/ACN). The relevant fractions were concentrated under reduced pressure to remove any ACN, then flash frozen and lyophilized to yield the product as a white powder. Yield: 95 mg, quant. The <sup>1</sup>H NMR spectrum was (DMSO-d<sub>6</sub>): δ 2.40 (t, 2H), 2.51 (s, 3H), 2.87 (d, 2H), 4.02 (dd, 1H), 4.09 (s, 1H), 4.22 (s, 1H), 4.28 (dd, 1H), 4.69 (q, 1H), 5.29 (d, 1H), 5.43 (d, 1H), 5.90 (d, 1H), 6.93 (t, 1H), 7.03 (t, 1H), 7.08 (s, 1H), 7.31 (d, 1H), 7.43 (s, 1H), 7.48 (d, 1H), 7.63 (s, 2H), 7.94 (s, 1H), 8.15 (s, 1H), 10.68 (s, 1H). <sup>13</sup>C NMR (126 MHz, DMSO): δ 9.31, 19.31, 21.96, 23.76, 26.35, 28.68, 32.17, 38.09, 46.21, 48.33, 53.85, 67.69, 71.48, 73.76, 83.26, 87.42, 109.99, 111.67, 115.25, 116.36, 118.46, 118.74, 121.16, 122.40, 127.67, 132.02, 136.46, 136.67, 141.39, 142.48, 145.41, 165.85, 177.92.



**Synthesis of 2',3'-Isopropylidene-5'-O-[(3-Indolyl)-1-Ethyl]Carbamoyl Ethenoadenosine.** MD-3-41 (250 mg, 0.69 mmol) and 4-nitrophenyl chloroformate (307 mg, 0.96 mmol) were added to a round bottom flask and dissolved in pyridine (10 ml). The reaction was stirred for 2.5 hr at room temperature. To the reaction mixture was added tryptamine (310 mg, 1.94 mmol) dissolved in pyridine (4 ml). The reaction was stirred overnight at RT. The reaction was concentrated under reduced pressure. The crude mixture was taken up in ethyl acetate and sodium bicarbonate. The organic layer was extracted twice and combined. The organic layer was washed with sodium bicarbonate, brine and water. The organic layer was collected, dried over MgSO<sub>4</sub>, filtered, and dried under reduced pressure. The product was purified using flash chromatography (0-15% DCM/MeOH). The relevant fractions were pooled and concentrated under reduced pressure. The product was carried forward as mixture of starting material and product. Crude yield: 169 mg, 36%. ESI-MS [M+H] 517.3.



**5'-O-[(3-Indolyl)-1-Ethyl]Carbamoyl Ethenoadenosine.** MD-3-45 (150 mg, 0.30 mmol) was added to a scintillation vial with 4:1 TFA/H<sub>2</sub>O (2.5 ml). The reaction stirred at RT for 30 min. The reaction was transferred to a round bottomed flask with 0.1% TEA/Ethanol and subsequently concentrated under reduced pressure. 3 rounds of 50 ml of 0.1% TEA/Ethanol were used to quench the reaction. The crude product was purified using reverse phase flash chromatography 85-0% H<sub>2</sub>O/ACN). The relevant fractions were concentrated under reduced pressure to remove any acetonitrile, then flash frozen and lyophilized to yield the product as a white powder. Yield: 96.5 mg, 69%. The <sup>1</sup>H NMR spectrum was (DMSO-d<sub>6</sub>): δ 2.75 (t, 2H), 3.19 (m, 2H), 4.09 (m, 3H), 4.22 (dd, 1H), 4.61 (q, 1H), 5.36 (d, 1H), 5.53 (d, 1H), 6.00 (d, 1H), 6.90 (t, 1H), 6.98 (t, 1H), 7.08 (d, 1H), 7.26 (d, 1H), 7.39 (t, 1H), 7.45 (d, 1H), 7.50 (d, 1H), 8.02 (d, 1H), 8.47 (s, 1H), 9.24 (s, 1H), 10.73 (s, 1H). <sup>13</sup>C-DMSO-d<sub>6</sub>: δ 25.99, 41.69, 71.07, 73.94, 83.15, 87.88, 111.83, 112.06, 112.73, 118.66, 118.71, 121.37, 123.10, 123.51, 127.66, 133.25, 136.69, 137.66, 139.05, 140.37, 140.94, 156.45. ESI-MS [M+H] 477.3.

## HINT1 Inhibition Curves

Figure S1

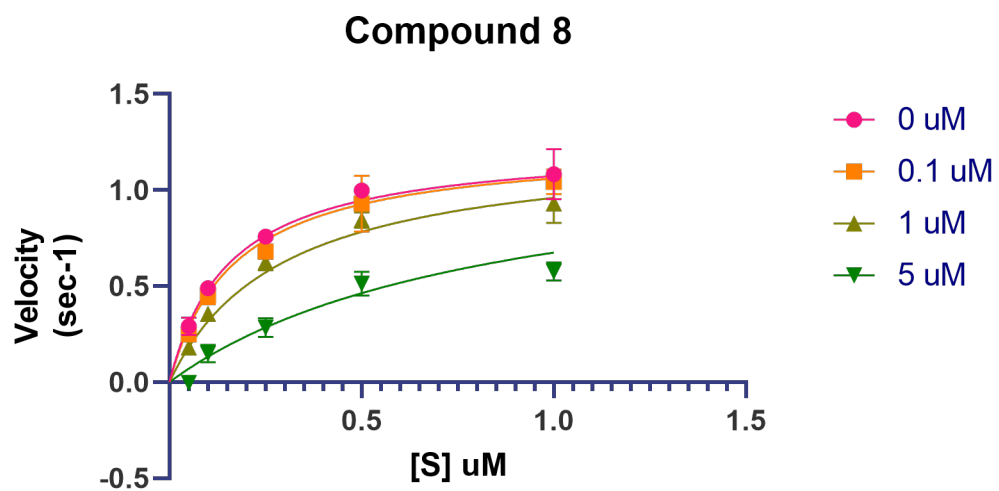


Figure S2

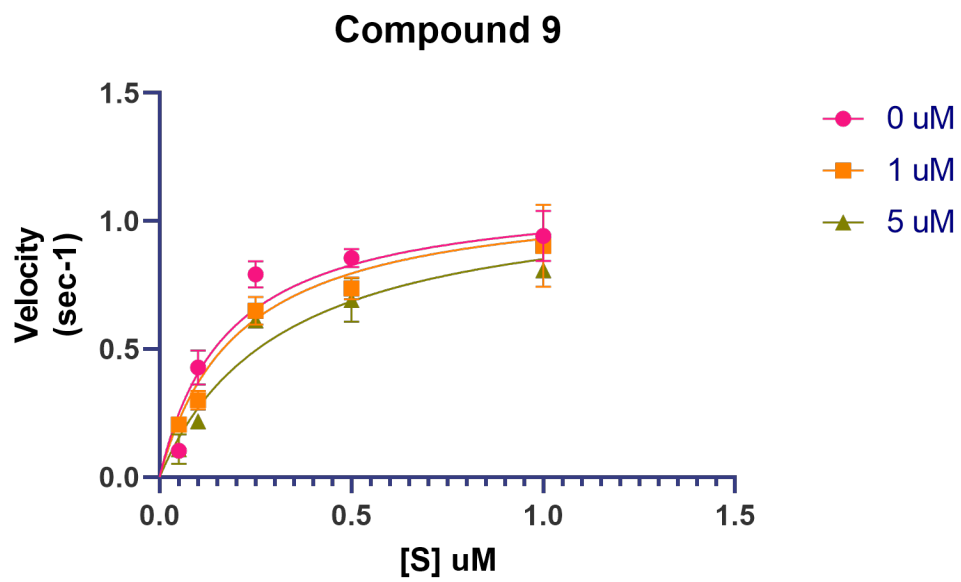


Figure S3

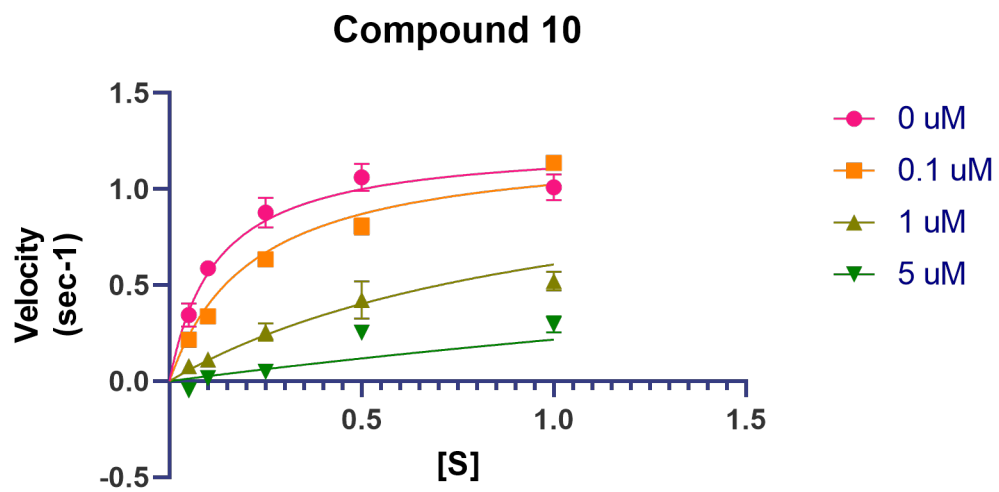


Figure S4

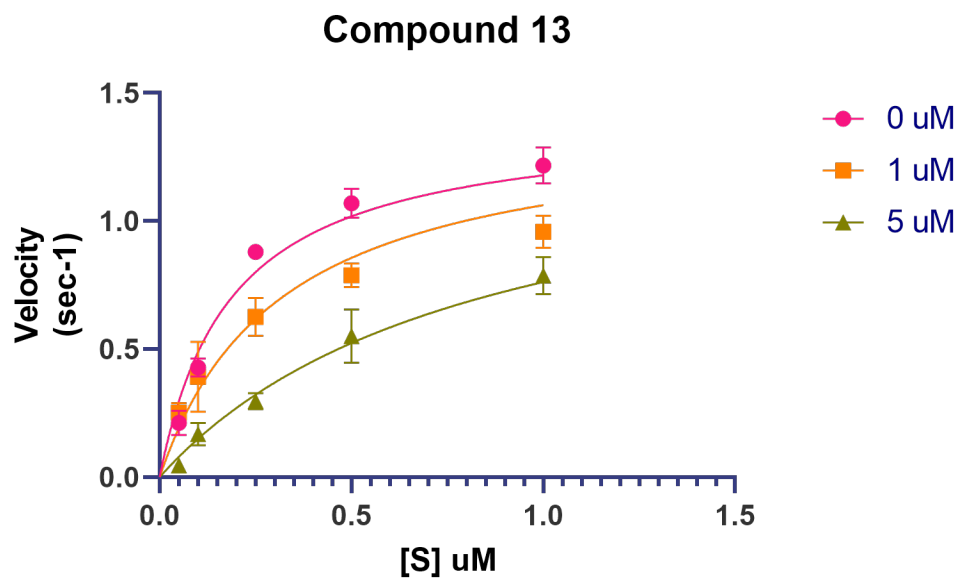
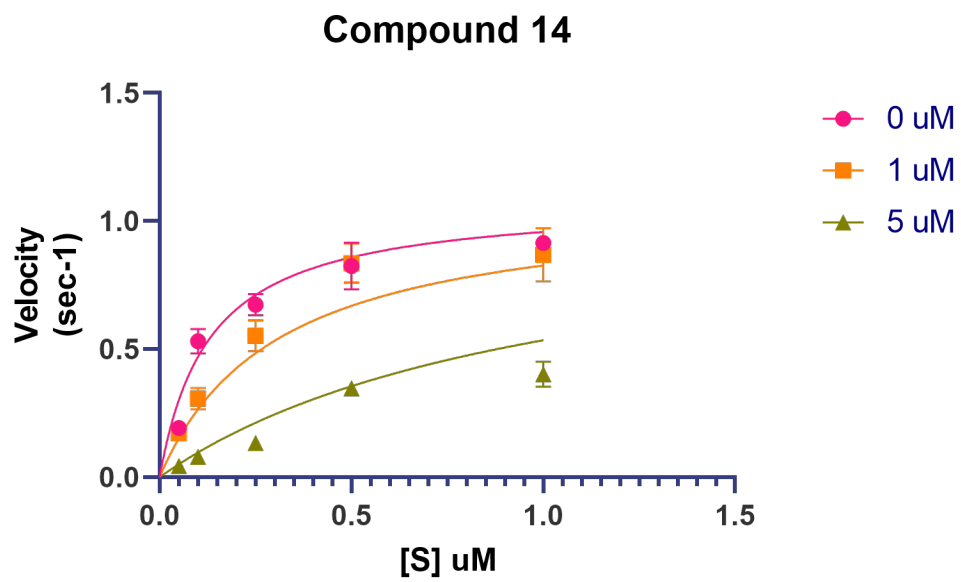




Figure S5



**Table S1. Crystallographic parameters and data collection statistics.**

PDB ID	8P8P	8PA6	8PA9	8PAF	8PAI
Crystallization conditions	10 % w/v PEG4000, 0.1 M sodium cacodylate pH 6.0	12 % w/v PEG4000, 0.1 M sodium cacodylate pH 6.0	12 % w/v PEG4000, 0.1 M sodium cacodylate pH 6.0	14 % w/v PEG4000, 0.1 M sodium cacodylate pH 6.0	10 % w/v PEG4000, 0.1 M sodium cacodylate pH 6.0
Crystal size ( $\mu\text{m}$ )	70 × 40 × 40	70 × 40 × 40	70 × 40 × 40	70 × 40 × 40	70 × 40 × 40
Ligand	TrpEtAdC	Trp2AEtAdC	Trp2MAEtAdC	Trp2AEtAdAS	Trp2MAEtAdAS
Ligand code	X7I	XKB	XKF	XKK	XKO
Soaking time (min.)	10	10	20	3	5
X-ray source	Rigaku XtaLAB Synergy-S				
Wavelength ( $\text{\AA}$ )	1.54184				
Detector	HyPix-6000HE				
Detector distance (mm)					
Oscillation width ( $^{\circ}$ )	0.38	0.38	0.38	0.38	0.38
Temperature (K)	100	100	100	100	100
No. of frames	609	1326	1316	788	989
Space group	<i>C2</i>	<i>C2</i>	<i>C2</i>	<i>C2</i>	<i>C2</i>
Unit-cell parameters					
<i>a</i> ( $\text{\AA}$ )	78.73	78.84	78.60	79.19	77.67
<i>a</i> ( $\text{\AA}$ )	46.55	46.32	46.31	46.55	46.43
<i>c</i> ( $\text{\AA}$ )	64.10	63.97	64.01	64.11	63.79
$\alpha$ ( $^{\circ}$ )	90.00	90.00	90.00	90.00	90.00
$\beta$ ( $^{\circ}$ )	94.74	94.80	94.71	94.84	94.62
$\gamma$ ( $^{\circ}$ )	90.00	90.00	90.00	90.00	90.00
Total no. of reflections	71108 (3434)	169719 (5651)	186288 (5964)	72260 (6027)	119678 (4221)
Unique reflections	18317 (1200)	31671 (1554)	36820 (1815)	13742 (1116)	21127 (1216)

Completeness (%)	99.6 (98.7)	99.9 (100)	99.8 (98.9)	99.8 (99.9)	99.8 (99.8)
Resolution (Å)	19.22-1.90 (1.94-1.90)	19.10-1.58 (1.61-1.58)	18.45-1.50 (1.53-1.50)	18.48-2.10 (2.16-2.10)	19.04-1.80 (1.84-1.80)
$R_{\text{merge}}^a$	0.100 (0.331)	0.074 (0.661)	0.062 (0.444)	0.082 (0.229)	0.087 (0.369)
$R_{\text{p.i.m}}$	0.057 (0.220)	0.035 (0.396)	0.028 (0.315)	0.039 (0.108)	0.039 (0.226)
Multiplicity	3.9 (2.9)	5.4 (3.6)	5.1 (3.3)	5.3 (5.4)	5.7 (3.5)
Mosaicity	1.34	1.19	1.32	1.53	1.47
Wilson $B$ factor	9.2	8.2	9.0	10.3	10.0
Mean $I/\text{sd}(I)$	8.9 (2.5)	15.3 (2.1)	14.2 (2.3)	14.9 (6.6)	12.6 (3.0)
$CC(1/2)$	0.994 (0.891)	0.998 (0.742)	0.999 (0.840)	0.998 (0.963)	0.997 (0.893)

**Table S2. Refinement statistics.**

PDB ID	8P8P	8PA6	8PA9	8PAF	8PAI
No. of reflections used in refinement	17388	30046	34937	13141	20130
No. of reflections used to $R_{\text{free}}$	910	1625	1878	592	982
$R_{\text{cryst}}$ ( $R_{\text{free}}$ )	0.154 (0.190)	0.147 (0.191)	0.149 (0.179)	0.136 (0.187)	0.149 (0.191)
No. of non H-atoms					
Protein	1887	1886	2000	1857	1901
Solvent	267	390	332	291	238
Ligand	35	36	37	39	40
R.m.s.d.s from ideal values					
Bond lengths (Å)	0.008	0.010	0.011	0.008	0.008
Bond angles (°)	1.461	1.540	1.657	1.461	1.528
Ramachandran plot					
Favoured [%]	98.7	98.7	99.1	99.1	98.7
Allowed [%]	1.3	1.3	0.9	0.9	1.3
Outliers [%]	0	0	0	0	0

## Appendix









